FUNCTIONAL NETWORK CONNECTIVITY ANALYSIS OF HUMAN BRAIN

Ph. D. Thesis

by

YOGESH KUMAR SARIYA

DEPARTMENT OF ELECTRICAL ENGINEERING
INDIAN INSTITUTE OF TECHNOLOGY ROORKEE
ROORKEE – 247667 (INDIA)
JULY, 2018

FUNCTIONAL NETWORK CONNECTIVITY ANALYSIS OF HUMAN BRAIN

A THESIS

Submitted in partial fulfilment of the requirements for the award of the degree

of

DOCTOR OF PHILOSOPHY

in

ELECTRICAL ENGINEERING

by

YOGESH KUMAR SARIYA

DEPARTMENT OF ELECTRICAL ENGINEERING
INDIAN INSTITUTE OF TECHNOLOGY ROORKEE
ROORKEE – 247667 (INDIA)
JULY, 2018

INDIAN INSTITUTE OF TECHNOLOGY ROORKEE
ROORKEE

CANDIDATE'S DECLARATION

I hereby certify that the work which is being presented in the thesis entitled "**FUNCTIONAL NETWORK CONNECTIVITY ANALYSIS OF HUMAN BRAIN"** in partial fulfilment of the requirements for the award of the Degree of Doctor of Philosophy and submitted in the Department of Electrical Engineering of the Indian Institute of Technology Roorkee, Roorkee, is an authentic record of my own work carried out during a period from July, 2013 to July, 2018 under the supervision of Dr. R. S. Anand, Professor, Department of Electrical Engineering, Indian Institute of Technology Roorkee, Roorkee.

The matter presented in this thesis has not been submitted by me for the award of any other degree of this or any other Institution.

(YOGESH KUMAR SARIYA)

This is to certify that the above statement made by the candidate is correct to the best of my knowledge.

(R. S. Anand)
Supervisor

Date:

ABSTRACT

Nowadays, the neurological disorders such as Alzheimer, epilepsy, autism spectrum disorder, Parkinson's disease, multiple sclerosis etc. has increased to an alarming level. Autism Spectrum Disorder (ASD), in this series, is an umbrella term for multiple neurodevelopmental conditions characterized by repetitive or stereotyped behaviors and pervasive deficits in social communications and interactions. The ASD is considered a lifelong disability which has an impact on both the individual and the family, as well as being a cost to society in general. Among these costs are additional health care, disability support in school and, in some instances, the loss of a productive working life and the provision of social security. By 2017, estimates of the prevalence of autism by the world health organization were 1 per 160 children, more than a 30-fold increase from the first studies of autism prevalence. From the perspective of social healthcare, it's an utmost requirement to understand their etiology.

Functional integration of the brain networks on a macroscopic level is being analyzed exhaustively to establish the biomarkers of neurological disorders. It is also termed as functional network connectivity analysis. During the past decade, the disrupted connectivity theory has generated considerable interest as a pathophysiological model for ASD. This theory postulates that deficiencies in the way the brain coordinates and synchronizes activity among different regions may account for the clinical symptoms of ASD. The most common version of this hypothesis proposes that individuals with ASD have weak connections between distant brain regions and increased connections within local regions.

The existing connectivity data in ASD are inconsistent and one possible explanation for the variability is that although altered connectivity is a pathogenic mechanism, there are insufficient specificity in existing hypotheses, insufficient precision in the techniques, excessive sensitivity to confounds, or insufficient power in studies to correctly identify the supporting evidence. The functional network connectivity in ASD significantly fluctuated in the research works carried out in this field because of methodological and subject choice contrasts. Early examinations regularly centered around locale differences in activation during tasks, with more recent studies utilizing resting state functional MRI concentrated in seed-based techniques and low-order ICA models. Developmental changes in functional connectivity have received inadequate attention and the discrepancies between findings of autism related hypo-

connectivity and hyper-connectivity might be reconciled by taking developmental changes into account as per the age range of the persons.

The present work emphasizes to bridge the inconsistencies in the literature and tries to establish a reliable biomarker which truly governs the signature manifestations of ASD patients. A resting-state examination is preferred rather a task-based one, because the imaging protocol is typically faster and the collected data serves multiple mapping purposes, thus fitting better into the usually limited patient scanning schedule. To accomplish this, the objectives of the present research work are formulated as: (1) comparing the ICA algorithms on the basis of their abilities to decompose the fMRI images, (2) building standard 3D templates for the naming of intrinsic connectivity networks, (3) age-stratified assessment of social and cognitive dysfunction of ASD through functional network connectivity (FNC), and (4) age-stratified functional network-based dynamic connectivity analysis in autism with higher order ICA model.

A variety of existing ICA algorithms have been implemented so far for fMRI images. With a view that algorithms that are overlooked may outperform the most opted, a comparative study is taken up in the first objective to analyze their abilities for the purpose of decomposition of fMRI images. In this work, ten independent component algorithms: Fast ICA, INFOMAX, SIMBEC, JADE, ERICA, EVD, RADICAL, ICA-EBM, ERBM, and COMBI are compared. Their separation abilities are adjudged on both, synthetic and real fMRI images. Performance to decompose synthetic fMRI images is being monitored on the basis of spatial correlation coefficients, time elapsed to extract independent components and the visual appearance of independent components. Ranking of their performances on task-based real fMRI images are based on the closeness of time courses of identified independent components with model time course and the closeness of spatial maps of components with spatial templates while their competencies for resting state fMRI data are analyzed by examining how distinctly they decompose the data into the most consistent resting state networks. Sum of mutual information between all the permutations of decomposed components of resting state fMRI data is also calculated. Based on all the acquired results, it is deduced that ERICA, EVD, and SIMBEC are not suitable algorithms for decomposition of fMRI images. Aggregate observations reveal that it is not worthwhile to use ERBM or ICA-EBM sepa-

rately but their combination is a better choice to use for fMRI decomposition. RADICAL is exceptionally sluggish and thus it is not a good choice. Among the overlooked algorithms and most opted algorithms, COMBI is a better choice for fMRI decomposition. The COMBI is fastest as well as it decomposes components quite distinctively.

The ICA finds the autonomous components of fMRI signal that represent a mix of 'true' brain networks and artifactual components from various sources such as cerebrospinal fluid, white matter, blood vessels and head motion. The separation of decomposed components into these two groups currently remains a semi-manual process, determined by quantitative metrics but reliant on the experience of the neuro-physicians. The labeling of RSN is being done either by utilizing the spatial correlation between the given 2D layout and component images or in light of the premise of ROIs effectively reported as the captivating anatomical part of those in past literary works. Splitting of components due to model order ambiguity, moderate advance in computer vision, higher likelihood of confusion of segments those are spread over more than one projection of the brain and repeating ROIs for different RSNs are the significant obstacles in utilizing 2D RSN layouts for the marking reason. To overcome this inadequacy, 3D templates are proposed in the second objective with the end goal of making RSN recognition automated. Proposed 3D templates are a superior substitute being free from these shortcomings. The use of volumetric overlap of decomposed RSN with 3D templates instead of the spatial correlation between RSN and 2D templates is expected to give more accurate results. These templates are developed by overlaying the manually labeled RSNs on 3D glass brain. These are selected from 100 decomposed components. The anatomic positions of them are based on the results of Talairach client where the toolbox was commanded to search in a cube of +/- 2mm. Images of manually labeled RSN are co-registered to sample image of multi-image analysis GUI (MANGO) toolbox (http://ric.uthscsa.edu/mango/) followed by the surface rendering. They are rendered on 3D glass brain for the purpose of better visibility. These 3D templates can be used as the standard for the labeling of RSN and are perfectly suitable for RsfMRI studies employing lower/higher order ICA model. Any RSN will get the name of the parent template which encompasses it and the quantification can be done based on the similarity indexes that measures the volumetric overlap viz., Dice coefficient or Jaccard coefficient.

Static functional network connectivity (sFNC) assessment to explore the limited cognitive ability of autistic subjects is executed in the third objective. The sFNC among six cognitive brain networks, viz. anterior default mode network, posterior default mode network, two frontoparietal networks (LFPN and RFPN), basal ganglia network (BG) and salience network (SN) have been examined. To understand the developmental trajectory of ASD, functional magnetic resonance imaging (fMRI) dataset of autistic children, adolescents and adults are considered. Constrained maximal lag correlation between each pair of networks of interest by calculating Pearsons correlation and constraining the lag between the time courses. The number of possible pair-wise combinations to examine between-network connectivity is 15 with six networks of interest. Subject-specific time-courses were detrended and despiked, then filtered using a fifth-order Butterworth low-pass filter with a cutoff frequency of 0.15 Hz. The SN manifest aberrant patterns of brain connectivity in the various stages of developmental trajectory. Attention allocation to stimuli, salient to the individual, is a conventional responsibility of the SN and atypical development of the SN may lessen interest in social interaction which is a signature characteristic of ASD. For the underlying two formative stages, the two frontoparietal networks are not connected and thus no availability of connectivity between them for the atypical population. This may be one of the reasons behind their hallmark behavioral characteristics.

The fourth objective of this study is to explore a whole brain dynamic functional network connectivity differences in a developmental trajectory. The dynamic FNC are evaluated utilizing a sliding window approach instantiated in the dFNC toolbox in GIFT toolbox. First, the time-courses were detrended and despiked using 3D despike in the AFNI software followed by filtering using a fifth-order Butterworth low-pass filter with a cutoff frequency of 0.15 Hz. Then, FNC covariance matrices were calculated between all pairwise RSNs for each subject using the correlations derived from previously done ICA analysis by moving a Gaussian window in 1 TR (time of repetition) increments across the subject time-courses. Successive FNC matrices for each window were then concatenated to form an array [number of RSNs x number of RSNs x (number of window units)] representing a state transition vector, or how the FNC state changed through time for each subject. Subsequently, a clustering analysis is done to examine the structure and frequency of FNC patterns that recurred in the state transi-

tion vectors. The k-means clustering algorithm was applied to the individual arrays of FNC covariance matrices using the City method and the algorithm iterated a maximum of 200 times before convergence. The results of this objective are dissimilar to the speculations that hyper-connectivity of brain networks are prevalent in young children with ASD, while hypo-connectivity are more common in young people and adults with the disorder when compared to typically developing cohorts. The statistically significant functional network connectivity differences (fdr<= 0.05) are sparse in the group of children and adults and even the significant intra-connectivity differences do not influence over the interconnectivity differences in the children's group of ASD.

ACKNOWLEDGEMENTS

First and foremost, I would like to thank God Almighty for giving me the strength, knowledge, ability and opportunity to undertake this research study and to persevere and complete it satisfactorily. Without his blessings, this achievement would not have been possible.

I express my sincere gratitude to Dr. R.S.Anand, Professor, Department of Electrical Engineering, Indian Institute of Technology Roorkee, Roorkee for his valuable guidance throughout my research work. His technical and clinical discussions, everlasting moral support and faith played a vital role in the completion of my thesis work. Apart from the this, his immense concern during tough and good times of my Ph.D. is indeed very memorable and highly appreciable.

I extend my sincere thanks to the members of student research committee Dr. Manoj Tripathi, Dr. M. V. Kartikeyan and Dr. Barjeev Tyagi for their valuable suggestions and assistance during my study period at IIT Roorkee. I would also like to thank the Head of the Department and other faculty members of Electrical Engineering Department, IITR for their moral support and providing the excellent laboratory facilities during this research work at Indian Institute of Technology Roorkee.

I am quite blessed and lucky to be working with a wonderful team of research scholars at IIT, Roorkee. I acknowledge the help rendered by my fellow researchers Dr. Nagashettapa Biradar, Dr Arvind R. Yadav, Mr. Jayendra Kumar, Dr. Arun Balodi, Dr. Deep Gupta, Dr. Sunil Sharma, Dr. Shashank Saini, Dr. Amol Sarkate, Dr. Bhavik Patel, Mr. Swapnil Jaiswal, Mr. Haresh Sabhadiya, Mr. Krishna Murari, Mr. Tushar Tyagi, Mr. Surender Hans, Mr. Gaurav Shukla, Mr. Shivam, Mr. Rinku, Mr. Ashish Rohilla, and Dr. Nabab Alam who never hesitated in lending a helping hand and made my stay at IIT Roorkee most memorable one. I extend my thanks to all whom I have missed mentioning.

I extend my thanks to office superintendent Mr. Mohan Singh, and other staff members particularly Mr. Rishab Verma, Mr. Shushil Kumar, Mr. Amir Ahmed, and all others who were quite helpful during my stay at IIT, Roorkee. I also wish to thank Mr. Jogeshwar Prasad, Mr.Rajiv Gupta, Mr. Dinesh Kumar, and Mr. Veer Chand, staff of Applied Instrumentation (AI) lab and Instrumentation and signal processing (ISP) Lab.

I express my sincere gratitude to Dr. Vince Calhoun for making the Group ICA for fMRI toolbox available for research purpose. I am obliged to the founders of the Human Connectome Project, Particularly the Autism Brain Data Exchange for giving me the opportunity to work on such a sophisticated data for my research work. I extend my sincere thanks to Dr. Yingying Wang, Dr. Andrew Jahn, Dr. Jason S. Nomi, and Mr. Srinivas Rachakonda who always tried to shed light on my doubts.

Last, but not least by any measures I am highly indebted to my beloved parents, siblings, and Ms. Seema Rajput for their unconditional support. I also thank the entire Biomedical Department of SGSITS, Indore for their supporting attitude.

(Yogesh Kumar Sariya)

CONTENTS

LIST OF FIGURES

LIST OF TABLES

Acronyms

2D	Two Dimensional
3D	Three Dimensional
ABIDE	Autism Brain Imaging Data Exchange
ASD	Autism Spectrum Disorder
AUD	Auditory Network
BGN	Basal Ganglia Network
BOLD	Blood Oxygenated Level Dependent
CBF	Cerebral Blood Flow
CCN	Cognitive Control Network
CCS	Connectome Computation System
CNR	Contrast to Noise Ratio
DCS	Direct Cotical Stimulus
dFNC	Dynamic Functional Network Connectivity
DMN	Default Mode Network
DTI	Diffusion Tensor Imaging
EEG	Electroencephelograph
ERBM	Entropy Rate Bound Minimization
ERICA	Equivalent Robust ICA
ERP	Event related potential
EVD	Eigenvalue Decomposition
FC	Functional Connectivity
FDR	False Discovery Rate
fMRI	Functional Magnetic Resonance Imaging
FNC	Functional Network Connectivity
FP	Frontoparietal
FWER	Family-Wise Error Rate
GIFT	Group ICA for fMRI Toolbox
HC	Healthy Control

HRF	Hemodynamic Response Function
ICA	Independent Component Analysis
ICA-EBM	ICA by Entropy Bound Minimization
ICN	Intrinsic Connectivity Network
INDI	International Neuroimaging Data-sharing Initiative
JADE	Joint Approximate Diagonalization Of Eigenmatrices
MANGO	Multi-image Analysis GUI
MEG	Magnetoencephelography
MNI	Montreal Neurological Institute
MRI	Magnetic Resonance Imaging
PET	Positron Emission Tomography
PCA	Principle Component Analysis
PCP	Preprocessed Connectome Projest
PLS	Partial Least Square
RADICAL	Robust, Accurate, Direct ICA aLgorithm
RsfMRI	Resting State Functional Magnetic Resonance Imaging
RSN	Resting State Network
SPM	Statistical Parametric Mapping
TPN	Task Positive Network
TNN	Task Negative Network
TMS	Transcranial Magnetic Stimulation

CHAPTER 1

INTRODUCTION

The investigations of the etiology of autism spectrum disorder has profited from the expanding conceptualization of behavior and cognition as stemming from atypicality of brain networks. Despite the fact that ASD is related with changed patterns of over-and under-connectivity, specifics are yet an issue of open deliberation. This chapter presents an prologue to ASD, fMRI and state of the art techniques. Thesis organization is mentioned at the end.

1.1 Motivation

The quest of probing the brain has always fascinated the research community. Historically correlating brain injury and behaviour was one of the only methods to infer the task of brain regions [1]. Today, neuroscientists can select from a wide range of brain imaging techniques viz., event related potential (ERP), magnetoencephalography (MEG), functional magnetic resonance imaging (fMRI), positron emission tomography (PET), single photon emission computerized tomography (SPECT) and transcranial magnetic stimulation (TMS). These techniques can be evaluated on the basis of spatial resolution, temporal resolution, mode (whether the technique measures activation or interferes with the region's function) and cost. The fMRI is non-invasive, gives a good spatial resolution (Fig 1.1) and doesn't require any exogenous contrast agent thus became the preferable technique. Since its inception, the fMRI has been applied for functional segregation of the human brain viz., sensation, perception and attention to cognition, language and emotion in healthy and atypically developing population as well [2, 3]. Today, interest has shifted slightly towards identifying that how the brain regions are connected functionally as well as anatomically. Functional connectivity (FC) analysis can shed light on the root of neurodegenerative and neurodevelopmental disorders. Functional connectivity examines temporal statistical dependencies among distant brain regions by means of seed-based analysis or independent component analysis (ICA).

Preponderance of people diagnosed with autism spectrum disorder has drawn attention of researchers around the globe to probe the neurobiology of this complex neurodevelopmental disorder. Neuroimaging and posthumous studies gives the testimony of atypical functional

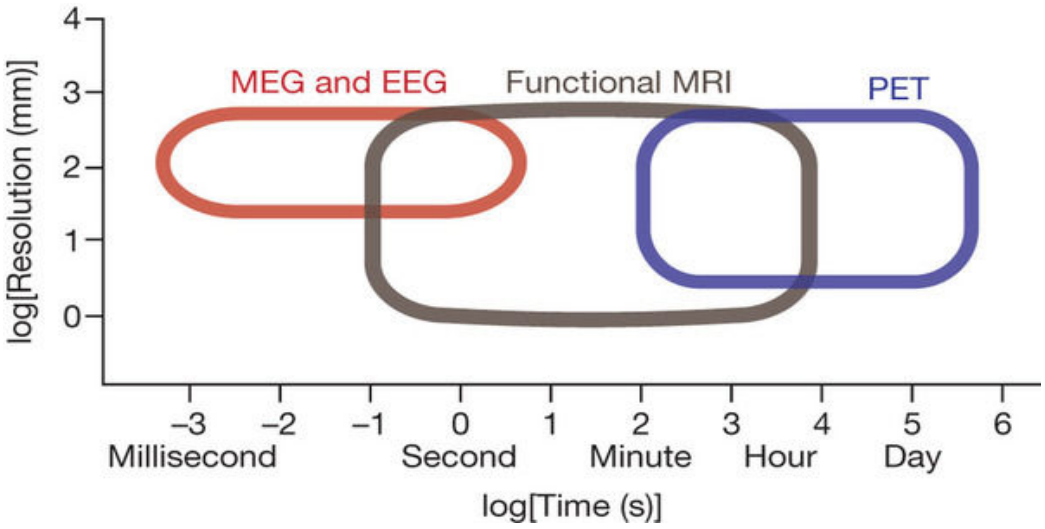

Fig. 1.1: Functional neuroimaging methods and their temporal and spatial resolution. Magnetoencephalography (MEG) and electroencephalography (EEG) image the electromagnetic effects of neuronal (assembly) action; their temporal resolution can be on the order of milliseconds whereas their spatial resolution tends to be less than that of fMRI, which images blood flow or oxygenation effects of neuronal activation, and PET, which uses radioisotopes to label molecules in the brain. fMRI and PET, in turn, are limited in their temporal resolution to several 100 ms (for fMRI) and minutes (for PET). Figure courtesy of (Andreas Meyer, 2010)

integration and structural connectivity of brain regions of individuals with ASD [4]. Author have proposed corrections in intermediate stages of functional network connectivity analysis (FNC) and thereafter explored the FNC patterns of ASD population.

1.2 Autism Spectrum Disorder

Autism is a neurodevelopmental disorder which was once a rarely found disease. USA's Center for Disease Control and Prevention recently released a data, quoting that the prevalence of autism at an alarming level of one in 68 children in March 2014, which was once at one in 88 in 2012. India has about 10 million people diagnosed with autism. It is an incurable disease, but early diagnosis and treatment have helped more and more people to reach their full potential. Understanding the severity of the disease, a USA based organization "Autism Speaks" invested $2.3 million for the research on autism. Since the persons diagnosed with

autism exhibit a range of symptoms, it is referred as autism spectrum disorder (ASD). People impaired by ASD may display obsessive tendencies, outrageous tangible affectability, hindrance to change in routine and repeated body movements. The ASD has turned into the most usually diagnosed childhood disorder. [5,6]. Autism can affect anyone, and is not based on ethnic, racial, or social backgrounds.

The analysis of ASD at a beginning period is pivotal for better evaluation and examination of this perplexing disorder. There has been a considerable endeavors to analyze ASD utilizing distinctive methodologies, for example, neuroimaging techniques, hereditary strategies, and behavior reports. Neuroimaging techniques have been widely used for ASD diagnosis in clinical/research applications, and a standout amongst the best ones is magnetic resonance imaging (MRI), where it has indicated guarantee of the ASD related variations from the norm specifically. The MRI modalities have risen as capable means that provide non-invasive clinical diagnostics of various diseases and abnormalities since their initiation in the 1980s. After the advent of the nineteen-eighties, MRI soon became one of the most promising non-invasive modality for visualization and diagnostics of ASD-related abnormalities. Along with its main advantage of no exposure to radiation, high contrast, and spatial resolution, the recent advances in MRI modalities have notably increased diagnostic certainty. Numerous MRI modalities, for example, different types of structural MRI (sMRI) that inspects anatomical changes, and functional MRI (fMRI) that gives proxy measurement of neuronal activity by checking cerebral blood flow changes, have been utilized to investigate aspects of ASD with end goal to better comprehend this perplexing disorder.

1.3 Physiology of the signal

1.3.1 Functional Magnetic Resonance Imaging

The origin and the primary attributes of the fMRI signals are briefly introduced here in this subsection for the basic acquaintance of the reader.

1.3.1.1 Source of the signal

The end goal of this subsection is to comprehend the characteristics of the functional counterpart of magnetic resonance imaging signals and it can be achieved by covering both, its association with the neuronal activity and the physics that captures this action. The fMRI is a

measurement of back end neuronal firing. [7–12]. The brain activity can actuate the cerebral blood flow and the fMRI signal is actually the proxy of neuronal activity in terms of this haemodynamic reaction to the neuronal electrification. Neuronal firing denote the utilization of oxygen and lead to uproot of molecules responsible for vasoactive signaling and thereby regulate the mechanism of vasoconstriction and dilation. This effect is known as Blood Oxygen Level Dependent (BOLD) response. The BOLD response results thus strictly related to neuronal activity, yet, it is characteristically influenced by other components, for example, the anatomy of capillary, vessels and veins distribution. Temporal resolution of the BOLD fMRI signals is relatively low by virtue of the neuronal activity. Since, it depends on haemodynamic response (HRF) (Fig. 1.2), it is of the order of 5-10 seconds which is much lower than the temporal resolution of neuronal firing as it vanishes within milliseconds.

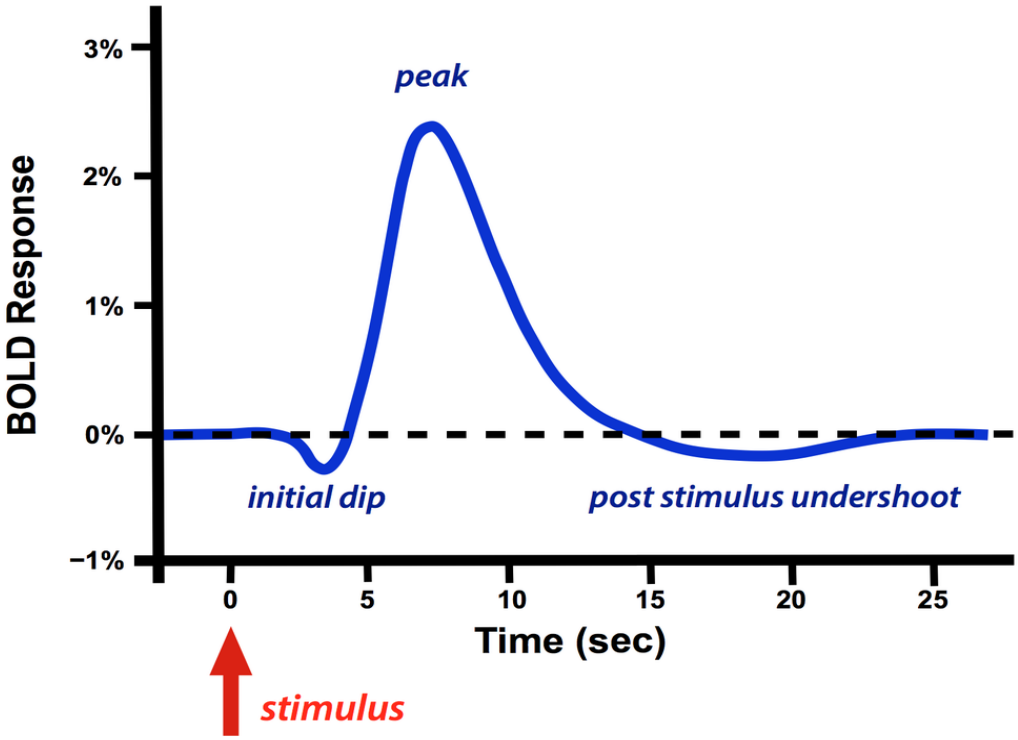

Fig. 1.2: Hemodynamic response function (HRF). The HRF typically demonstrates a small initial dip, followed by a tall peak, and then a variable post-stimulus undershoot. Figure courtesy of (http://mriquestions.com/does-boldbrain-activity.html)

1.3.1.2 Measured signal

The whole fMRI strategy depends on those matters whose characteristics are in cooperation with magnetic fields. At the point when putting in an magnetic field, protons (in this case protons of hydrogen) tend to align to the magnetic field itself, generating a magnetization vector whose magnitude is proportional to the magnetic field strength. With a specific end goal to disturb the magnetization vector a specific extent of energy need to be provided, and it can happen at a specific frequency, termed as Larmor frequency, which depends on the nature of protons and on the value of the magnetic field. This means that the energy transmitting system and the protons must be in resonance. Once perturbed protons tend to realign with the magnetic field emitting a signal which can be finally measured and exploited. The BOLD related deoxyhaemoglobin works as an endogenous contrast agent within blood flow and volume, whose magnetic properties bring forth the deliberate fMRI signal.

1.3.1.3 Image generation

As expressed over, a disturbed hydrogen nuclei emits a signal during its reorientation with hotelier external magnetic field whose acquisition can be materialized to figure out the locality of the nuclei. Some mechanism is required to encode the spatial information in order to create an image. Gradient coils of MRI machine serve this encoding purpose and total three gradient coils are used. These coils adjust resonance frequency with the goal that specific position in a 2D axial slice of the brain can be portrayed by different phase and frequency values. By doing so its possible to attain a higher spatial resolution in the reconstructed brain images and even it is done noninvasively, which has made it a well-received neuroimaging modality that is suitable to answer neuroscientific questions.

1.3.1.4 Image contrast

As per the explanation given in the previous subsection various matters and tissues are portrayed by various resonance frequencies. Subsequently by gauging the transient orthogonal transverse and longitudinal components it is feasible to capture the signals radiated by different tissues. Where lower T_2^* reflect lower concentration of deoxygenated hemoglobin and the reverse in higher T_2^*. Consequently the activated brain region appears brighter in fMRI images.

1.4 Univariate Analysis of fMRI

1.4.1 General Overview

One very intuitive way to design the fMRI and PET experiments is to advise the volunteers to execute both test and control assignments in succession [13–15]. The resultant haemodynamic response at each individual voxel might get affected by different distributive processes and they might not be of interest too viz., physiological (breathing and pumping of the heart), head motion, machine artifacts etc. and consequently a blend of informations of varying frequencies might constitute the signals gathered from those voxels. The regional differences between the brain images in most of the PET examinations till 1980s were characterized by researchers utilizing the manually drawn region of interests [16]. This approach abbreviated huge number of voxels to a modest bunch of ROI examination, in a fairly uncertain anatomical manner. The prevalence of univariate analysis at that time was solely governed by the undeniable need of voxelwise deductions regarding brain reactions in the absence of any a priori hypothesis regarding anatomical mapping of those responses.

The univariate analysis is a common statistical approach for neuroimaging analysis and it identifies voxelwise signal changes reliably. This is carried out by first creating an identical design matrix (for each voxel) whose columns correspond to the effects that have been built into the experiment or may confound the results [17, 18]. These are alluded to as regressors and are made by convolving onsets of each state of the experimental task with a fixed model of the HRF. A general linear model is conducted after the creation of design matrix and for the further statistical parametric mapping [SPMs; [19]] it aids parameter estimation as well as a wide range of hypothesis testing. Statistical parametric mapping alludes to the construction of spatially expanded statistical processes (usually derived under parametric assumptions) to test the null hypothesis about specific effect in a voxel-by-voxel manner. Put simply, if one applies t/F tests for every voxel variable, an image of t or F statistics, called the t or F statistical parametric map, is obtained. Voxels crossing some defined threshold are labeled as active voxels.

1.4.2 Limitations of univariate analysis

Despite the fact that an univariate investigation approach is fairly simple in effective computation, it has some inherent shortcomings. Most importantly, it goes with the assumption that all voxels or group of voxels under investigation are independent variables [20] but the correlation among voxels is inevitable [21]. Furthermore, such an approach regularly overlooks cooperations between brain regions (i.e. functional integration) by just endeavoring to recognize a brain region(s) with a particular capacity (i.e. functional segregation).

Being a hypothesis driven method is a second major issue with univariate analysis and it implies that there should be a model a priori which mimic the changes in fMRI signals in reaction to the experimental events. This approach is not compatible when reactions to the experimental paradigm is either unknown or heterogeneous among voxels. Typically univariate analysis is able to capture those activations whose signal changes mimic canonical HRF. A reliable activation can not be attained when the changes in signal deviates from the HRF.

Third, since in univariate analysis signal changes are identified voxelwise, null hypothesis needs to be executed out for each region, across tens of thousands of voxels. Consequently, correction for multiple comparisons is a basic concern. Probability of false discovery (i.e. falsely declaring a voxel active when it is not) increases with the increase in the number of statistical tests conducted. One potential fix, to overcome the multiple comparisons problem is to limit the number of false positives, or to control for family-wise error rate (FWER), for instance by using a Bonferroni correction. This is achieved by lowering an acceptable false positive rate (i.e. alpha value) in extent to the number of independent statistical tests. Bonferroni correction successfully diminishes false positives, it increases false negatives (i.e. type II errors, failing to identify voxels with actual arousal). Along these lines, it can be deduced that the absence of a gold standard method for the multiple comparisons problem has been a genuine problem.

Fourth, it is usual in univariate analysis to investigate indicators of task differences (using ANOVA or t- test), while indicators for likeness are mostly depreciated which implies that in a run of a typical univariate voxelwise technique (e.g. SPM), subtraction paradigm has been used to a great extent to investigate differences between tasks instead of looking at both

differences and similarities.

Given the previously mentioned methodological caveats of univariate analyses, a basic inquiry is whether there is a complementary statistical framework that can mitigate the shortcomings. Multivariate analysis is presented as a potential complementary approach to the univariate analysis in the next section.

1.5 Multivariate Analysis of fMRI

The univariate analysis was introduced in previous section as the most well known way to deal with the investigation of fMRI data. Despite the fact that this technique has represented the real piece of the development of fMRI over the previous decade, it may not be an appropriate framework in connection with various possibly vital research objectives. For example, univariate analysis is not a good choice to seek for systematically intrinsic variations in the fMRI data due to the absence of a model. Such exploratory queries in regard to the fMRI data can be addressed by multivariate approaches which are data driven techniques. These methodologies parse the 4D fMRI time-series into a set of components (i.e. common features), that comprise of a bunch of voxels and their temporal profile. Each component is either task-related or task-unrelated (e.g. noise, movement artifacts) and accounts for certain amounts of variation in fMRI data.

Although multivariate techniques are not subjected to the inherent problems of hypothesis driven univariate framework viz., avoiding functional integration, imprecise models and variability in HRF but they do suffer with interpretative challenges. It is highly dependent on algorithms used to decompose the fMRI time series and the selection criteria for meaningful component. Independent component analysis is one such multivariate approach which is a clan of blind sourse separation (BSS) and is totally model free. Partial least square (PLS) is another example of multivariate analysis which slightly depend on the experimental paradigm to shape a component. Principle component analysis is also a model free multivariate approach.

Next, principal component analysis (PCA) and independent component analysis (ICA) are introduced briefly as two examples of completely model-free multivariate approaches.

1.5.1 Principle Component Analysis (PCA)

This is a statistical tool usually applied for dimension reduction of a big data, it rationally chops the data relatively in a simple manner while keeping the dimensions with most variances. The components are sorted from highest to lowest variance. Based on the requirement the variance window is set and obviously this window starts from the highest variance. As each component is estimated from the remaining portion of the variance that was not captured by the former component(s), the components are orthogonal to each other. Every component hold an eigenimage portraying spatial patterns of activation across voxels. Eigenvector contains the temporal profile of eigenimage and the associated eigenvalue gives the amount of variance of it thus the component with highest eigenvalue has the most variance of the data.

Although there is no thumb rule mentioning how many components should be held, but there are some usual practices and one such option is to retain all those components having eigenvalue at least one [22]. Another way is to apply elbow criteria in which number of components are estimated using the plot of eigenvalues. Given that each subsequent component represents a lessening of variance in the data in relation to the former component, the plot resembles a decreasing exponential function. The number of components to be retained can be estimated from the point where the curve begins to flatten out.

Friston and colleagues [23] first introduced an application of PCA to a verbal fluency task based PET study. They recruited two components that accounted for the most variance in data, and those components were claimed as the network of interest responsible for verbal fluency and attentional bias, respectively. Recently, Ecker and colleagues [24] have supplemented their univariate findings in visual cortex with PCA to explore the functional connectivity within those regions identified by the univariate approach. Moreover, PCA has been utilized to distinguish an average pattern of response in regions of interest [25–27] and for noise reduction in fMRI time series [28].

Despite the fact that PCA is by all account a valuable method to recognize the partitioned nature of a brain function, this possesses few pitfalls. Foremost it is a variance based disintegration technique and proposes to keep those components who contribute the most variation of the data and thereby it may produce imprecise results if the change in signal of interest account for a little piece of total variance. Moreover, the identified components are sometime

hard to interpret. Additionally, no thumb rule exist to examine the statistical significance of the decomposed components.

1.5.2 Independent Component Analysis (ICA)

The signal to noise ratio of fMRI signals are by default very poor as a consequence a big share of the total variance of the data are of non-task related components viz., physiological noises, head motion and machine artifacts. Along these lines, variance based examinations such as PCA might prompt one sided identification of components of interest which implies that the initial few decomposed components might be all noisy thus the subsequent components get affected by the previous noisy components due to the orthogonality condition of PCA. A contemporary data driven approach known as ICA was introduced few years back to the inception of fMRI and it is free from the noted pitfalls of PCA because it decomposes the data using a more robust criteria i.e. statistical independence. Orthogonality among the decomposed components is an essential criteria in PCA whereas ICA bank upon a higher order statistics i.e. independence (two orthogonal components are linearly independent but the reverse is not necessarily true). Pictorial Illustration of ICA for fMRI data analysis is given in Fig. 1.3

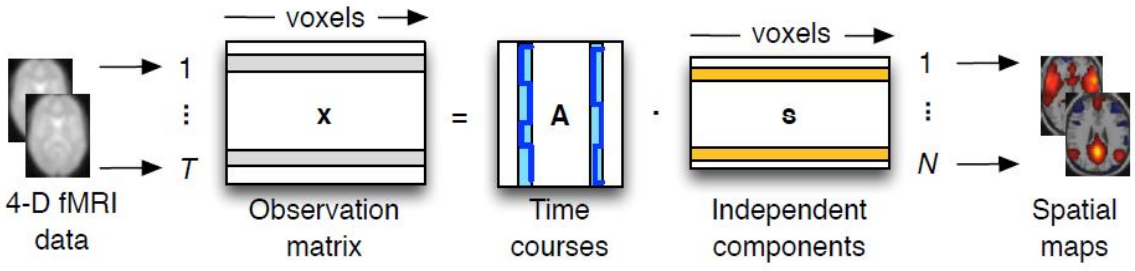

Fig. 1.3: Illustration of ICA for fMRI data analysis Figure courtesy of (http://users.ics.aalto.fi/whyj/publications/thesis/thesis_node8.html)

The components decomposed by ICA would be independent in either dimension (i.e. space or time) and the comparison between their superiority is under constant debate as far back as the first occasion that fMRI data was dealt with ICA [29], there has been a debate regarding the choice of spatial or temporal ICA. Despite the fact that spatial ICA has over-

whelmed the functional imaging literature, probably because of higher spatial than temporal dimensions, in this way being more affordable computationally, tICA has also been applied to fMRI studies. It is a genuine expectation to get the same results by applying any of the two protocols of ICA in the case of uncorrelatedness among the components but if there are correlations among them either spatially or temporally this choice matters a lot [30].

The framework of ICA looks unfit for group based studies and it is due to the fact that the time courses for all the volunteers might not be the same, thus does not seem to be naturally suitable for drawing group level inferences. This is because different individuals may have different time courses, and these time courses might be sorted differently. Despite this fact there are many group-level ICA investigations [30–32]. In the majority of those studies group data was concatenated first either spatially or temporally and then ICA was directly applied on that concatenated data. In connection with it, creation of subject specific maps were drawn and were used to infer group differences [a more rigorous description can be found in [32]].

Particularly for group-based fMRI investigations, ICA has been the most preferred multivariate framework [30–37] and its data driven nature can be understood very nicely in [35] which is a study conducted by Calhoun and colleagues. A complex experimental design was constructed in that investigation which had three blocks of fixation, acting simulated driving and watching simulated driving. From the decopmosed components they recruited six who were representing the dynamics with regard to the simulated drive. Without an a priori model it is not feasible to parameterize these naturalistic task with univariate analysis. Along with such unimodel problem the ICA is also capable to deal with multimodel queries such as to find out whether one modality (e.g. sMRI, DTI) is governing the change in the other (e.g. fMRI). One such question was addressed by Calhoun and colleagues for an oddball detection task and the objective was to find whether the differences in gray matter volume between the schizophrenia and typically developing population has to do anything with their functional capabilities. A direct correlation between the gray matter volume and the cognitive abilities was found in that investigation.

To map the decomposed component with the underlying physical phenomenon is a big challenge because irrespective of the experimental paradigm it simply extract the components. This issue can be resolved simply by including any relevant hypothesis driven statistics

i.e. ICA can be followed by a multiple regression to look for task-related components. Despite the aforementioned limitation, ICA, and most of the multivariate approaches, provide valuable insights into fMRI data.

1.6 Task based fMRI and Resting state fMRI

A conventional but potential protocol with the fMRI modality is the task-based protocol which has been utilized to map the brain regions associated to the execution of a particular task [38, 39]. However in comparison with the direct cortical stimulus (DCS), the specificity and sensitivity of task-based fMRI is modest [40].

A relatively newer counter protocol is the resting-state fMRI (RsfMRI) which is named so due to the fact that while scanning the functional images the volunteers do not perform any task. The RsfMRI scans manifest BOLD signal fluctuations in the lower range of frequency (<0.1 Hz) [41–43]. Many resting-state networks also known as intrinsic networks has been extracted from the RsfMRI data viz., default mode networks, somatosensory, cognitive control [31]. Decomposed components with similar time profile are bunched together and are considered as intrinsic networks [44, 45]. Preliminary results show that resting-state fMRI can also identify the language network [46–48].

The RsfMRI convention has many benefits over the traditional task-based protocol. Although the ratio of BOLD signals for two conditions is relatively tiny in this contemporary protocol but the SNR is almost three times to that achieved with the conventional method [43]. No task is the another crucial benefit of RsfMRI convention and it is logical to expect better execution of a task from healthy controls but not justified with the population suffering from some neurological disorder [49–51]. Measurement using RsfMRI protocols usually do not contain activity confounds because in the absence of the task, probability of occurrence of any auxiliary activity is relatively lower (in a language based experimental paradigm visual activity is often complementary) [43]. On the top of these mentioned superiorities the RsfMRI protocol is faster too as well as the data collected in such manner is fit for functional segregation [52], thus fitting better in to the usually limited patient scanning schedule.

1.7 Functional Connectivity

A large portion of the recent fMRI studies are framed to explore the brain activity pattern responsible for the phenomena of interest. These patterns are often termed as the neural basis. These studies are sought to test the functional integration hypothesis. In such studies any kind of interrelationships are evaluated among those voxels who are significantly related to the experimental task. It can be achieved by measuring the similarity/dissimilarity between their time courses. Though it does not provide any information about the relations or dependencies among the brain regions that those voxels delineate.

Because fMRI data are collected over time and have a temporal structure, several methods utilize the information about the coherence of activity over time to identify functional connectivity, which represents the pattern of functional relations among brain regions, independent of a particular task-induced activation. This class of methods includes cross-correlation [53], partial least squares [20], and data driven methods such as flat [54] and hierarchical clustering [55], principal component analysis [19], multidimensional scaling [19], and independent component analysis [29].

1.7.1 Brain Connectivity

There are two complementary theories with regard to the organization of human brain, consequently two distinctive approaches to explain it's functions [56]. Functional segregation is the first approach where brain functions are mapped to specific brain areas. The principle of modularity is the sole of segregation approach. It professes that the brain can be split into bunches of innate neurons having particular functionalities. Although this modularity approach is an eminent concept but it is not able to clarify the functions of brain to the full extent. Functional integration approach is the other concept with the notion that brain regions either adjacent or distant interact with each other to execute a function. Nowadays this distributed information processing concept is on the anvil and it is called functional connectivity (FC). By this newer approach researchers are trying to decode " transferred and transformed effects within the segregated regions " [56].

Brain connectivity term covers several facets of the brain configuration viz., functional connectivity, structural and effective connectivity (Fig. 1.4) [57, 58]. Structural connectivity

basically deals with the architectural studies of the brain and several time structural atrophies are declared to be responsible for the aberrant manifestations of subjects affected by neurological disorders. Another perspective to probe the brain organization is to look for the FC among the brain regions. In this functional category of brain connectivity the simultaneous activation or deactivation of various brain regions are explored irrespective of any anatomical connection between those regions and it can be measured using either spectral coherence [20] or covariance [19]. Both the categories explained above do not take into the account the causal effects between the events. Effective Connectivity is the third category of brain connectivity which does explores this causality and it is often considered as the intersection of the other two connectivity approaches. Effective connectivity requires some model a priori which involve anatomical parameters and connections of interest [59].

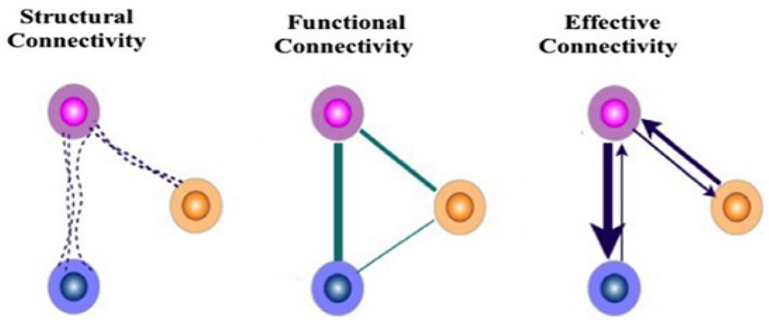

Fig. 1.4: The fiber pathway structural connectivity, the functional connectivity (correlations), and effective connectivity (information flow) between brain regions. Figure courtesy of (Daniele Poli and colleagues, 2015)

1.8 Literature Survey

In order to understand the etiology of the ASD, author surveyed the fMRI modality based literature and particularly those which follows resting-state protocol as it is well suited to scan the population with limited ability. The very first research article on resting-state functional connectivity analysis goes in the credit of Cherkassky and group which got published in the year 2006. The author have tabularised the literature survey in table 1.1 for the purpose of better understanding. It contains the author's name and year of publishing of the article followed by the seed region taken into account along with findings of their FC.

Table 1.1: Research articles furnishing macroscopic justification of manifestations of ASD. Author's name, seed regions and the corresponding FC results are embodied in this table.

Cherkassky etal. (2006) [60]

Numerous	General underconnectivity
Anterior cingulate cortex	Reduced connectivity to posterior cingulate cortex
L parahippocampal gyrus	Reduced connectivity with multiple ROIs

Kennedy &Courchesne (2008) [61]

-	Connectivity within the task negative network comprising of dorsal and ventromedial prefrontal cortex, posterior cingulate cortex/precuneus, left and right angular gyrus, right temporal pole, and right superior temporal gyrus/superior temporal sulcus

Monk et al.(2009) [62]

Posterior cingulate cortex	Reduced connectivity to right superior frontal gyrus
Posterior cingulate cortex	Increased connectivity to right temporal lobe and right-parahippocampal gyrus

Weng et al. (2010) [63]

Posterior cingulate cortex	Reduced connectivity to most of the default mode network nodes

Olivito et al. (2016) [64]

Dentate nucleus (DN)	underconnectivity between the left cerebellar DN and cerebral regions

Paakki et al.(2010) [65]

-	Reduced regional activity coherence in right superior temporalsulcus, right inferior frontal and middle frontal gyrus, bilateral cerebellar crus I, right insula, and right postcentral gyrus

-	Increased regional activity coherence in right thalamus, left inferiorfrontal gyrus, left inferior, medial, and superioroccipital gyri and fusiform gyrus with optic radiation, left middle cingulate cortex with corpus callosum, right middle temporal gyrus

Assaf et al.(2010) [66]

-	Reduced connectivity strength in precuneus
-	Reduced connectivity strength in medial prefrontal cortex/anteriorcingulate

Dinstein et al. (2011) [67]

Superior temporal gyrus and Inferior frontal gyrus	Reduced strength and spread of inter-hemispheric correlations

Di Martino et al.(2011) [68]

-	Increased connectivity in striatal-cortical circuitry, including the right superior temporal gyrus and insular cortex
-	Striatal functional hyperconnectivity with the pons
-	Broad patterns of hyperconnectivity of brainstem area, with bilateral insular cortices

Anderson et al.(2011) [69]

-	Reduced interhemispheric functional connectivity between homologous gray matter voxels (sensorimotor cortex, frontal insular cortex, and superior parietal lobule extending from the parieto-occipital junction to the intraparietal sulcus)

Ebisch et al.(2011) [70]

R anterior insular cortex	Lost connectivity to amygdala and thalamus
R anterior insular cortex	Lost connectivity to dorsal postcentral gyrus
R posterior insular cortex	Lost connectivity to dorsal postcentral gyrus

L anterior insular cortex	Lost connectivity to orbitofrontal cortex and posterior insularcortex
R anterior insular cortex	Reduced connectivity to right dorsal anterior cingulate cortex
R anterior insular cortex	Reduced connectivity to amygdala
R anterior insular cortex	No significant difference in connectivity to dorsal anterior cingulate cortex

Wiggins et al. (2011) [71]

R superior frontal gyrus	Reduced connectivity to posterior superior frontal gyrus

Gotts et al.(2012) [72]

-	Lower connectedness to other ROIs for social brain network regions such as ventromedial prefrontal cortex, left amygdala, left hippocampus, bilateral ventromedial anterior temporal lobes, left temporoparietal junction, bilateral postcentral gyrus, right lateral occipital cortex
-	Lower connectedness to other ROIs for right anterior middle temporal gyrus/superior temporal gyrus, left inferior and right posterior temporal gyrus, and left cerebellum
Posterior parahippocampal gyrus	No change in connectivity to the rest of the brain

Rudie et al.(2012) [73]

-	Reduced overall default mode network connectivity
Posterior cingulate cortex	Reduced connectivity to medial prefrontal cortex in combined genotyped groups
Posterior cingulate cortex	Reduced connectivity to medial prefrontal cortex in the MET- homozygous (risk) group, irrespective of ASD
Posterior cingulate cortex	Reduced connectivity to medial prefrontal cortex within ASDgroup (MET-homozygous < MET-heteromozygous < nonrisk)

Posterior cingulate cortex	Reduced connectivity to medial prefrontal cortex (MET CC ASD < MET CC typically developing, and MET CG ASD< MET CG typically developing)

von dem Hagenet al. (2013) [74]

-	Reduced correlation between the salience network and the medial temporal lobe network
Medial prefrontal cortex	Reduced connectivity to temporoparietal junction/posteriorsuperior temporal sulcus
Amygdala	Reduced connectivity to left anterior insular cortex

Lynch et al.(2013) [75]

Posterior cingulate cortex	Increased connectivity to inferior frontal and middle frontal gyrus, dorsal medial prefrontal cortex, posterior insular cortex, lingual gyrus, posterior parahippocampal gyrus, temporal pole, posterior superior temporal sulcus, and anterior supramarginal gyrus
Retrosplenial cortex	Reduced connectivity to cuneus, caudate, and dorsal and medial thalamic nuclei
Precuneus	Reduced connectivity within default mode network nodes and other functional networks

Washington et al. (2013) [76]

Various regions	Reduced connectivity within default mode network nodes and other functional networks
Dorsal anterior cingulatecortex/Medial prefrontalcortex	Reduced connectivity to ventral anterior cingulate cortex and medial prefrontal cortex

Tyszka et al.(2014) [77]

-	No significant between group differences for networks identified by independent component analysis
-	No significant between group differences for ROI-based analysis

-	Residual effect of subject motion was larger than the effect of diagnosis

Uddin et al.(2013) [78]

Anterior cingulate cortex	Increased connectivity to superior frontal gyrus, thalamus, and bilateral insular cortex
Precuneus	Increased connectivity to posterior cingulate cortex and left angular gyrus
Superior temporal gyrus	Increased connectivity to middle temporal gyrus
Postcentral gyrus	Increased connectivity to precentral gyrus, left posterior insular cortex, and thalamus
L lateral occipital cortex	Increased connectivity to intracalcarine cortex, and occipital pole

Redcay et al.(2013) [79]

Medial prefrontal cortex	Increased local connectivity within ROI
Anterior medial prefrontal cortex	Increased long distance connectivity to right lateral parietal region
R lateral parietal region	Reduced connectivity to cerebellar tonsils

Neilsen et al. (2013) [80]

-	Classification accuracy analysis; No connectivity changes reported/studied

Maximo et al.(2013) [81]

-	Increased local connectivity in right middle frontal gyrus, bilateral striate and extrastriate cortices, parahippocampal gyrus, middle temporal gyrus, and supramarginal gyri
-	Reduced local connectivity in left superior frontal gyrus andbilateral middle cingulate cortex/posterior cingulate cortex,right paracentral cortex, left perisylvian and frontopolar regions (anterior prefrontal cortex), left insular cortex, bilateral precuneus

Starck et al.(2013) [82]

-	No significant between group differences for local connectivity
Medial prefrontal cortex	Reduced connectivity to posterior subnetworks of default mode network, dorsal (the central-posterior precuneus andthe posterior cingulate cortex) subnetworks of default modenetwork, and to ventral (retrosplenial cortex) subnetworks of default mode network

DiMartino et al. (2013) [83]

Precuneus	Decreased DC (i.e., number of direct connections to precuneus) Increased DC for bilateral limbic areas including the superficial and latero-basal amygdala, the adjacent parahippocampus (posterior parahippocampal gyrus and fusiformgyrus), planum temporale, and temporal cortex

DiMartino et al.(2013) [84]

-	Corticocortical intrinsic functional connectivity across all functional domains with paralimbic and unimodal association regions having the highest proportions of affected connections
-	Intrinsic functional connectivity for subcortical regions, particularly between subcortical (thalamus and globus pallidus) and primary parietal sensorimotor regions
L posterior insular cortex	Reduced VMHC, ReHo and DC in cluster extending from the left posterior insula to the central and parietal operculum
R superior frontal cortex	Increased fALFF, ReHo and DC in cluster located in right dorsal superior frontal cortex

-	Reduced in at least 2 of ReHo, VMHC, fALFF, or DC in clusters in thalamus, posterior cingulate, bilateral middle-insula, and left middle occipital gyrus

Abrams et al.(2013) [85]

Posterior superior temporal sulcus	Reduced connectivity to components of reward pathways such as bilateral ventral tegmental area, nucleus accumbens and putamen of the basal ganglia, ventromedial prefrontal cortex,as well as the left caudate, anterior insular cortex, and orbitofrontal cortex

Mueller et al.(2013) [86]

-	Lower connectivity for dorsal attention network to a cluster including the right precentral gyrus, which reached into theright parietal lobe, and right parietal and precuneal cortex
Superior temporal gyrus	Reduced connectivity to default mode network
Medial prefrontal cortex	Reduced connectivity to left anterior cingulate cortex

Cardinale et al. (2013) [87]

-	Significant rightward asymmetry in ASD for all components

You et al.(2013) [88]

-	Increased modularity of network
-	No between group difference in global efficiency of networks

Alaerts et al.(2013) [89]

Posterior superior temporal sulcus	Reduced connectivity with inferior parietal lobule, precentral gyrus, supramarginal gyrus, inferior frontal gyrus (pars triangularis)
Posterior superior temporal sulcus	Increased connectivity with lingual gyrus, calcarine gyrus, fusiform gyrus

Posterior superior temporal sulcus	Reduced connectivity with right inferior parietal lobule, left premotor area, fusiform gyrus and bilateral superior occipital gyrus
Posterior superior temporal sulcus	Increased connectivity with left thalamus and right inferior frontal gyrus

Verly et al.(2014) [90]

Arcuate fasciculus	No between group difference for connectivities observed for bilateral arcuate fasciculus seed
L Broca's area (part ofinferior frontal gyrus)	Reduced connectivity to bilateral Wernicke's area (superior temporal gyrus) in ASD group with only unilateral arcuate fasciculus
-	Reduced interhemispeheric connectivity (besides arcuate fasciculus)

Nair et al.(2013) [91]

-	Several clusters of underconnectivity in ASD, especially for right prefrontal cortex, right parietal-occipital, and bilateral motor and bilateral somatosensory seeds
R thalamus	Increased connectivity to temporal seed
Thalamus	Reduced connectivity to prefrontal, parietal-occipital, and somatosensory cortical seeds

Keown et al.(2013) [92]

-	Increased local connectivity in temporo-occipital regions (including inferior temporal gyrus and middle temporal gyrus, temporal pole, middle and superior occipital gyri, calcarine cortex, right parahippocampal gyrus, right fusiform gyrus, and left cuneus) and right middle frontal and superior frontal gyrus
Middle cingulate	Small clusters of local underconnectivity
R inferior parietal sites	Small clusters of local underconnectivity

L lateral and bilateral polar and medial frontal cortices Posterior brain regions	Low-severity ASD subgroup < typically developing Higher-severity ASD subgroup > typically developing (predominantly)

Alaerts et al. (2015) [93]

pSTS	underconnectivity between the left pSTS and typical dopaminergic areas

Doyle-Thomas et al. (2015) [94]

mPFC, ACC and MTG	Both over and underconnectivity based on region.

1.9 Research Objectives

Generalizing the FNC patterns based on either narrow age group or selected seed regions are the major research gaps found by the author. Additionally, dynamic counterpart of FNC analysis is not much explored for the ASD and auto recognition and the naming of the RSN is over the anvil but yet to establish. Based on these research gaps author have framed following objectives.

1. **Finding the best suitable ICA algorithm for the parceling of fMRI images:** Accuracy of the FNC maps definitely depends on all the steps that constitute the baseline of FNC analysis. In ICA based FNC studies the very first step is to decompose the fMRI data where INFOMAX and FastICA have been applied preferably to do so. The first objective is to conduct a comparative study of the ICA algorithm when the input to decompose is a fMRI image.

2. **Accurate and automatic labeling of RSN:** Identifying which component is a resting state network (RSN) and which component is not, is the second step of ICA based FNC examinations and it is preceded by the marking of RSN. The traditional method is cumbersome and indeed the automation is needed. A very usual way is to carry a spatial correlation between existing 2D templates of various RSN and the one which has been already identified as an RSN but not labeled yet. It will get the name of that RSN with whose template it gets the highest spatial correlation score. Accuracy check

of this procedure and establishment/confirmation of standard templates is the second objective.

3. **The FNC analysis of ASD population for the different developmental stages:** As it is mentioned above that the inclusion of a narrow range of participant's age could be the possible reason behind the discrepancies in the connectivity data of ASD, conducting an FNC study for three different groups i.e. children, adolescents and adults, is the last objective.

1.10 Organization of the thesis

The thesis contains six chapters, out of that, the first chapter deals with the introduction, literature review and research objectives of the present study. The remaining part of the thesis is structured as follows:

Chapter 2 presents the brief theoretical background of the state-of-the-art independent component analysis techniques used for the decomposition of fMRI images. Further, the effectiveness of the ICA techniques are evaluated in terms of the parcellation of fMRI images done by them.

Chapter 3 raises the issue of the current use of two dimensional RSN templates for the labeling of intrinsic connectivity networks and also presents the networks labeled wrongly by conventional 2D spatial correlation. Alternative three dimensional templates are proposed in this chapter.

Chapter 4 presents the conventional state-of-the-art static functional network connectivity (sFNC) analysis. Further, the sFNC maps derived for ASD and typically developing population are analyzed interpreted to highlight the connectivity differences between the two population.

Chapter 5 presents the contemporary state-of-the-art dynamic functional network connectivity (dFNC) analysis. Further, the dFNC states derived for ASD and typically developing population are analyzed interpreted to highlight the connectivity differences between the two population.

Chapter 6 presents the aggregate conclusion of the present work and covers the scope for future research in the field.

CHAPTER 2

COMPARISON OF SEPARATION PERFORMANCE OF ICA ALGORITHMS FOR FMRI IMAGES

There are numbers of independent component analysis algorithms available, but only a few of them have been used frequently so far for fMRI images. With a view that algorithms that are overlooked may outperform the commonly used algorithms, a comparative study is taken up in this chapter to analyze their abilities for the purpose of synthesis of fMRI images. In this chapter, ten independent component algorithms: Fast ICA, INFOMAX, SIMBEC, JADE, ERICA, EVD, RADICAL, ICA-EBM, ERBM, and COMBI are compared. Their separation abilities are adjudged on both, synthetic and real fMRI images. Performance to decompose synthetic fMRI images is being monitored on the basis of spatial correlation coefficients, time elapsed to extract independent components and the visual appearance of independent components. Ranking of their performances on task-based real fMRI images are based on the closeness of time courses of identified independent components with model time course and the closeness of spatial maps of components with spatial templates. Their competencies for resting state fMRI data are analyzed by examining how distinctly they decompose the data into the most consistent resting state networks. Sum of mutual information between all the combinations of decomposed components of resting state fMRI data are also calculated.

2.1 Background and Motivation

Independent component analysis is one of the most versatile exploratory methods which has been frequently used for functional magnetic resonance imaging data analysis. The utility of ICA in the fMRI studies spans over unmixing the underlying signal sources from physiological artifacts, assessment of activations with unknown stimulus type, multivariate pattern analysis and resting state functional connectivity [95]. The ICA is preferable over PCA, another data-driven technique because it uses more robust criterion for the task of blind source separation which is independence. However, the use of independence as a source separation norm for fMRI data is highly criticized and some other mathematical characteristic is suggested by Daubechies et al. [96].

Many ICA algorithms have been designed and applied fruitfully to analyze fMRI data. They are either deterministic or iterative type. Their reliability checkup [97] in terms of the consistency to produce the same independent components (ICs) and even comparison of their performances [98,99] have been done by many researchers, but they compared few algorithms. Although there are many algorithms, it is expected to pick up the one which is more promising for fMRI data. In the above perspective, the present chapter aims at performing an exhaustive study to evaluate the performances of various available ICA algorithms.

The fMRI can be used for studying both, functional segregation and functional integration of the brain [100]. Biswal et al. (1995) observed that regions that are co-activated during a task are also temporally correlated at rest [101, 102]. This temporal correlation among the anatomically separated brain regions reflects a level of ongoing functional connectivity among brain regions during rest [103, 104]. The fluctuations in the blood oxygenation level-dependent signal during rest reflects the neuronal baseline activity (intrinsic activity) of the brain . Resting state fMRI (RsfMRI) is a method to study this intrinsic activity.

In the last two decades, several RsfMRI studies have been done, looking for the functionally relevant resting state networks. Although, these studies incorporate a different group of subjects, methods and types of magnetic resonance (MR) acquisition protocols, they are highly similar in their results supporting the robustness of RSN [105, 106]. Approximately, eight RSN have been reported such as visual network, the motor network, two lateralized networks consisting of superior frontal and superior parietal regions and the so-called default mode network (DMN) [106–108]. The DMN is reported in positron emission tomography [109] and fMRI [103, 110] study. It has been suggested that the activity and connectivity of the DMN are involved in the integration of emotional and cognitive processing and monitoring the world around us [106].

To grade the performance of ICA algorithms phantom / synthetic images and real fMRI images are utilized in this work. Three sets of simulated fMRI like components with different contrast to noise ratios (CNR) are created using SimTB toolbox [111]. This toolbox was developed in Medical Image Analysis Laboratory (MIALAB). Multi-site real fMRI data are exploited here in this work.

2.2 Materials and Methods

2.2.1 Phantom Image

To quantify the performances of ICA algorithms there is a need to generate fMRI like synthetic images. A good understanding of the possible sources of BOLD fMRI images would help to create phantom images. Sources whose reflection are the BOLD fMRI image may be grouped into signals of concern and signals, not of concern [112]. The signals of concern are task-related, transiently task-related and function-related whereas physiology-related, scanner-related and motion-related are the signals who are not of concern [112, 113]. The signal of concern are typically focal but the artifactual signals are more varied and thus, their distributions are supergaussian and subgaussian, respectively [99]. Synthetic data are simulated with SimTB, a MATLAB based toolbox, which is available freely for download (http://mialab.mrn.org/software). The data generation model exploited in SimTB is invariable to the assumption of spatiotemporal separability which says that data is basically the product of timecourses (TCs) and spatial maps (SMs). There is a flexibility to choose the number of subjects, components, voxel size and CNR in SimTB. The data is simulated for single subjects with four components of interests. Simulated images are of 148×148 voxels, TCs are 260 time points longer and the repetition time (TR) is kept 2 seconds. Three sets of synthetic images with varying CNR (0.5, 1, 2) are simulated. Total 30 components which altogether cover sinuses (component 6), white matter (components 16 and 17), cerebrospinal fluid (components 14 and 15) and gray matter (rest components) are shown in Fig. 2.1 The components of interest are shown in Fig. 2.2 Synthetic Images are made noisy by adding Rician noise relative to a specified CNR [114]. The CNR is expressed as $\hat{\sigma_s}/\hat{\sigma_n}$ where $\hat{\sigma_s}$ is the temporal standard deviation of true signal and $\hat{\sigma_n}$ is the temporal standard deviation of the noise.

2.2.2 fMRI Images

Medical Image Analysis Lab has made available Group ICA of fMRI toolbox (GIFT) along with one example dataset. This dataset contains brain scans of three subjects generated against visuomotor paradigm. More details can be had from [115]. The visual stimuli are made up of presenting an 8 Hz reversing checkerboard pattern to the right and left visual

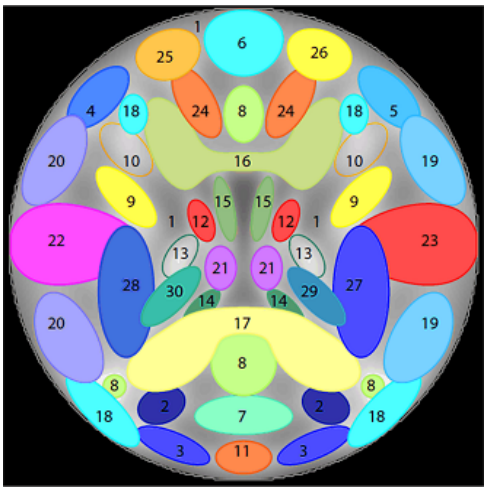

Fig. 2.1: A template of the 30 default spatial maps (SMs), which are modelled like the components usually seen in axial slices of real fMRI data. They are labelled 1 to 30 and can be selected manually by the SimTb user to make the synthetic images. Overall they represents all the four tissue types viz., SM6 sinus signal dropout, SM14,15 cerebrospinal fluid, SM16,17 white matter and rest gray matter.

hemi-field sequentially. First, present the stimuli to right visual hemi-field for a duration of 15 seconds followed by an asterisk fixation of 5 seconds. Further, the stimuli are presented to left visual hemi-field for 15 seconds but the asterisk fixation is now 20 seconds longer. This set of events of 55 seconds duration is repeated four times. Volunteers had to touch their left thumb to all of their fingers sequentially back and forth at a self-paced rate when the stimuli are presented to left hemi-field and had to do the same with right thumb in another case.

The RsfMRI data used in the present work can be found at the autism brain imaging data exchange (ABIDE I) website: http://fcon1000.projects.nitrc.org/indi/abide/abideI.html along with complete phenotypic and scanning information. The ABIDE is a part of International Neuroimaging Data-Sharing Initiative (INDI) and 1000 Functional Connectomes Project (FCP: http://fcon 1000.projects.nitrc.org/fcpClassic/FcpTable.html). The INDI (INDI: http://fcon 1000.projects.nitrc.org/indi/pro/nki.html) is a collaboration of 16 international sites [84]. The Preprocessed Connectomes Project (PCP) allows open sharing of preprocessed ABIDEI data. The data of 14 individuals suffering from autistic spectrum disorder (ASD) and of 13 neurotypical individuals, collected at Carnegie Mellon University and preprocessed using

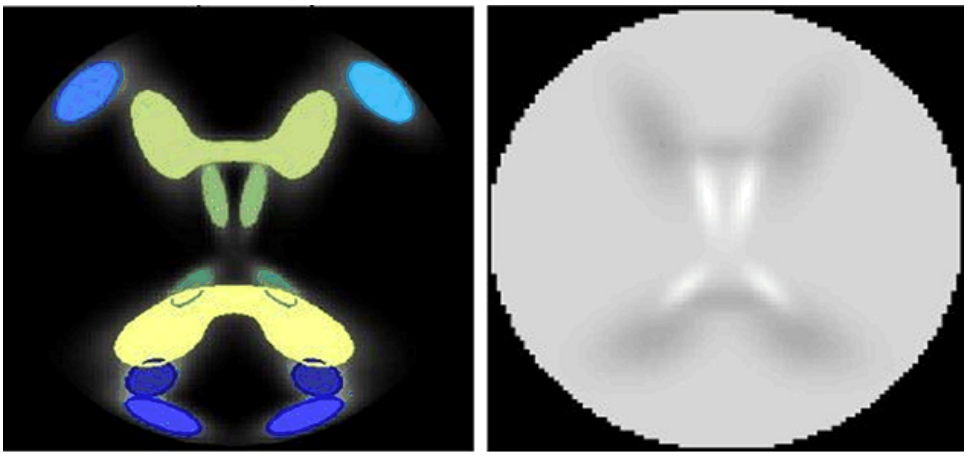

(a) (b)

Fig. 2.2: Selected default spatial maps to make the synthetic images (b) the baseline map obtained by assigning intensity levels (w) to spatial maps viz.,$w_6 = 0.3, w_{14,15} = 1.5, w_{16,17} = 07$ and $w_{rest} = 1$.

Connectome Computation System (CCS) protocol under PCP project, are opted here for a comparison of segregation performance of ICA Algorithms. The preprocessing in the CCS pipeline begins with leaving first four volumes followed by slice timing correction, motion realignment and intensity normalization. This strategy includes band-pass filtering in the frequency band of 0.01 - 0.1 Hz and global signal regression.

2.2.3 BSS Algorithms considered

Blind source separation (BSS) is basically an explorative tool established for the analysis of images and sound. They extract sources from mixtures where mixing coefficients are not known, hence called blind methods. The ICA is a clan of methods for BSS formed on some statistical independence of the source signals. Here in this paper, the focus is on the spatial ICA model [112].

Assume the ICA model as $X = AS$, Where A is the mixing matrix of $M - by - N$ dimension whose columns represent the time courses of respective sources. $S = [s_1.....s_N]^T$ is a $N - by - V$ source matrix, where N is the number of sources, V is the number of voxels and s_i is the i^th source. The ICA determines the decomposing matrix W such that the burried sources are extracted as $\hat{S} = WX$ with the assumption of statistical independence of spatial components.

A brief overview of the adopted ICA algorithms is given below. At a whole the adopted algorithms incorporate all the major approaches for measuring the independence.

2.2.3.1 INFOMAX

[116] This is one of the most frequently used ICA algorithms. Infomax uses mutual information for independence measurement. It favors partition of super-Gaussian sources. Since fMRI images contain subgaussian signals (physiological noises) also, Extended Infomax should be used instead of infomax.

2.2.3.2 FastICA

[117] This has been one of the obvious choices for fMRI applications. The negentropy (higher order statistics approach) is the measurement of independence here because as negentropy increases non-Gaussianity also increases. Four nonlinearities tanh, pow3, skew, and gauss are the contrast function of Fast ICA. If the convergence problem persists stabilized version of the algorithm is advisable.

2.2.3.3 JADE

[118] Joint approximate diagonalization of eigenmatrices exploits fourth order cumulant to separate the constituents of the mixture. It performs joint approximate diagonalization by Jacobi technique on the fourth order cumulant.

2.2.3.4 SIMBEC

[119] Simultaneous blind extraction using cumulants is basically a deterministic algorithm which makes use of natural gradient ascent in a stiefel manifold thereby extracting sources with higher order cumulant as contrast function.

2.2.3.5 ERICA

[120] Equivalent robust ICA uses information theoretic approach for independence measurement. It uses entropy as a cost function instead of a nonlinearity. The ERICA uses quasi - Newton iteration to converge at a saddle point of the cumulant based differential entropy cost function.

2.2.3.6 EVD

[121] Eigenvalue decomposition separates sources by deploying both second-order statistics and higher order correlation functions. It creates and sums a set of shifted cross variance matrices, subsequently applies singular-value decomposition to achieve source separation. This is fast and useful when the spectra of the components are different.

2.2.3.7 COMBI

[122] Algorithm COMBI offers a novel scheme for combining weights-adjusted second-order blind identification (WASOBI) and efficient FastICA (EFICA), making use of the strengths of both techniques. Realistic mixtures usually present both diverse time-structure and non-Gaussianity and since WASOBI and EFICA are severely suboptimal for such mixtures, it is better to use the combination of these two.

2.2.3.8 RADICAL

[123] RADICAL is an acronym for Robust, Accurate, Direct Independent Components Analysis algorithm. This non-parametric method is based on spacing estimators of entropy, which is computationally efficient, simple, and insensitive to outliers.

2.2.3.9 ICA-EBM

[124] The ICA by entropy bound minimization furnishes flexible density matching using four measuring functions who are based on the maximum entropy principle. With multiple measuring functions, it is possible to model super- and sub-Gaussian densities. The performance of this method can be improved by adding some more measuring functions.

2.2.3.10 ICA-ERBM

[125] The ICA by entropy rate bound minimization utilizes both non-Gaussianity and sample correlation by minimizing mutual information rate. It assumes that the sources are outputs of linear systems and those systems are driven by independently and identically distributed (i.i.d.) noise, thereby converting the entropy rate estimation to an entropy estimation problem solved using EBM.

2.3 Software and Hardware details

The whole simulation work was based on an in-house MATLAB implementation (MATLAB 2012) that exploits the code available with the group ICA of fMRI toolbox (GIFT) [126] toolbox for image processing. The PC used to run the simulations was an INtel(R) Core(TM) i3-4010 U CPU @ 1.70 GHz equipped with 4GB of RAM and running a Windows 8 32-bit OS. The GIFT is a MATLAB based toolboxes that implement a number of efficient algorithms for BSS and it furnishes execution time information along with the decomposed components of fMRI data. In GIFT, there is a provision to sort the ICs temporally and spatially thereby comparing the model's time course and spatial templates with component's time course and spatial map.

2.4 Results of ICA Comparisions

All the ten ICA algorithms described above were applied to the three sets of synthetic images and the resultant decomposed components are shown in Figs 2.3, 2.4, 2.5. The spatial correlations among the decomposed components and the templates are arranged in table 2.1.

Table 2.1: Spatial correlation between decomposed components of interest of synthetic images and spatial templates.

Algorithm	**COMP 1**	**COMP 2**	**COMP 3**	**COMP 4**	**Required Time (seconds)**
CNR = 0.5					
FastICA	0.9873	0.9912	0.9951	0.9957	16.2787
INFOMAX	0.9901	0.9926	0.9949	0.9958	7.4843
SIMBEC	0.971	———	———	0.9955	6.8406
JADE	0.9894	0.9909	0.9949	0.9957	7.6522
ERICA	0.9281	———	———	0.9877	7.3857
EVD	———	———	———	———	6.8043

RADICAL	0.9871	0.991	0.9947	0.9957	189.3987
ICA-EBM	———	0.9927	0.9918	———	8.3961
ERBM	0.9903	0.9921	———	0.9949	49.9969
COMBI	0.9888	0.9912	0.995	0.996	4.9388
CNR = 1					
FastICA	0.9907	0.9939	0.9961	0.9963	10.3756
INFOMAX	0.9921	0.9954	0.9962	0.9963	7.7758
SIMBEC	———	———	———	———	6.7946
JADE	0.9902	0.9951	0.9962	0.9962	7.0135
ERICA	———	———	———	———	7.4633
EVD	———	———	———	0.993	6.8961
RADICAL	0.991	0.9958	0.9962	0.9963	191.0547
ICA-EBM	———	———	0.9929	0.9936	9.2952
ERBM	———	0.9627	———	0.9932	33.7969
COMBI	0.9914	0.9948	0.9962	0.9963	5.3986
CNR = 2					
FastICA	0.9907	0.9933	0.9961	0.9957	10.2979
INFOMAX	0.9926	0.9947	0.996	0.996	8.0558
SIMBEC	———	———	———	———	6.7824
JADE	0.9898	0.9948	0.9961	0.9957	7.054
ERICA	———	———	———	———	7.4225

EVD	———	———	0.9929	———	6.66
RADICAL	0.9913	0.9955	0.9961	0.996	189.9249
ICA-EBM	0.9634	———	———	0.9922	9.305
ERBM	———	0.9728	———	0.9936	44.9287
COMBI	0.9671	0.9954	0.9963	0.9959	5.2328

FastICA, INFOMAX, JADE, RADICAL and COMBI are the five algorithms accomplishing the decomposition of fMRI images into the constituent components with tidiness irrespective of the noise level instilled into the images. The RADICAL seems an outlier among this five in terms of time consumption, thus, although RADICAL decomposes components very cleanly but it is not wise to opt it for fMRI data decomposition as it is sluggish.

After utility check for synthetic images, algorithms were tested on real fMRI data collected with the visuomotor paradigm. The data was reduced using PCA. Results were scaled to Z - scores and the threshold was set to Z = 2. Twenty independent components (ICs) were found for each algorithm, further sorted temporally and spatially to get the two most task-related components. For all ICs, time courses and spatial maps are generated. Temporal sorting is an approach to compare the time course of the model with the time course of the component, whereas in spatial sorting the comparison would be among the spatial maps obtained and the spatial templates. Spatial templates are available in the template library of GIFT toolbox and the design matrix is available with the sample data.

Fig 2.6 shows the expanded view of TCs of the two task-related components decomposed by INFOMAX along with their temporal sorting score. For the iterative type of algorithms, ten runs are performed and due to the convergence issue stabilized version of Fast ICA is used. Extracted components of ICA algorithms have both sources of interest and not of interest. Regression values for the two most task-related components who represent left and right visual cortex are given in table 2.2. Spatial maps of these two task-related components are depicted in Fig 2.7.

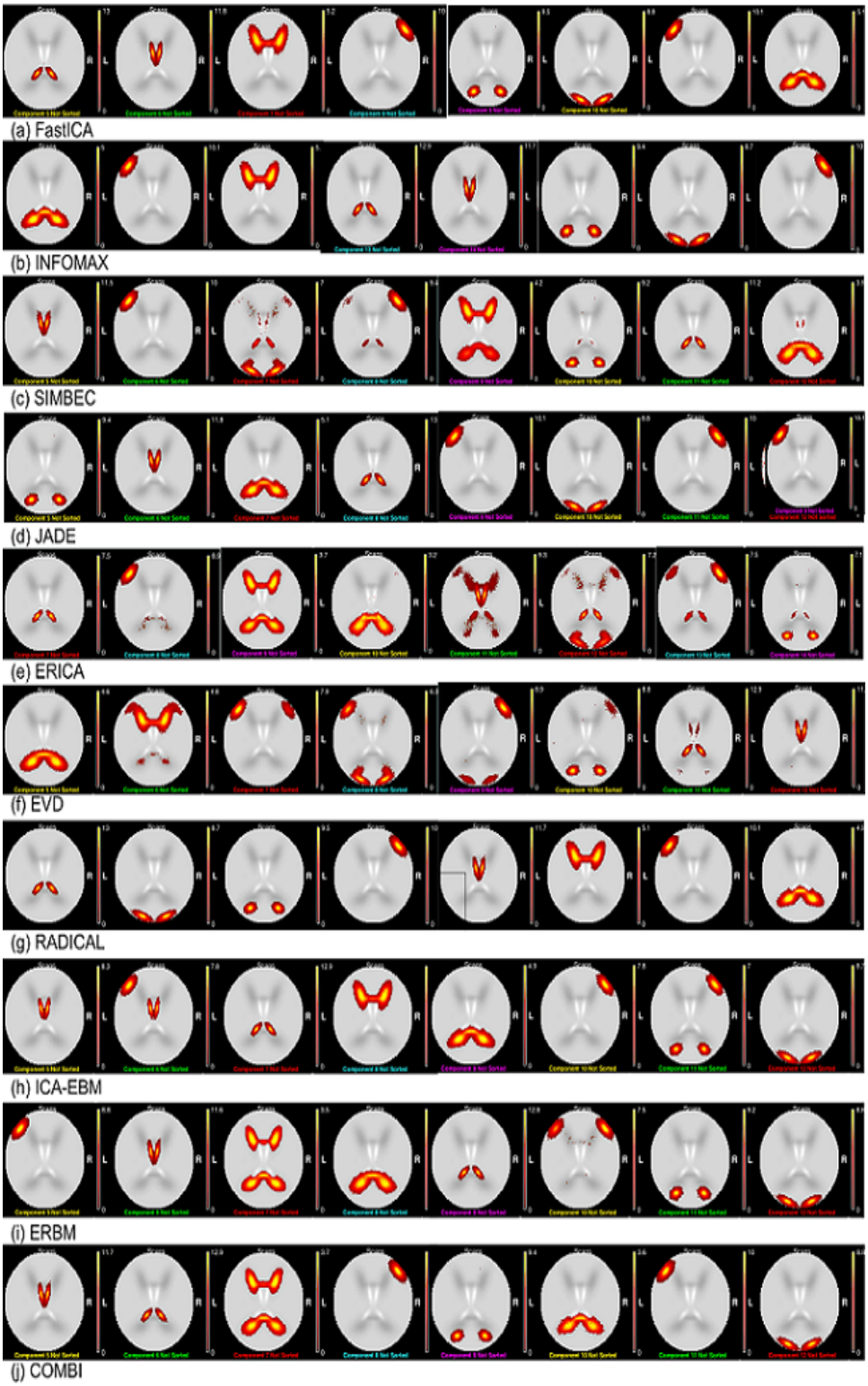

Fig. 2.3: Decomposition of synthetic fMRI images (CNR = 0.5) by all the ten ICA algorithms considered for comparison. Decomposed components include task-related components as well as the artifacts.

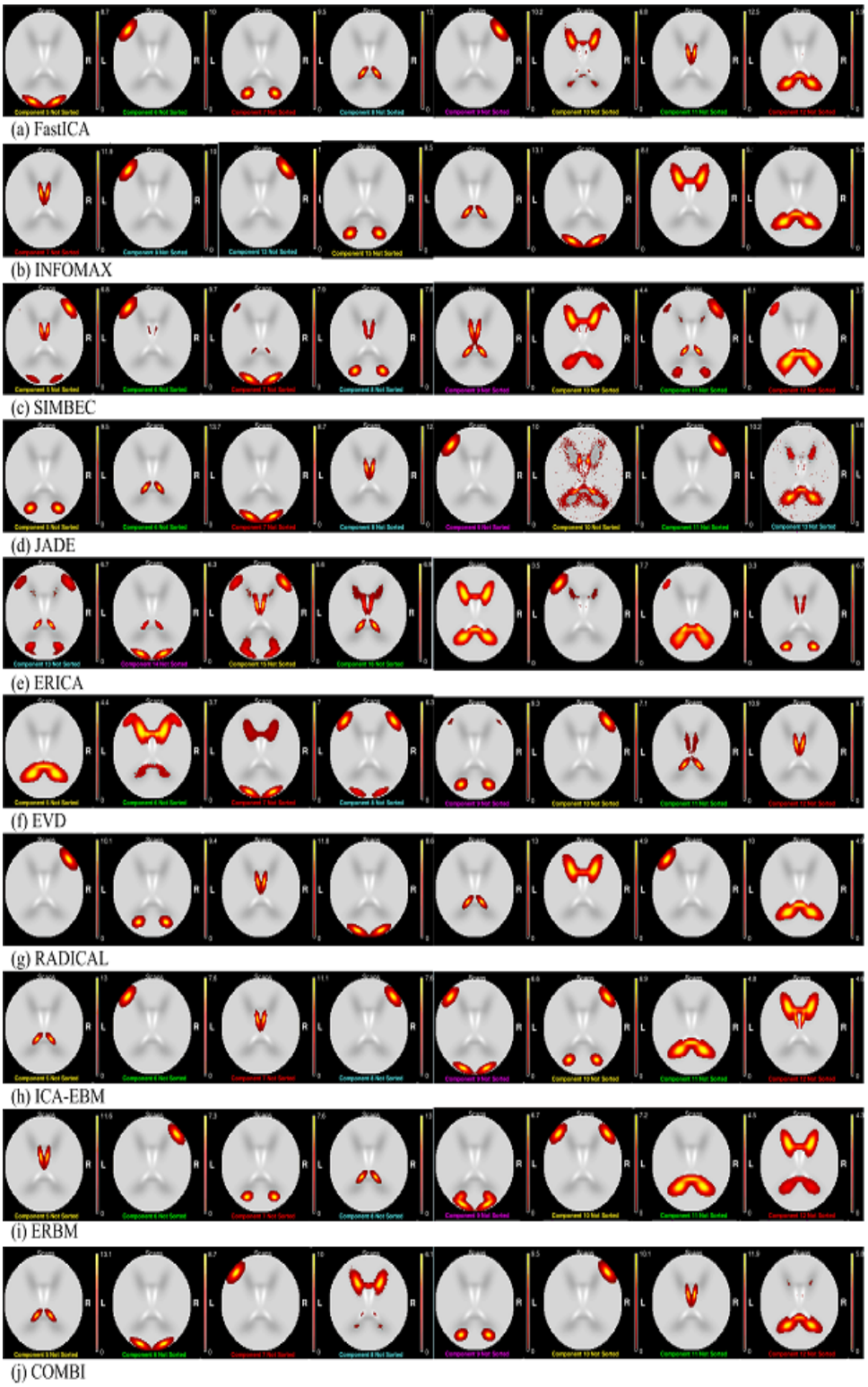

Fig. 2.4: Decomposition of synthetic fMRI images (CNR = 1) by all the ten ICA algorithms considered for comparison. Decomposed components include task-related components as well as the artifacts.

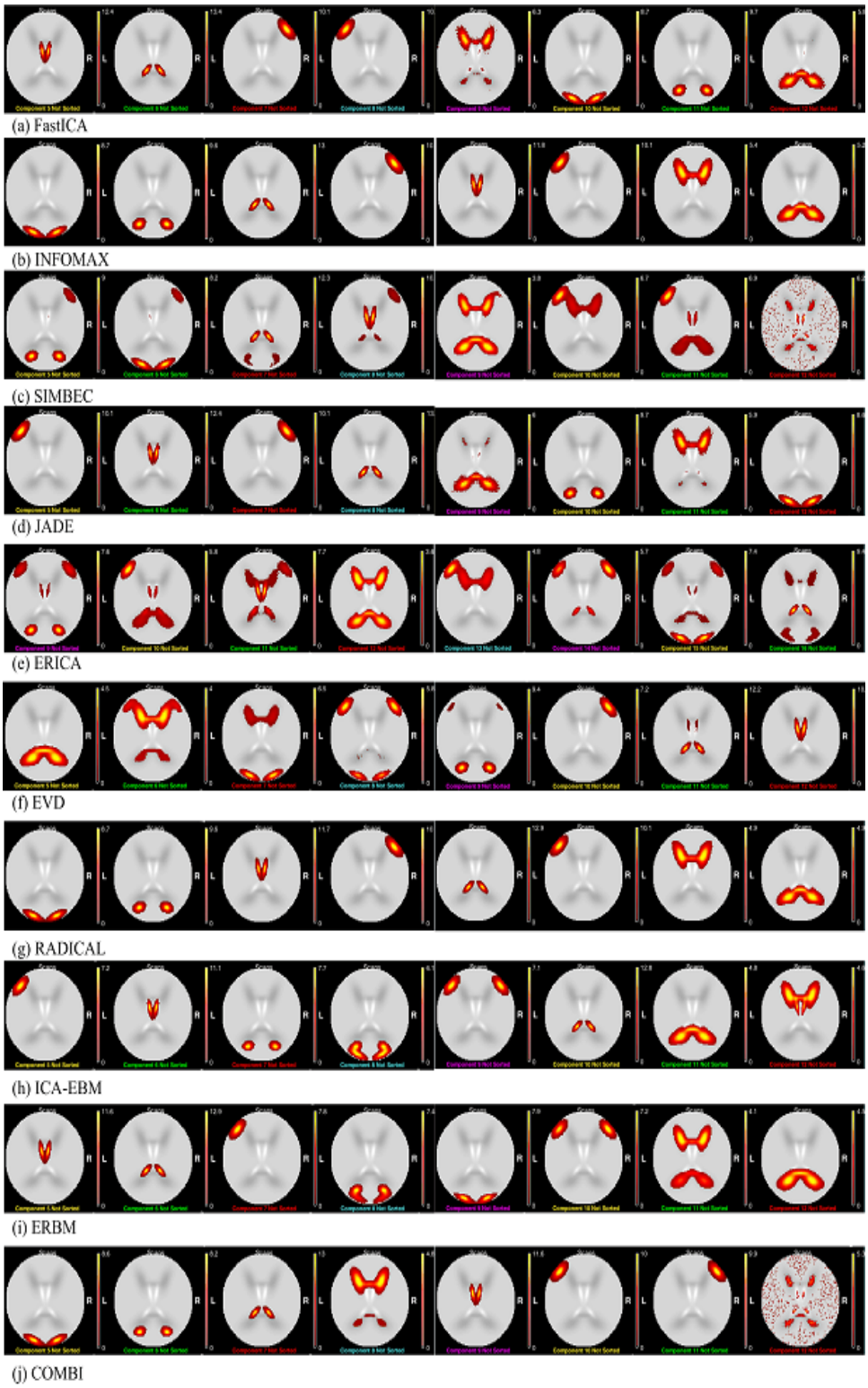

Fig. 2.5: Decomposition of synthetic fMRI images (CNR = 2) by all the ten ICA algorithms considered for comparison. Decomposed components include task-related components as well as the artifacts.

The judgment of their decomposition capabilities on the basis of the tabulated sorting scores go against ERICA, EVD, SIMBEC and ERBM but while comparing the overall performance and taking into account the visual appearance and time consumption, ICA-EBM and RADICAL also disappoint.

Table 2.2: Temporal and spatial sorting scores of the two task-related components extracted by all algorithms.

S. No.	Algorithm	Multiple Regression (Temporal Sorting)		Multiple Regression (Spatial Sorting)		Time elapsed (seconds)
		left	right	left	right	
1	FAST ICA	0.8655	0.6997	0.7218	0.7337	4.80149
2	INFOMAX	0.846	0.7862	0.7376	0.7348	6.71056
3	SIMBEC	0.7531	0.4584	0.6274	0.5957	2.38564
4	JADE	0.8674	0.7092	0.7279	0.6002	4.31545
5	ERICA	0.7807	0.4678	0.4755	0.366	2.44439
6	EVD	0.7678	0.5265	0.4427	0.255	2.45602
7	RADICAL	0.8195	0.7177	0.7339	0.7146	738.7942
8	ICA-EBM	0.804	0.8367	0.7141	0.6954	17.81147
9	ERBM	0.6436	0.8976	0.5573	0.3002	171.2499
10	COMBI	0.8383	0.7826	0.7405	0.732	1.25181

Since many works have used ICA on RsfMRI data, the separation performance of ICA algorithms are compared with resting state data too. The RsfMRI images of 14 individuals

suffering from ASD and of 13 neurotypical individuals (mean age 24 years) was collected from the ABIDEI website. Here, only the most consistent RSN are included [41] out of the 30 components extracted and they were recognized by visual inspection. The RSNs testimony were also cross-checked with the help of dynamic range and low frequency (LF) to high frequency (HF) power ratio values [127, 128]. These RSNs extracted using the ten algorithms are depicted in Fig 2.8,2.9,2.10,2.11.

All the consistent RSNs depicted here are centered at the peak of their distribution. The peak coordinates of the RSNs extracted by INFOMAX and COMBI are exactly same and the coordinates of those who were extracted using ERBM, RADICAL and ICA-EBM are almost same to INFOMAX. On the other side SIMBEC, ERICA and EVD were not able to disintegrate all the consistent RSNs. Time consumed by these algorithms are enlisted in the table 2.3. Sum of mutual information between all the permutations of decomposed components of RsfMRI data are calculated for the ten ICA algorithms which are tabulated in table 2.4.

Table 2.3: Time consumed (in seconds) by ICA algorithms while extracting components from RsfMRI data.

FastICA	109.67	EVD	105.54
INFOMAX	107.20	RADICAL	2496.50
SIMBEC	105.19	ICA-EBM	163.19
JADE	111.42	ERBM	516.63
ERICA	106.58	COMBI	75.61

Table 2.4: The sum of mutual information between all the permutations of decomposed components for all the ten ICA algorithms.

FastICA	197.36	EVD	203.91
INFOMAX	198.31	RADICAL	198.94
SIMBEC	205.21	ICA-EBM	200.99
JADE	198.38	ERBM	192.52
ERICA	201.91	COMBI	199.26

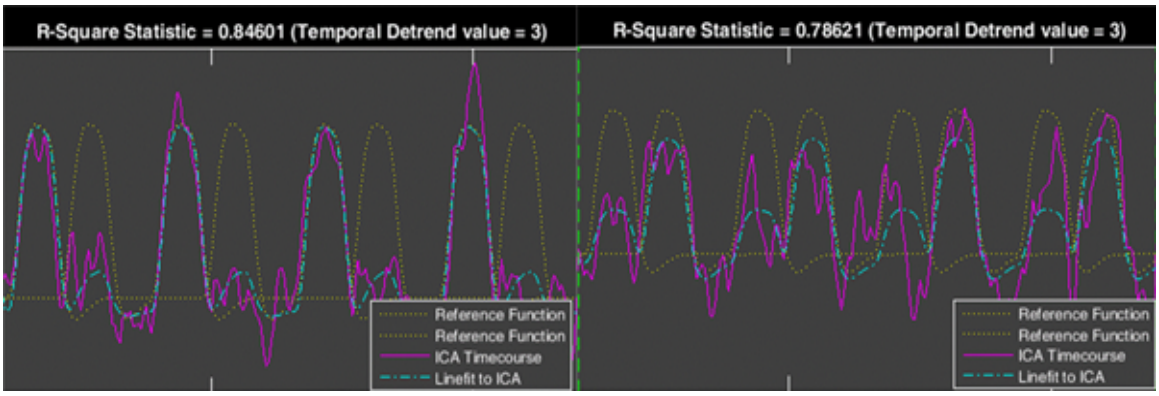

Fig. 2.6: Time courses of the two task-related components decomposed by INFOMAX. Temporal sorting scores is done by regressing these time courses with model time courses and the resultant values are also given in the figure.

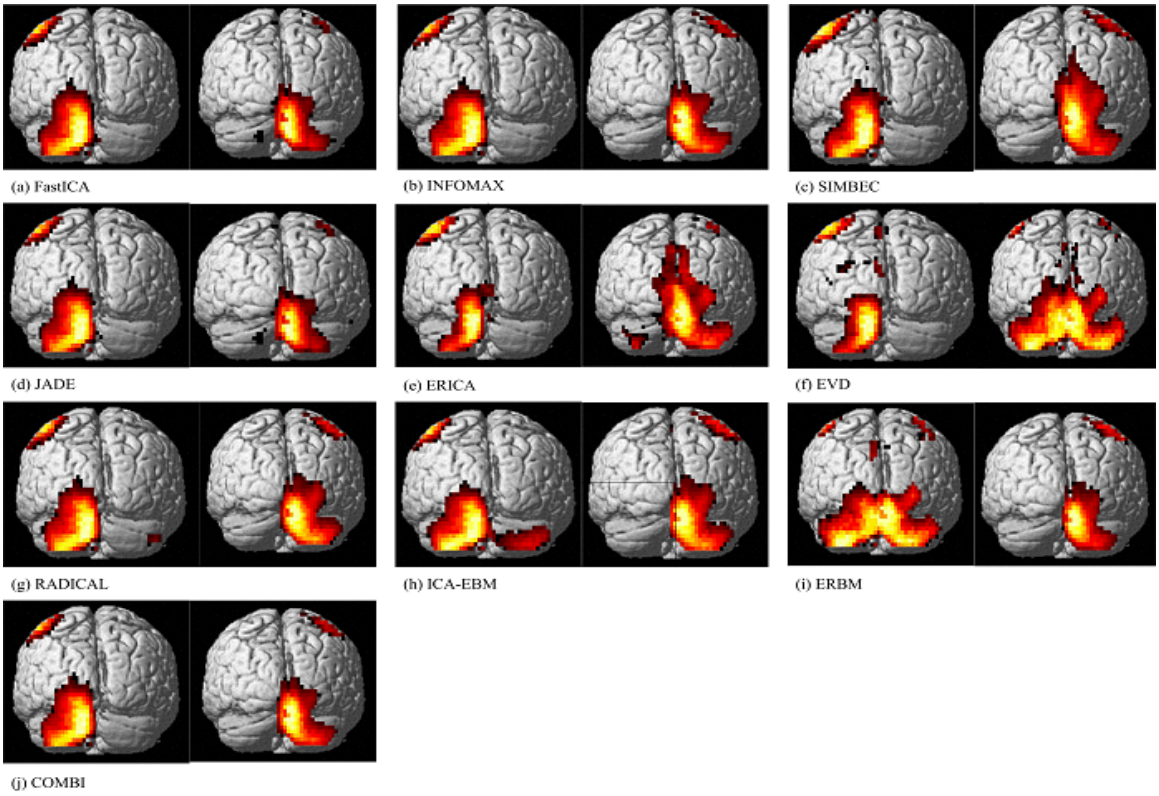

Fig. 2.7: Spatial maps of the two most task-related components decomposed by all the ten ICA algorithms. These maps are rendered on the human brain. Components decomposed by ERICA, EVD, ICA-EBM and ERBM are not distinctive.

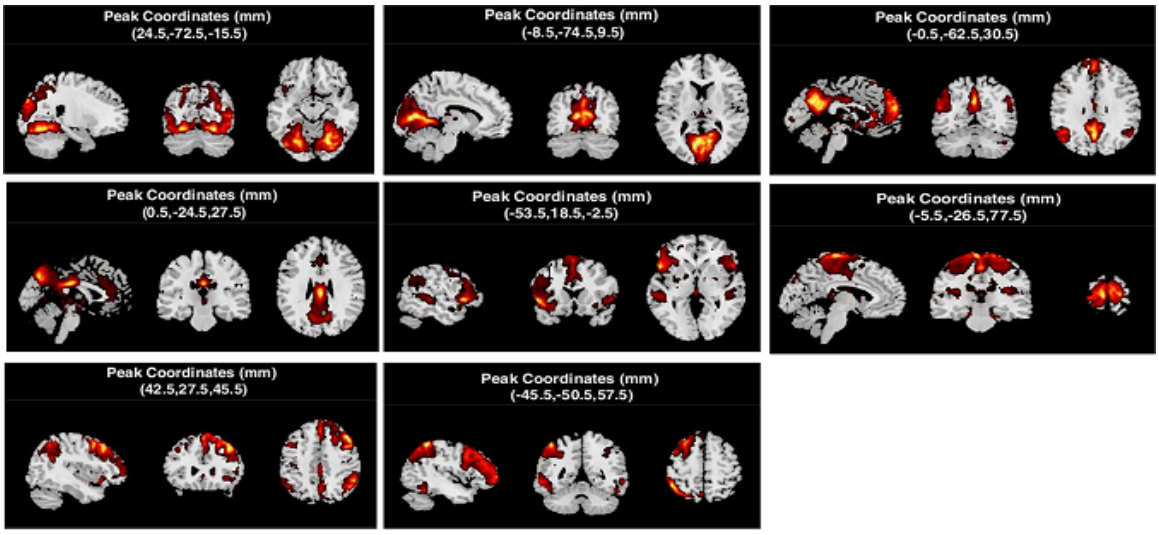

(a) FastICA

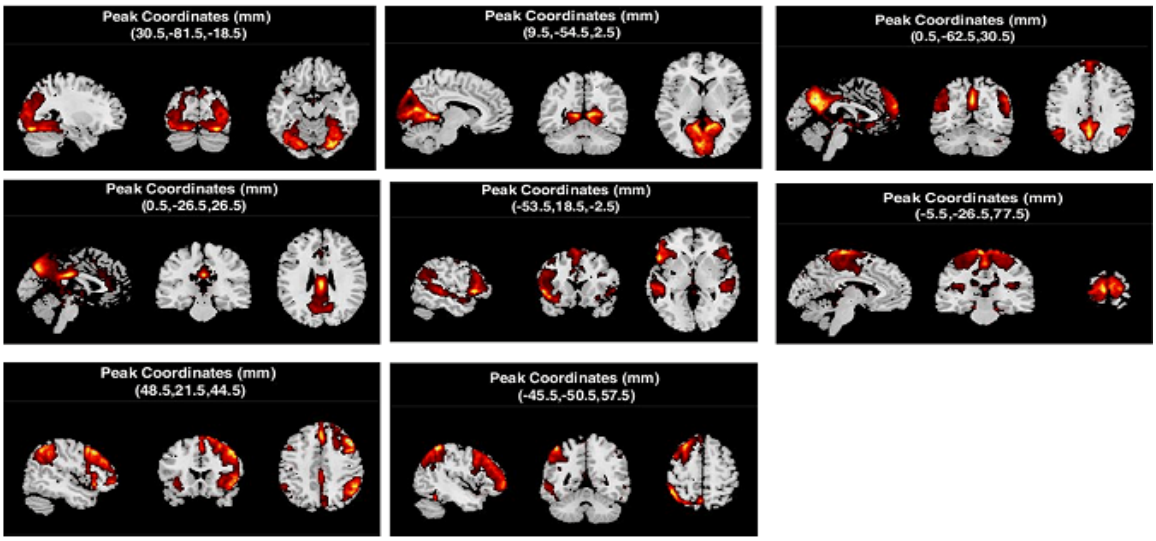

(b) INFOMAX

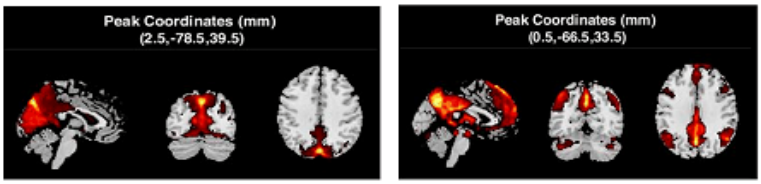

(c) SIMBEC

Fig. 2.8: Resting State networks decomposed from resting state data by (a) FastICA, (b) INFOMAX and (c) SIMBEC. Screening left to right in (a) and (b), these networks are visual occipital, visual medial, DMN I, DMN II, auditory, sensorimotor, left fronto-parietal and right-frontoparietal. Only two of the eight could be decomposed by SIMBEC.

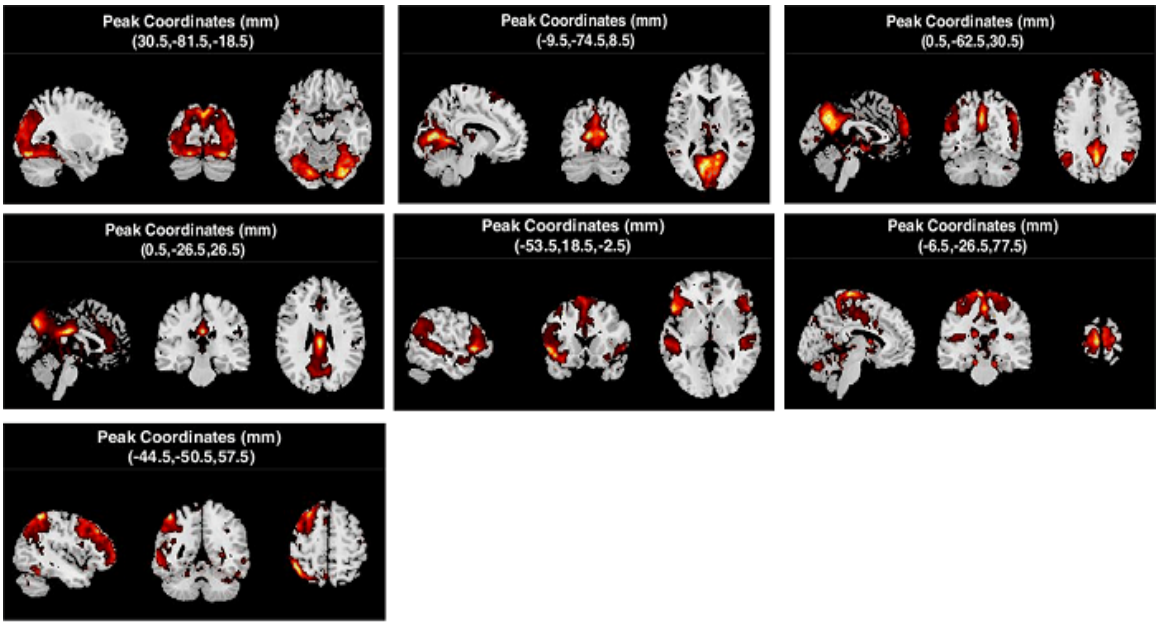

(d) JADE

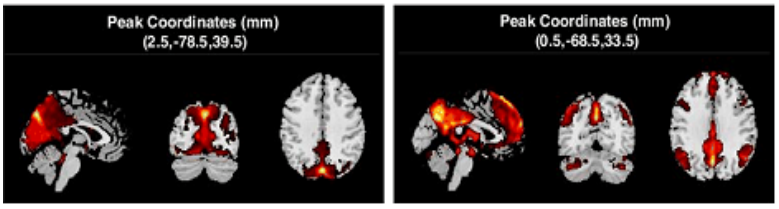

(e) ERICA

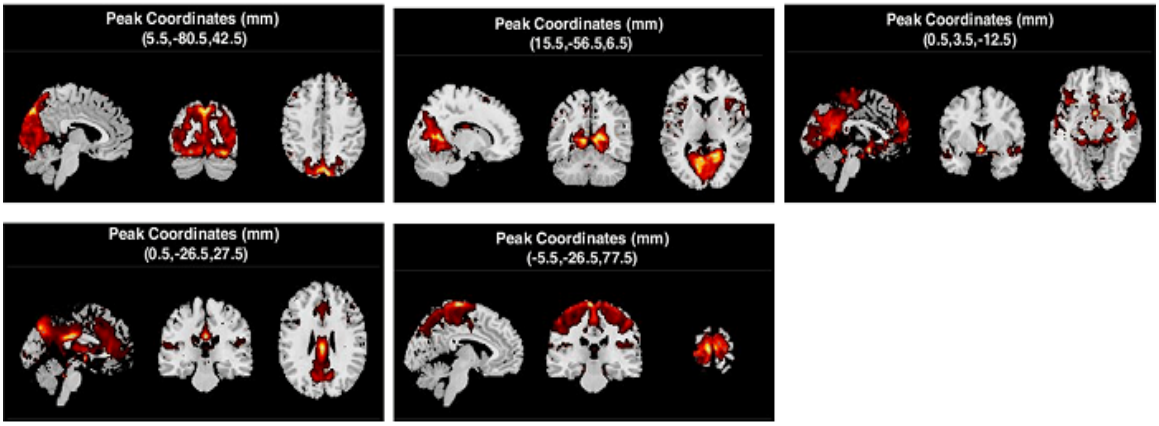

(f) EVD

Fig. 2.9: Resting State networks decomposed from resting state data by (d) JADE, (e) ERICA and (f) EVD. Screening left to right in (d) these networks are visual occipital, visual medial, DMN I, DMN II, auditory, sensorimotor, left fronto-parietal and right-frontoparietal. The ERICA and EVD could not decompose all the eight resting state networks. ERICA could recover only visual medial and DMNI, whereas EVD couldn't decompose auditory and the two fronto-parietal networks.

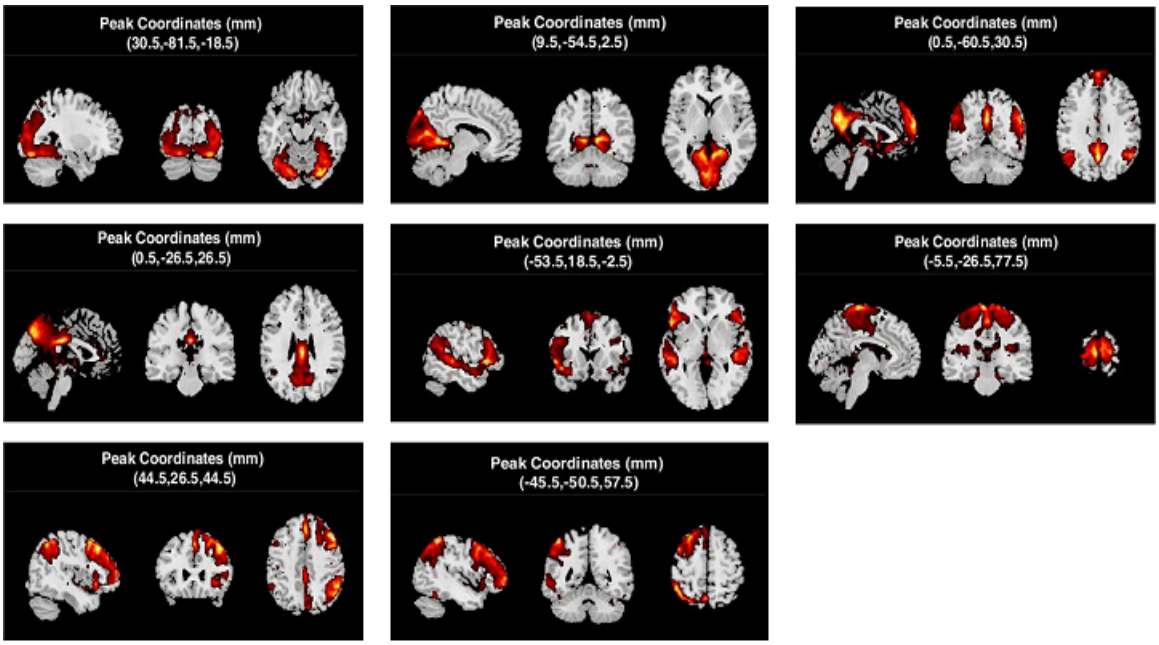

(g) RADICAL

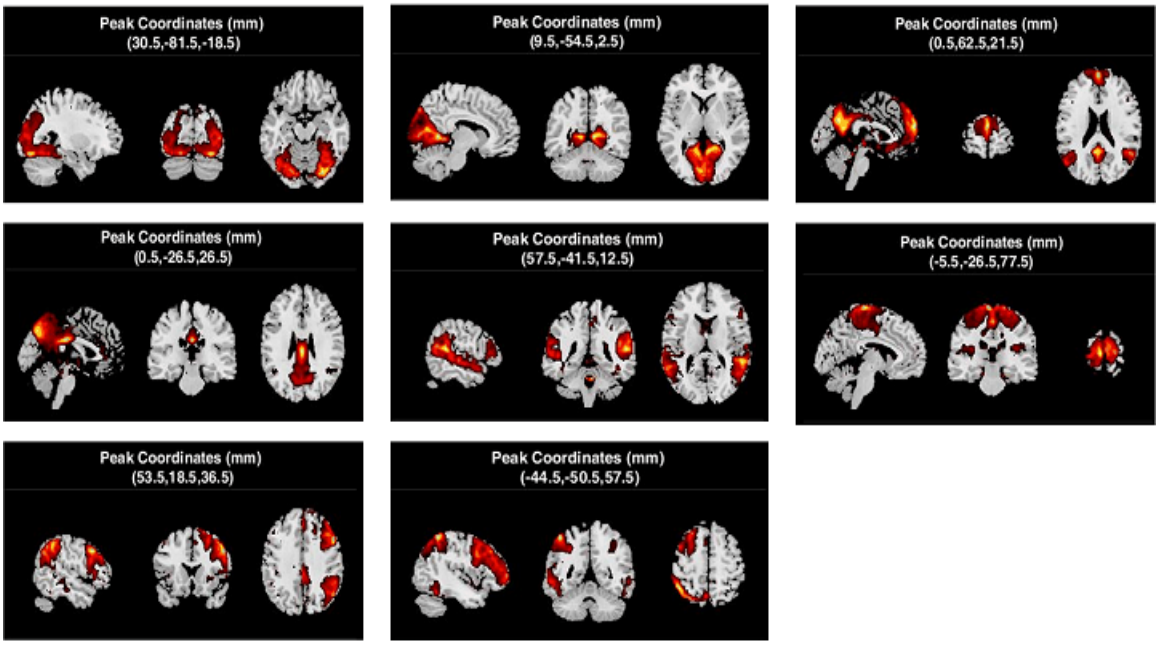

(h) ICA-EBM

Fig. 2.10: Resting State networks decomposed from resting state data by (g) RADICAL and (h) ICA-EBM. Screening left to right these networks are visual occipital, visual medial, DMN I, DMN II, auditory, sensorimotor, left fronto-parietal and right-frontoparietal.

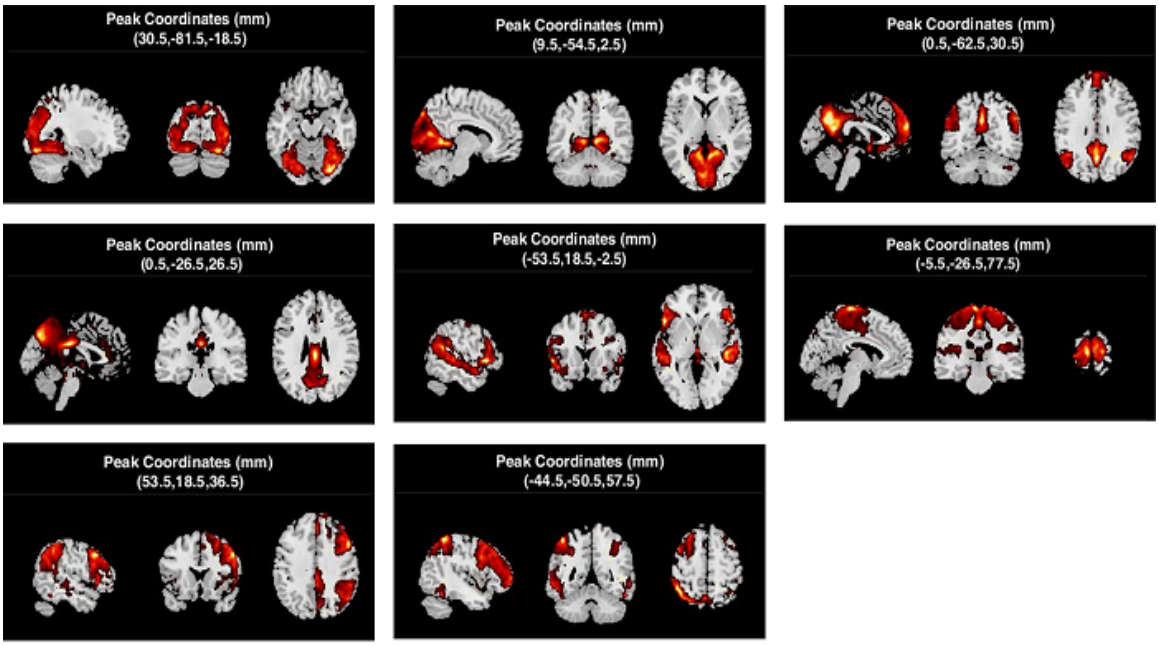

(i) ERBM

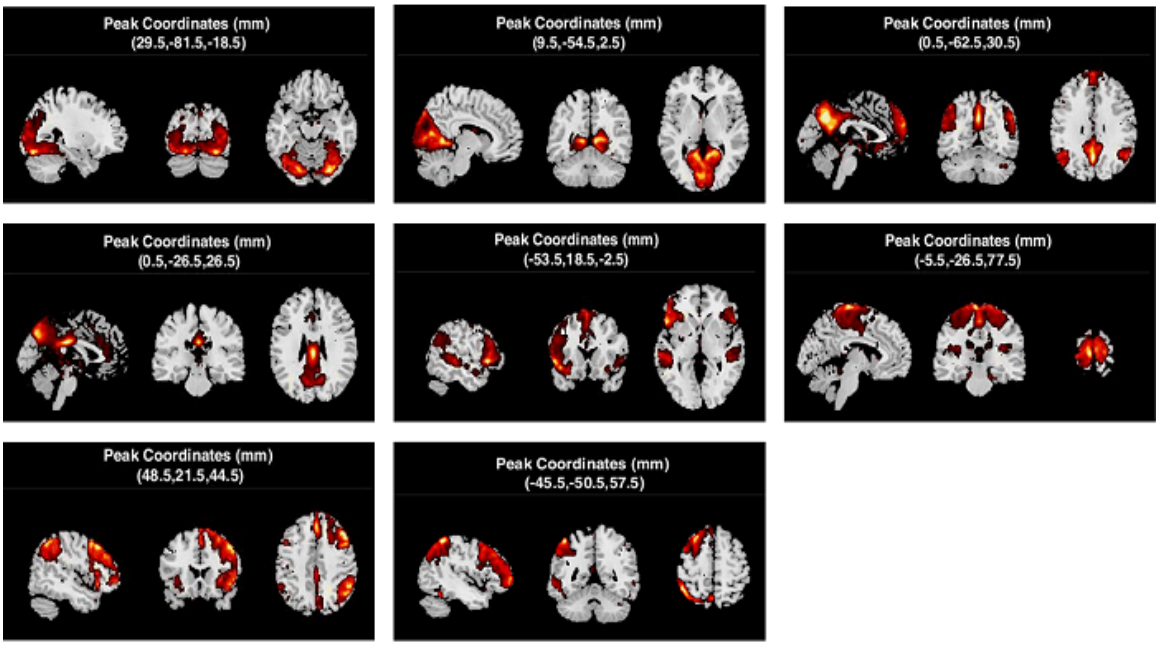

(j) COMBI

Fig. 2.11: Resting state networks decomposed by (i) ERBM and (j) COMBI. Screening left to right these networks are visual occipital, visual medial, DMN I, DMN II, auditory, sensorimotor, left fronto-parietal and right-frontoparietal.

2.5 Summary

The fMRI has gained tremendous attention by the researchers who are probing the brain and the ICA is one of the preferable explorative methods for the analysis of fMRI data. The ICA is elder than fMRI and many ICA algorithms are already framed, but FastICA, INFOMAX, and JADE have been applied repeatedly on fMRI data. It was a great opportunity to compare the performances of most opted ICA algorithm and those who were overlooked. Ten ICA algorithms are covered in this paper which encompasses nearly all the major approaches to measuring the independence. Their performances are quantified for synthetic and real fMRI images. Based on all the results obtained it can be deduced that ERICA, EVD and SIMBEC are not suitable algorithms for decomposition of fMRI images. Cumulative observations reveals that it's not fruitful to use ERBM or ICA-EBM separately but their combination is a better choice to use for fMRI decomposition. RADICAL is very sluggish and thus not a good choice. Among the overlooked algorithms and most opted algorithms COMBI is a better choice for fMRI decomposition. The COMBI is fastest as well as it's decomposed components are quite distinct.

CHAPTER 3

3D TEMPLATES FOR LABELING OF RSN

The Functional Magnetic Resonance Imaging, together with the interdisciplinary methodologies including computer science, mathematics, and physics, are cultivating interesting outcomes from computational neuroscience. Over the most recent two decades, several Resting state fMRI studies have been done, searching for the practically significant resting state networks. The naming of RSN are being done either by utilizing spatial correlation between's the given 2D layout and component images or in light of the premise of ROIs effectively reported as the captivating anatomical part of those RSN in past literary works. Because of nonexistence of any standard convention for ICA model order selection, 2D RSN templates cannot be used as standard layout for examination, moreover ROIs combinations are not unique for RSN. To overcome this inadequacy, 3D templates are proposed in this chapter with the end goal of RSN recognition.

3.1 Components of ICA based FNC Analysis

Brain study has entered into an era of grey box testing with advanced neuroimaging techniques. Noninvasive neuroimaging techniques have provided commendable insight into the architecture and functioning of the brain. The functional magnetic resonance imaging is progressively gaining attention because of its higher spatial resolution, but, as hemodynamic response is the proxy of neuronal response, its temporal resolution is relatively poor [129]. In the starting phase of its application fMRI was exploited to map the individual function of brain regions. Within the two decades it has gained confidence and now its clinical and real time applications are being explored such as biomarker identification of neurological disorders viz. schizophrenia, autism, epilepsy etc. [130–135].

To get to the bottom of brain functions, task based fMRI experimental paradigms used to be designed till the ground breaking finding of Biswal (1995). He observed that regions that are co-activated during a task are also temporally correlated at rest [101, 102]. This temporal correlation among the anatomically separated regions reflects a level of ongoing FC among brain regions during rest [104, 136]. The fluctuations in the BOLD signal during rest

reflect the neuronal baseline activity (intrinsic activity) of the brain. Resting state fMRI is a method to study this intrinsic activity. The utilization of resting state fMRI for the assessment of unconstrained changes in the BOLD signal has a few advantages over conventional task based fMRI [137,138]. One vital favorable benefit of this technique is that it can be performed notwithstanding when the patient can't perform the task. This will empower us to perform fMRI mapping on numerous populaces already avoided from customary assignment based systems, for example, youthful kids, patients with psychological impedances, and patients that are deadened, aphasic, or in need of a hearing aid. Spontaneous fluctuations have been appeared to hold on under states of rest and diverse levels of anesthesia [139], in this manner a moment preferred standpoint of this procedure is that it can be performed in disturbed patients and in youthful kids under sedation. A third favorable position of this technique is that one data acquisition can be utilized to concentrate a wide range of brain networks, in this manner perhaps decreasing the procurement time when numerous frameworks are assessed.

The fMRI information has been broke down by the two opposing techniques, theory driven and information driven methodologies. Among the information driven methodologies, Independent Component Analysis has been appeared to give an effective technique to the exploratory investigation of fMRI data [140, 141]. The ICA empowers recuperation of underlying signals, or independent components (ICs) from linear data mixtures. Along these lines, it is an incredible technique to be connected for the spatial localisation and transient portrayal of sources of BOLD activation. Spatial ICA has overwhelmed so far in fMRI applications on the grounds that the spatial measurement is considerably bigger than the temporal measurement in fMRI [138].

3.1.1 Identification of RSN

The ICA can disentangle intrinsically connected brain regions known as resting state network (RSN). The ICs can be categorised into RSNs and physiological components by utilizing their temporal features. Contrasts in the frequency structure of RSN and physiological components prompt two features as the basis for classification. These have been marked "Dynamic Range" - the difference in power between the maximum and the minimum of the distribution, and "Low to High Power Ratio" - the ratio of the integral of power in the region of the spectrum

below 0.02 Hz to the total spectra [128]. Nearly 10 RSNs have been recognized yet and they are over and over recreated at various research facilities.

3.1.2 RSN Labeling

Oftentimes experienced practitioners label the RSN as being of physiological origin. Neuroimaging is an interdisciplinary area where researchers from non-medical background also participate. As neuroimaging research taking a strong move towards their clinical contribution, its utmost necessity to develop a protocol to label the RSNs automatically. As a first attempt, and as a baseline reference, automated RSN identification was investigated with a simple correlation classifier by calculating spatial correlation to a 2D template [103,130,142]. Demertzi et al. [143] addressed the methodological challenge when opting for multiple RSN investigations in patients with severe brain damage. In particular, by using a single template-matching goodness-of-fit procedure at a time, one runs the risk to erroneously identify a component as the RSN of interest. For specific component labeling, [143] used ICA and a univariate template matching method with an additional step of "neuronality" classification to label RSN.

The work done by Vergun [144] combines two established methods, ICA, and machine learning, to develop an automatic process of extracting and identifying (classifying) network maps. With respect to the study by [143], this work adds the investigation of the performance of different, complementary multivariate machine learning algorithms for IC spatial map labeling and the evaluation of the labeling method. Chamberland et al. [145] in their 3D interactive tractography validated RSN using 3D overlap matrics viz. Dice coefficient and Jaccard coefficient. These spatial matching approaches of labeling have some major limitations and thus it may be misleading. First, different RSNs may have a same spatial correlation with a template as shown in Fig 3.1, consequently, two different components may get the same name and it is most probably with those components who extend to different lobes i.e. fronto-parietal networks. Second, there is no standard order of ICA thusly decomposed RSN might be of various morphology based on ICA model order. The RSN splits with increase into the ICA order. With this ambiguity, 2D overlap measurement is not a decent decision to quantify the similarity between the component and the template because a low

value may result in wrong labeling.

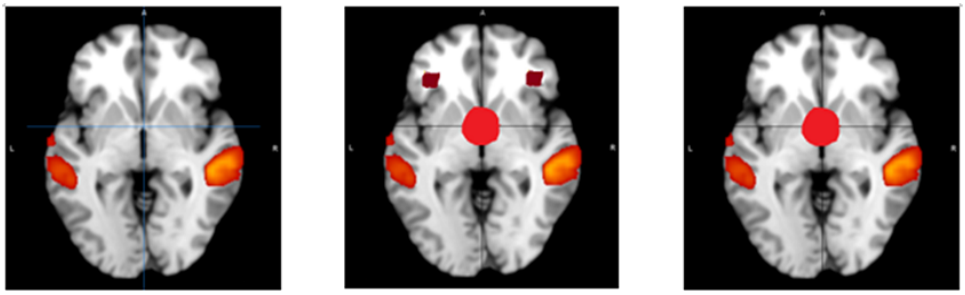

Fig. 3.1: Axial slice in the left is a RSN template and the other two slices represent two different decomposed components. Naming of them can be done by their spatial correlation values with the template but both will produce same spatial correlation values with the 2D template.

Tomasi et al. identified 7 bilateral functional networks [146] and the labels of their constituting regions are checked using Automated Anatomical Labelling (AAL) atlas [147] and the Brodmann atlas. The RSNs have all the earmarks of being like the Task-Based Networks (TBNs) that rise up out of the examination of substantial troupes of activation studies gathered with various psychological undertakings found in vast functional imaging databases [146, 148]. Pushed by this reality, Mesmoudi et al. [149] portrayed anatomo-functional bunches of RSN in view of their cover with two reference sets [i.e.,Brodmann Areas (BAs) and TBNs]. Rosazza el al. [150] hailed the brain areas where the reliably discovered RSNs are identifiable in their survey paper . These definitions are altered in [151] in light of the method of reasoning that associations inside RSNs ought to be one of a kind. While quantifying the consistency of RSN, Damoiseaux et al. [41] mapped their occupancy into Brodmann areas to label them. Labelling the RSNs has been carried out by observing their overlap with Brodmann areas. In ICA based analyses, it's a practice to find clusters of individual RSN and locate and label them using some atlas, but the BAs and regions constituting them are not unique thusly becomes exhaustive and error-prone.

Here in this chapter 3D templates are proposed for the labeling of RSN. These templates are developed by overlaying the manually labelled RSN on 3D glass brain. The manual labelling of RSN are based on the results of Talairarch client where the toolbox was com-

manded to search in a cube of +/- 2mm. These 3D templates are made for the standardization of RSN labeling. Using the 2D overlap measurement to quantify the similarity of decomposed RSN with templates, one runs the risk to erroneously identify a component as the RSN of interest. With the help of 3D templates, RSN labeling can be made automatic, accurate as well as faster. Instead of 2D overlap measurement, one needs to identify the inhabitancy of the RSN with templates. The RSN will essentially get the name of that 3D template which will contain it irrespective of how much space RSN occupy.

3.2 Making of 3D templates

The RsfMRI images in use for the template making are gathered from the autism brain imaging data exchange (ABIDE I) website alongside entire make up details and scanning details. ABIDEI is a subset of International Neuroimaging Information Sharing Initiative (INDI) and 1000 Functional Connectomes Project. The RsfMRI data present in this repository are collected from around 16 different laboratories.

The pre-processing is done as per the connectome computation system (CCS) protocol which starts with skipping initial four volumes followed by slice timing correction, motion realignment and intensity normalization. Confounding variables brought in either by scanner, head motion, breathing or pulsation are regressed out after primary processing of images. The global mean signal was incorporated with disturbance variable. The processed images were decomposed by spatial ICA (SICA), using the Group ICA fMRI Toolbox [152]. A higher model order i.e. 100 was selected for SICA. The COMBI algorithm was utilized to break down the datasets [122]. At last, the parts were back remade utilizing the group ICA tool. Spatial maps were guaranteed as RSN on the premise of the estimations of dynamic range and the proportion of power at low frequency to higher frequency. The MNI coordinates of the group maxima were changed to the Talairach stereotactic space. The brain areas were marked by the Talairach daemon tuned to an inquiry scope of 2mm. Components were visually inspected and RSN are labelled on the basis of their spatial scope. Detailed anatomic information of RSN network are tabulated in table 3.1.

Images of manually labelled RSN are coregistered to sample image of Multi-image Analysis GUI (MANGO) toolbox (http://ric.uthscsa.edu/mango/) followed by the surface render-

ing. They are rendered on 3D glass brain for the purpose of better visibility. Images of all the six sides are captured for better interpretation.

3.3 Results

The pre-processed data are decomposed into 100 independent components. The threshold for qualification of these components as RSN is set to 2 (low to high frequency ratio). Detailed anatomic information of RSN network, overlaid on 3D glass brain to make the 3D templates are included in table3.1. Images of anterior, posterior, superior, inferior, left and right views for the seven resting state networks are included in Fig 3.2. In the GIFT toolbox there is a provision to label the RSNs based on the spatial correlation between RSNs and the 2D templates. These templates are available online on the homepage of Functional Imaging in Neuropsychiatric Disorders (FIND) Lab. Labeling of RSNs were also carried out using this utility of GIFT toolbox and some of the wrongly labeled RSN are in Fig 3.3.

3.4 Discussion

The purpose of this work was to develop 3D RSN templates which has utility in clinical RsfMRI mapping. One very obvious way to identify the RSN is to sort it spatially as it is done in GIFT toolbox. Spatial sorting is an approach to compare the obtained spatial map with the available spatial templates. To date, only 2D templates are available and this is the first attempt to establish 3D RSN templates. RSN labelling by volumetric matching may by-pass the dissimilarity as describes as its limitation in introduction. It can be understood by examining the RSN who spread in more than one lobe i.e. fronto-parietal networks. Clusters of intriguing functional parts for it are in two different lobes and those clusters can be identified as two different RSN. The process of labelling with the help of 3D templates can be made more intuitive by using the coordinates of the decomposed clusters. A component lying in the occipital lobe should not undergo in the process of overlapping calculation with templates which actually belong to some other lobe of the brain.

A noteworthy issue is with the ICA model order, that is, the number of components to be decomposed. In particular, overestimation may prompt component splitting. The optimized number of components to be separated is not known from the earlier. Underestimating the model order may lead to information loss, while overestimating it might deliver spurious

outcomes or the part of intriguing segments into more segments. The utilization of higher model requests permitted discovery of intriguing neuroanatomical and functional parts. This model order ambiguity makes the use of 2D RSN templates doubtful. The proposed 3D templates are unaffected from this splitting of components as the surface rendering unite them again on the 3D brain.

There is a difference between ROIs of the same RSN into different ICA based RsfMRI studies. The contrast between ROIs incorporated into each RSN is obvious and makes disarray with respect to interesting anatomical and functional parts of them. The reason might be the contrast between the model order selection. Therefore it is difficult to think of a rundown of ROIs constituting the RSNs.

Table 3.1: Anatomical information of independent components rendered on the 3D glass brain to make the three dimensional templates.

IC	Talairach Coordinates			Hemisphere	Lobe	Gyrus	Tissue Type	Brodmann Area	Low to High Frequency power ratio
COGNITIVE CONTROL NETWORK									
1	36	41	-14	Right Cerebrum	Frontal Lobe	Middle Frontal Gyrus	Gray Matter	11	2.049911
2	50	35	14	Right Cerebrum	Frontal Lobe	Middle Frontal Gyrus	Gray Matter	*	3.444046
8	-42	43	-8	Left Cerebrum	Frontal Lobe	Middle Frontal Gyrus	Gray Matter	11	3.364123
18	53	20	-4	Right Cerebrum	Frontal Lobe	Inferior Frontal Gyrus	Gray Matter	47	3.338171

19	50	-52	50	Right Cerebrum	Parietal Lobe	Inferior Parietal Lobule	Gray Matter	40	7.541966
20	33	59	17	Right Cerebrum	Frontal Lobe	Superior Frontal Gyrus	Gray Matter	10	3.243869
28	36	53	25	Right Cerebrum	Frontal Lobe	Superior Frontal Gyrus	Gray Matter	10	3.55553
37	-51	16	29	Left Cerebrum	Frontal Lobe	Middle Frontal Gyrus	Gray Matter	9	4.510992
42	48	-35	60	Right Cerebrum	Parietal Lobe	Inferior Parietal Lobule	Gray Matter	40	4.350592
49	54	17	33	Right Cerebrum	Frontal Lobe	Middle Frontal Gyrus	Gray Matter	9	4.251517
53	38	22	-7	Right Cerebrum	Frontal Lobe	Inferior Frontal Gyrus	Gray Matter	47	4.964348
54	33	59	-1	Right Cerebrum	Frontal Lobe	Middle Frontal Gyrus	Gray Matter	*	3.953466
60	32	43	44	Right Cerebrum	Frontal Lobe	Superior Frontal Gyrus	Gray Matter	8	2.489772
80	26	-67	53	Right Cerebrum	Parietal Lobe	Superior Parietal Lobule	Gray Matter	7	4.256288

SENSORIMOTOR NETWORK									
10	60	-14	28	Right Cerebrum	Parietal Lobe	Postcentral Gyrus	Gray Matter	3	5.639205
11	-36	-21	61	Left Cerebrum	Frontal Lobe	Precentral Gyrus	Gray Matter	4	5.055152
46	30	-35	68	Right Cerebrum	Parietal Lobe	Postcentral Gyrus	Gray Matter	2	2.456195
48	0	9	65	Left Cerebrum	Frontal Lobe	Superior Frontal Gyrus	Gray Matter	6	2.871596
70	54	-30	57	Right Cerebrum	Parietal Lobe	Postcentral Gyrus	Gray Matter	2	4.228714
73	0	-20	64	Left Cerebrum	Frontal Lobe	Medial Frontal Gyrus	Gray Matter	6	2.992024
95	56	-4	25	Right Cerebrum	Frontal Lobe	Precentral Gyrus	Gray Matter	6	6.645517
AUDITORY NETWORK									
17	50	-24	-1	Right Cerebrum	Temporal Lobe	Superior Temporal Gyrus	Gray Matter	21	3.383204
34	62	3	6	Right Cerebrum	Frontal Lobe	Precentral Gyrus	Gray Matter	6	4.547463
51	-41	-31	13	Left Cerebrum	Temporal Lobe	Transverse Temporal Gyrus	Gray Matter	41	2.527898

52	-54	-57	27	Left Cerebrum	Temporal Lobe	Superior Temporal Gyrus	Gray Matter	39	5.894107
DEFAULT MODE NETWORK									
11	0	-56	38	Left Cerebrum	Parietal Lobe	Precuneus	Gray Matter	7	10.19038
23	15	-54	19	Right Cerebrum	Parietal Lobe	Precuneus	Gray Matter	31	6.643629
31	-21	-45	-7	Left Cerebrum	Limbic Lobe	Parahippocampal Gyrus	Gray Matter	37	4.125467
35	0	-4	39	Left Cerebrum	Limbic Lobe	Cingulate Gyrus	Gray Matter	24	2.503981
38	0	46	-4	Left Cerebrum	Limbic Lobe	Anterior Cingulate	Gray Matter	32	7.244612
39	0	25	30	Left Cerebrum	Limbic Lobe	Cingulate Gyrus	Gray Matter	32	5.60359
44	0	-38	38	Left Cerebrum	Limbic Lobe	Cingulate Gyrus	Gray Matter	31	7.426639
51	11	-47	5	Right Cerebrum	Limbic Lobe	Parahippocampal Gyrus	Gray Matter	30	4.385572
55	21	-21	-9	Right Cerebrum	Limbic Lobe	Parahippocampal Gyrus	Gray Matter	35	2.263749
58	20	-35	2	Right Cerebrum	Limbic Lobe	Parahippocampal Gyrus	Gray Matter	30	2.018515

64	5	-42	-10	Right Cerebellum	Anterior Lobe	Cerebellar Lingual	Gray Matter	*	2.346558
70	0	-4	30	Left Cerebrum	Limbic Lobe	Cingulate Gyrus	Gray Matter	24	3.348904
75	0	-49	14	Left Cerebrum	Limbic Lobe	Posterior Cingulate	Gray Matter	30	5.98791
78	0	-19	28	Left Cerebrum	Limbic Lobe	Cingulate Gyrus	Gray Matter	23	2.706604
80	0	-24	27	Left Cerebrum	Limbic Lobe	Cingulate Gyrus	Gray Matter	23	13.44533
83	0	59	25	Left Cerebrum	Frontal Lobe	Superior Frontal Gyrus	Gray Matter	9	8.989119
FRONTO-PARIETAL NETWORK									
9	53	-59	34	Right Cerebrum	Parietal Lobe	Angular Gyrus	Gray Matter	39	10.04026
25	-42	14	41	Left Cerebrum	Frontal Lobe	Middle Frontal Gyrus	Gray Matter	8	8.499725
VISUAL NETWORK									
22	3	-92	11	Right Cerebrum	Occipital Lobe	Cuneus	Gray Matter	18	5.96929
24	32	-70	39	Right Cerebrum	Parietal Lobe	Precuneus	Gray Matter	19	8.572919
27	11	-69	14	Right Cerebrum	Occipital Lobe	Cuneus	Gray Matter	18	3.981281
43	21	-71	-9	Right Cerebrum	Occipital Lobe	Lingual Gyrus	Gray Matter	18	4.875348

56	0	-76	35	Left Cerebrum	Occipital Lobe	Cuneus	Gray Matter	19	7.242336
68	0	-82	-6	Left Cerebrum	Occipital Lobe	Lingual Gyrus	Gray Matter	18	3.770719
100	41	-61	-12	Right Cerebrum	Temporal Lobe	Fusiform Gyrus	Gray Matter	37	2.773226
BSASAL GANGLIA NETWORK									
3	0	-13	-10	Left Brainstem	Midbrain	*	Gray Matter	Mammillary Body	2.083156
10	0	0	0	Right Cerebrum	Limbic Lobe	Anterior Cingulate	Gray Matter	25	2.054156
29	0	-20	10	Left Cerebrum	Sub-lobar	Thalamus	Gray Matter	Medial Dorsal Nucleus	2.482992
30	-3	6	8	Left Cerebrum	Sub-lobar	Caudate	Gray Matter	Caudate Body	3.035344
47	0	-23	-1	Left Brainstem	Midbrain	*	Gray Matter	Red Nucleus	2.067775
50	0	-26	5	Left Cerebrum	Sub-lobar	Thalamus	Gray Matter	*	2.383022
54	9	3	13	Right Cerebrum	Sub-lobar	Caudate	Gray Matter	Caudate Body	3.274689
65	-24	0	-8	Left Cerebrum	Sub-lobar	Lentiform Nucleus	Gray Matter	Putamen	4.609092

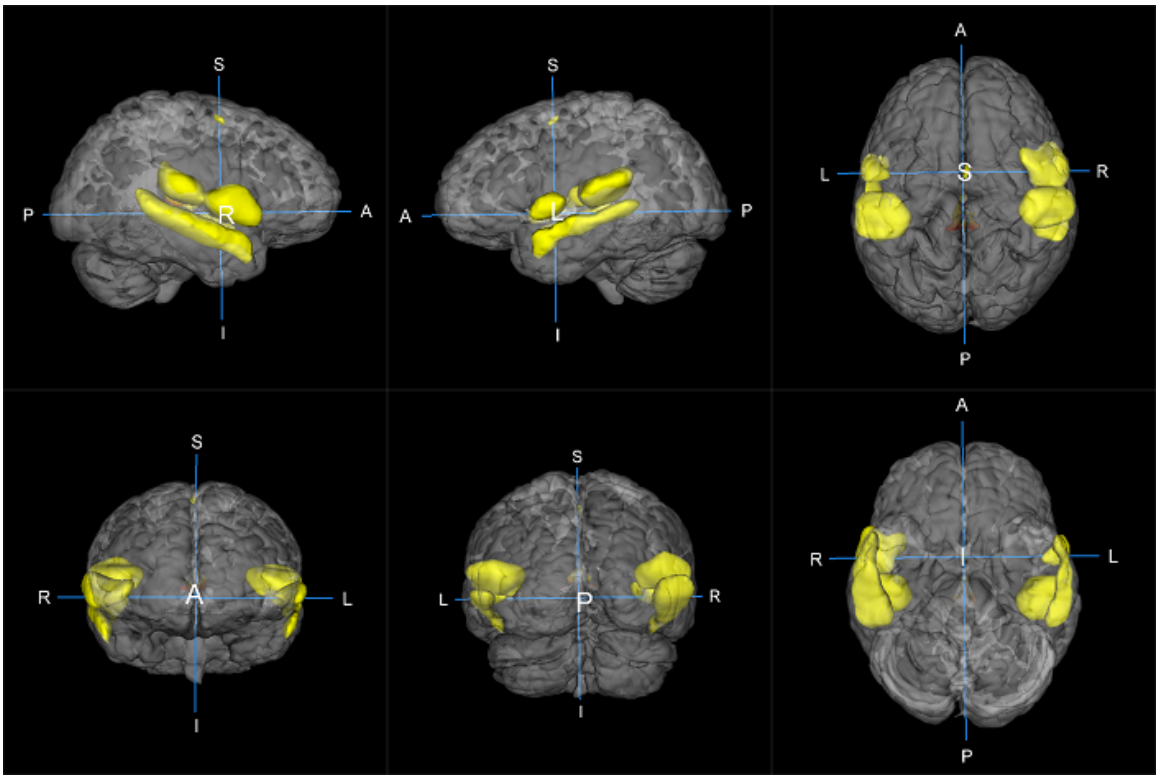

(a) Auditory Network

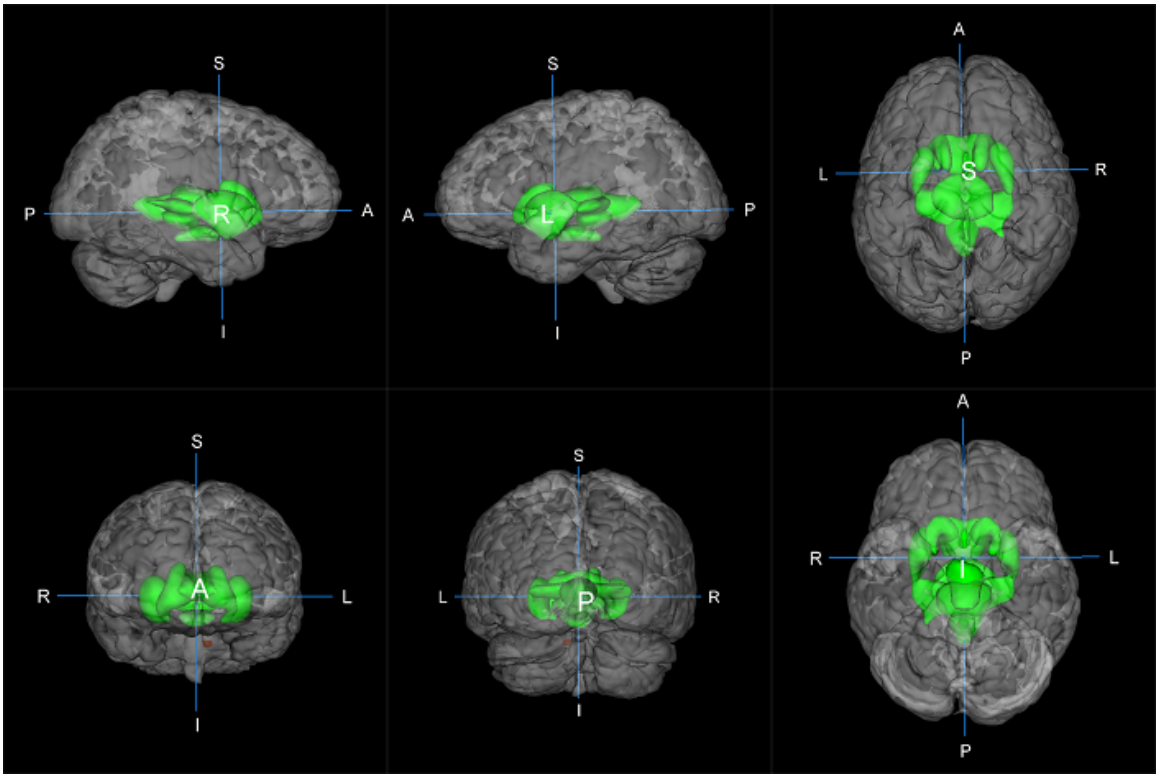

(b) Basal Ganglia Network

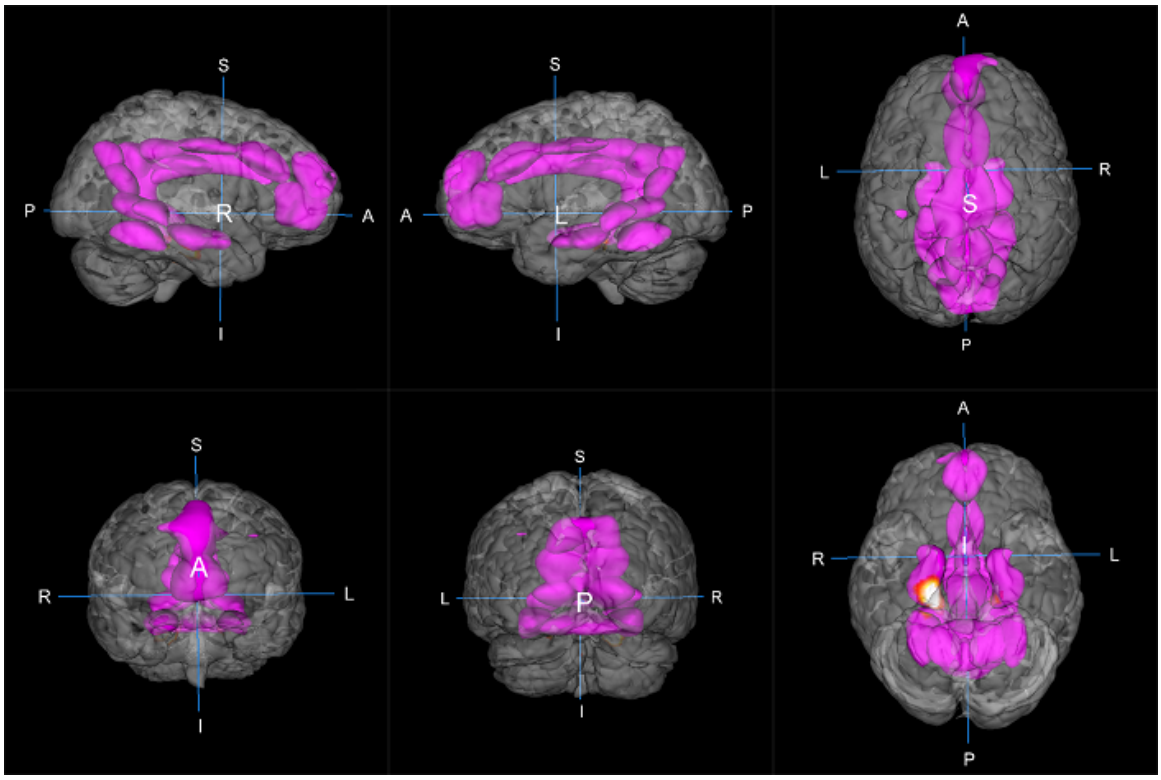

(c) Default Mode Network

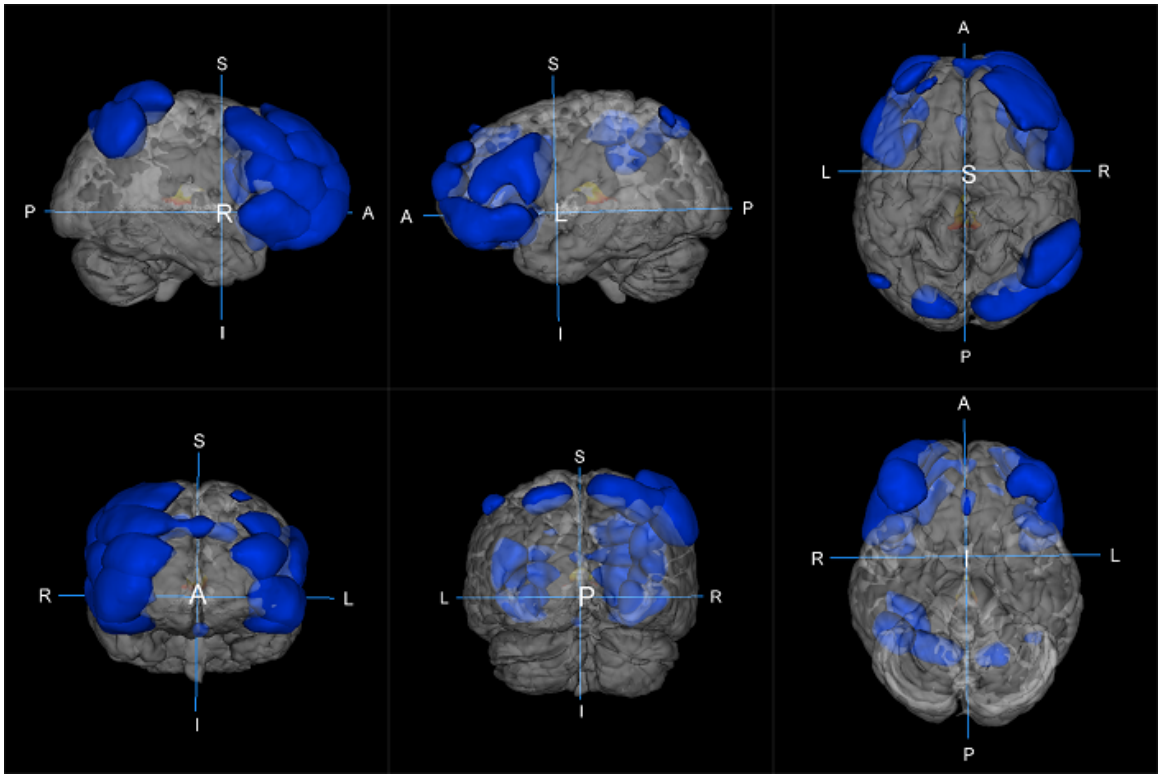

(d) Cognitive Network

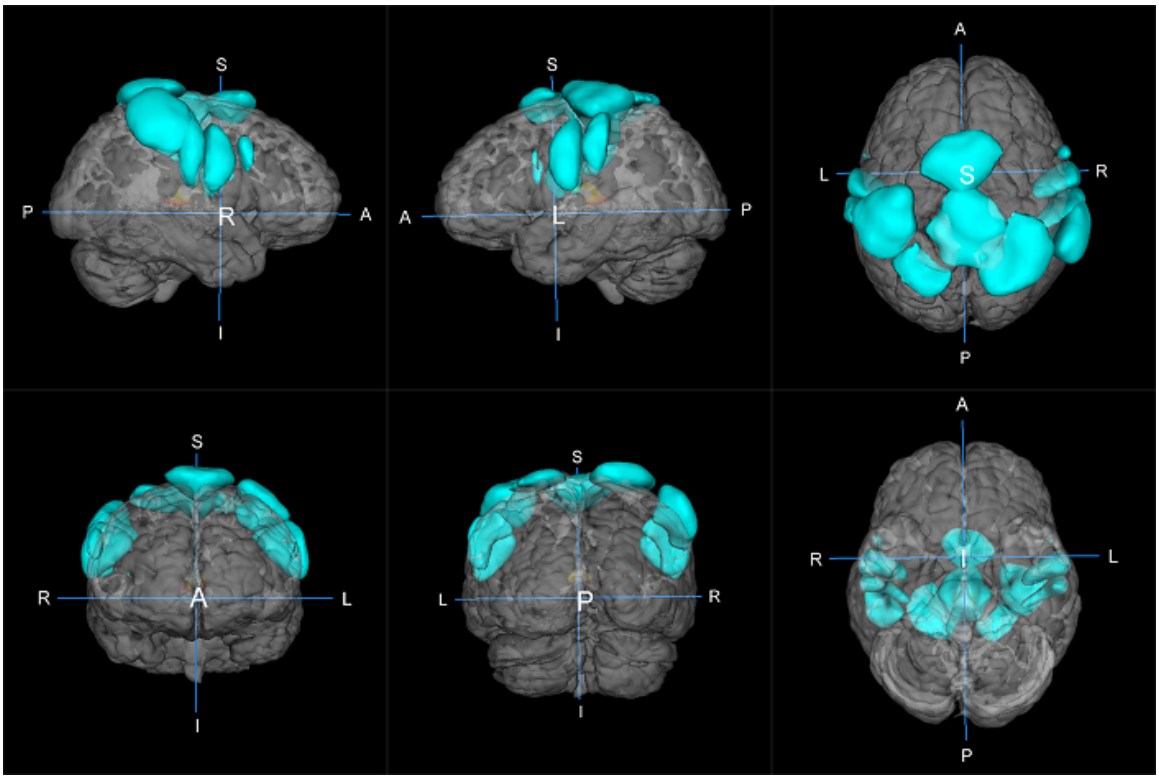

(e) Sensorimotor Network

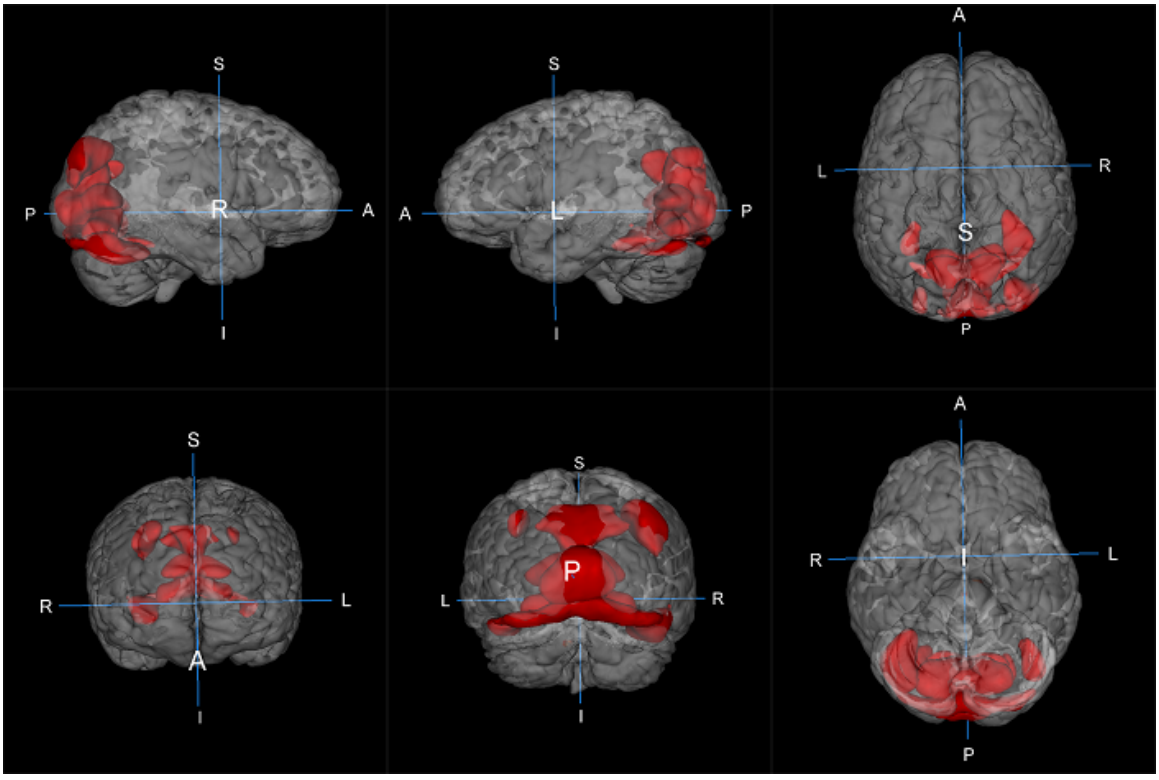

(f) Visual Network

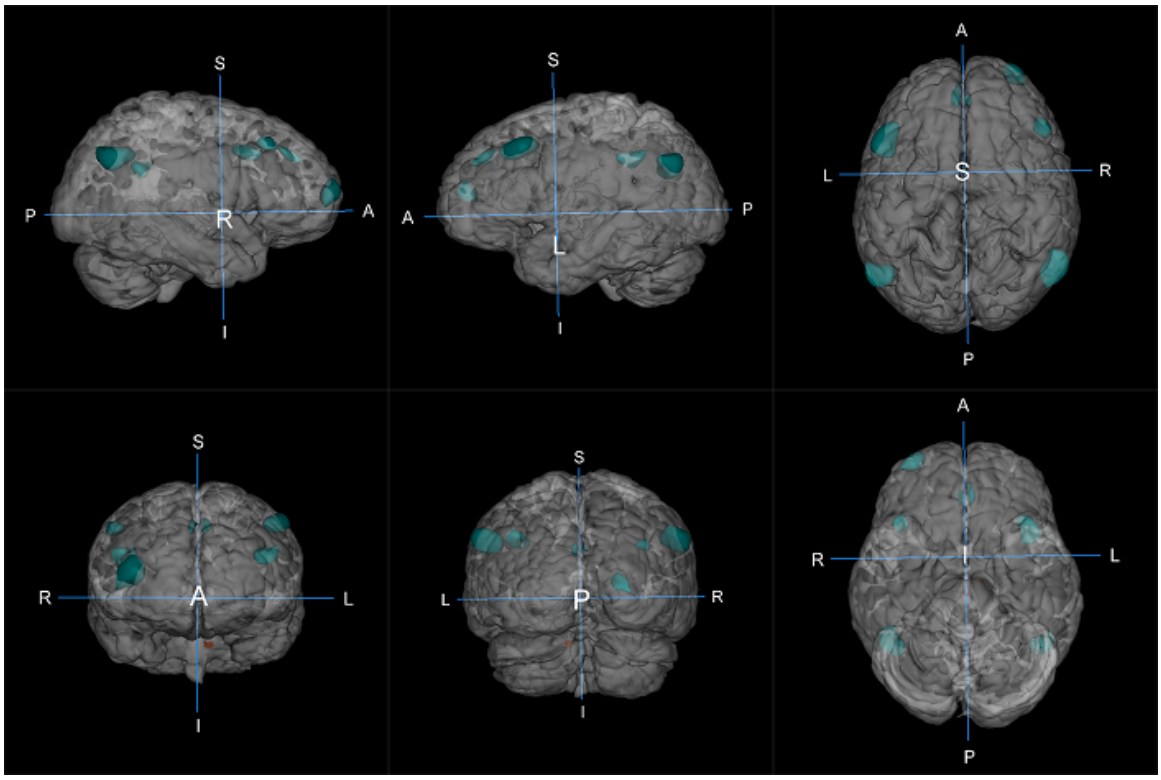

(g) Executive (fronto-parietal) Network

Fig. 3.2: Six principle views of RSNs, anterior, superior, Left side, Right side, inferior, and posterior. (a) Auditory Network, (b) Basal Ganglia network, (c) Default Mode network, (d) Cognitive network, (e) Sensorimotor network, (f) Visual network, and (g) Executive or fronto-parietal network.

Machines fall extremely a long ways behind people in "understanding pictures" in the feeling of producing rich semantic explanation. For instance, systems that endeavor to manage impediment, context, and unforeseen courses of action, all of which are effectively taken care of by individuals, regularly experience issues. Thus, there is no reason for planning an "opposition" between computer vision and human vision. Researchers from non medicinal foundation often experience issues accomplishing a spatial comprehension of 3D brain anatomy from (2D) pictures and content. The 3D layouts of RSN will profit such researchers to contribute in this interdisciplinary zone all the more intelligently.

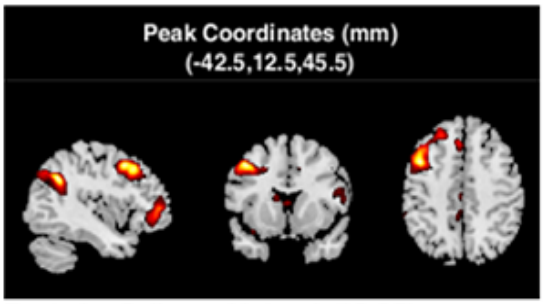

Posterior Salience Network (IC 25)

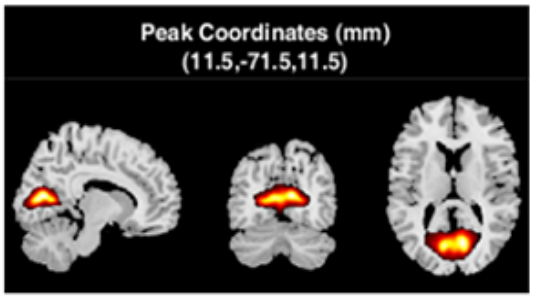

Ventral DMN Network (IC 27)

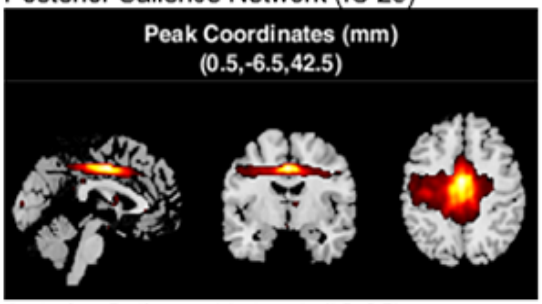

Anterior Salience Network (IC 35)

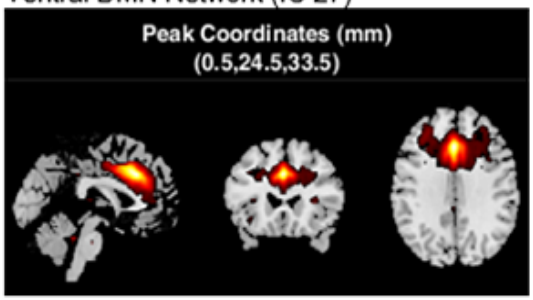

Anterior Salience Network (IC 39)

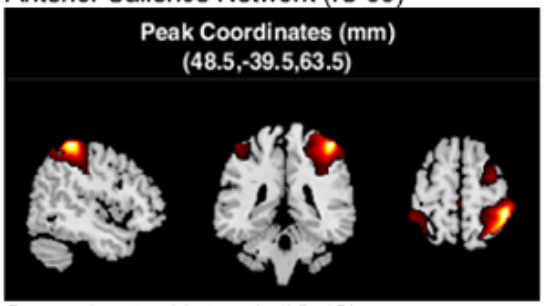

Sensorimotor Network (IC 42)

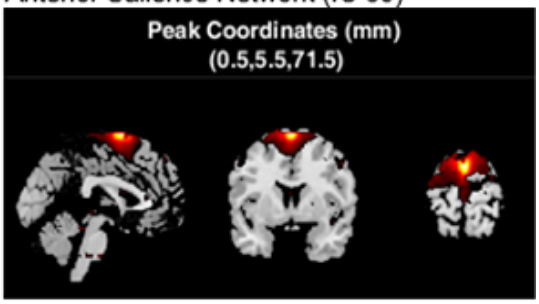

Anterior Salience Network (IC 48)

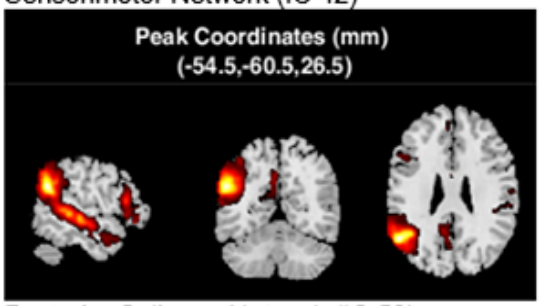

Posterior Salience Network (IC 52)

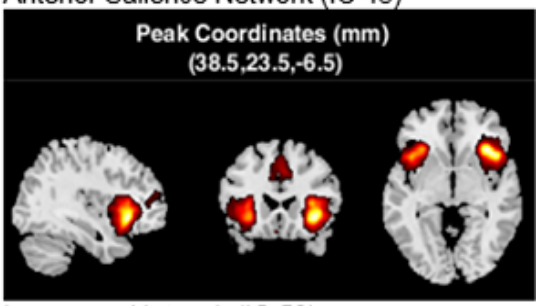

Language Network (IC 53)

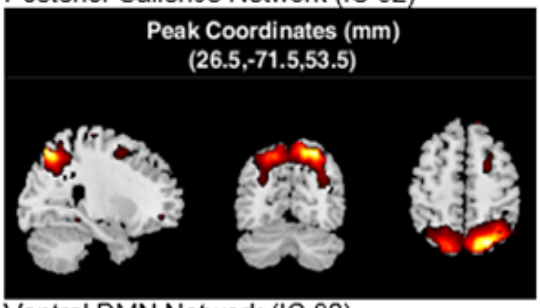

Ventral DMN Network (IC 80)

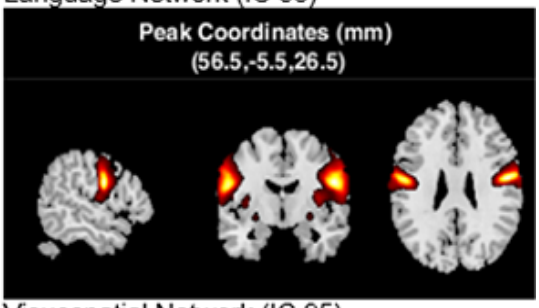

Visuospatial Network (IC 95)

(a)

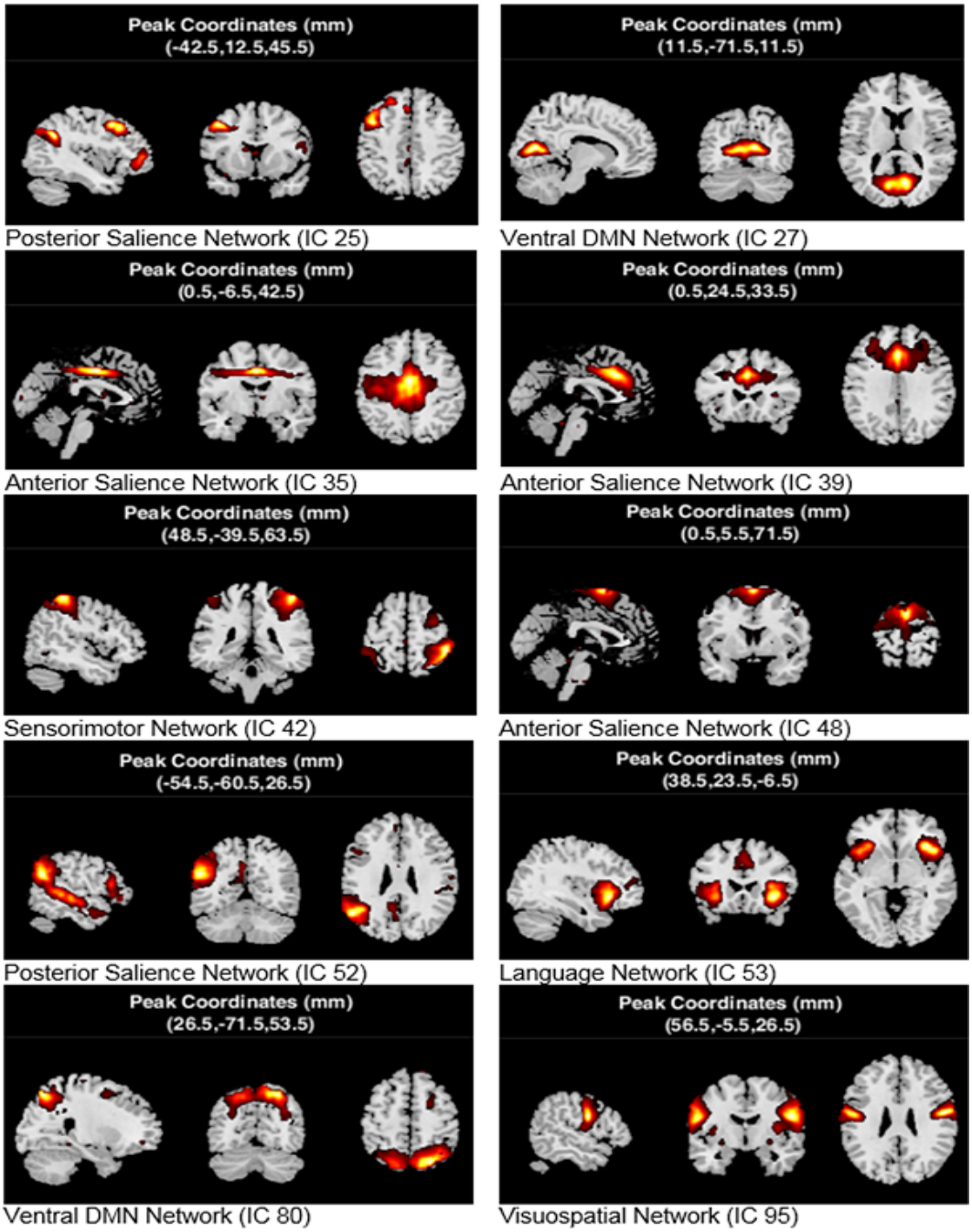

(b)

Fig. 3.3: Resting State Networks along with their naming identified using the RSN labelling utility of GIFT toolbox. Labelling of RSN is done in this utility by spatially correlating them with the resting state fMRI templates. Component numbers are mentioned along with the labels and they can be cross checked with the entries of Table 3 to get their right name.

3.5 Summary

Splitting of components due to model order ambiguity, moderate advance in computer vision, higher likelihood of confusion of segments who are spread over more than one projection of the brain and repeating ROIs for different RSN are the significant obstacles in utilizing 2D RSN layouts for the marking reason. Proposed 3D templates are a superior substitute which are free from these shortcomings also well simple to acknowledge even by a researcher from non-medicinal foundation and having just shallow information of brain anatomy.

CHAPTER 4

AGE-STRATIFIED STATIC FUNCTIONAL NETWORK CONNECTIVITY ANALYSIS OF ASD AND TYPICALLY DEVELOPING SUBJECTS

Autism spectrum disorder (ASD) is a neurodevelopmental disorder. Obsessive tendencies, language deficits, and social deficits are the hallmarks of ASD. Poor information integration across functional networks of the brain may be the root cause of these deficiencies. Functional network connectivity (FNC) assessment among six brain networks, viz. anterior default mode network, posterior default mode network, two frontoparietal networks, basal ganglia network (BGN) and salience network (SN) have been examined here in this chapter. To understand the development trajectory of ASD, functional magnetic resonance imaging (fMRI) dataset of autistic children, adolescents and adults are considered. The SN and BGN of participants with ASD had the most FNC differences with typically developing cohorts. The SN had hyperconnectivity with the rest five networks for autistic children while hypoconnectivity were observed for adolescents and adults. The two lateralized fronto-parietal network had no connectivity for the two initial developmental stages however for adults with ASD they had stronger functional connectivity.

4.1 Background and Motivation

To establish the functional network connectivity based biomarkers the fMRI has been used because of it's higher spatial resolution and reasonably good temporal resolution [153]. Distant brain regions are connected functionally to each other and it is defined as functional connectivity (FC) [101]. Lots of work has already been done on FC assessment of human brain and this technique has the potential to be used for the identification of biomarkers for neurological disorders such as autism, schizophrenia etc [78, 154–156]. ICA has the ability to unravel intrinsically connected networks (ICN) of RsfMRI images.

Nearly 10 RSN have been identified yet [136, 142] and they are repeatedly reproduced at different laboratories. Some of these RSN gets activated while performing the task and hence known as task positive networks (TPN) however task negative networks (TNN) also exist and they remain quiescent while performing the task [154, 157]. Based on, within network connectivity and/or between network connectivity, biomarkers for the neurological disorder have been reported [78, 131]. Between network

connectivity is called functional network connectivity (FNC) alternatively. Aberrant FNC may be responsible for signature behavioral characteristics of the atypical population.

Here in this chapter authors have compared FNC differences of the autistic and neurotypical population in the longitudinal direction. The fMRI data of volunteers, developing typically and with ASD, were taken from three different labs which are working in collaboration under International Neuroimaging Data-Sharing Initiative. Although the resting state data were generated with different MRI machines with different acquisition protocols, authors were able to decompose the data into same RSNs and this reflects the robustness of the resting state networks. The FNC of resting state networks associated with cognitive functions are determined here and these networks are anterior default mode network (DMNI), posterior default mode network (DMNII), right fronto-parietal network (RFPN), left fronto-parietal network (LFPN), salience network (SN) and basal ganglia network (BGN).

4.1.1 Baseline of Static Functional Network Connectivity

Spatial ICA disintegrates fMRI data into functional networks which is comprised of both the spatial map and the respective timecourse. It is represented in the foloowing equation $S(x,t) = \sum_{k=1}^{K} M_k(x)A_k(t)$ where K is the number of spatially independent components, M_k is the spatial map of component, and A_k is the timecourse of component k. The ICA based correlation between network x_1 and x_2:
$C_{ICA}(x_1,x_2) = \frac{\sum_{t=1}^{T}(\sum_{k=1}^{K} M_k(x_1)A_k(t)\sum_{l=1}^{K} M_l(x)A_l(t))}{\sqrt{\sum_{t=1}^{T} S^2(x_1,t)\sum_{t=1}^{T} S^2(x_2,t)}}$

arranging the terms $k = l$ and $k \neq l$ yields:

$$C_{ICA}(x_1,x_2) = \frac{\sum_k M_k(x_1)M_k(x_2)\sum_{t=1}^{T} A_k^2 t}{\sqrt{\sum_{t=1}^{T} S^2(x_1,t)\sum_{t=1}^{T} S^2(x_2,t)}} + \frac{\sum_{k\neq l} M_k(x_1)M_l(x_2)\sum_{t=1}^{T} A_k(t)A_l(t)}{\sqrt{\sum_{t=1}^{T} S^2(x_1,t)\sum_{t=1}^{T} S^2(x_2,t)}}$$

where the first term is the representation of the sum over within network connectivities (total WNC), and the second term is the sum over between network connectivities (total BNC). Hence, total connectivity:
$C_{ICA}(x_1,x_2) = TotalWNC + TotalBNC.$

4.2 Materials and Methods

4.2.1 Data

To contrast the FNC profile of people with ASD from neurotypicals longitudinally, participants of three developmental stages, viz., childhood, adolescence, and adulthood are considered. The RsFMRI

data used in the present work is downloaded from the autism brain imaging data exchange (ABIDE I) website [158] along with complete phenotypic and scanning information. ABIDEI is a part of International Neuroimaging Data-Sharing Initiative (INDI) and 1000 Functional Connectomes Project [159]. Data shared by Stanford University, Leuven University, and Carnegie Mellon University are used here in the present work and, the volunteers participated at these universities belongs to different age groups, children, adolescence, and adult respectively. The diagnosis of autistic disorder was established either using the autism diagnostic interview-revised (ADI-R) [160] or according to the diagnostic and statistical manual of mental disorders, fourth edition, Text Revision (DSM-IV-TR) criteria. Typically developing controls had no history of neurological or psychiatric conditions nor a current medical, developmental or psychiatric diagnosis. They did not report any language problems.

4.2.2 Image preprocessing and independent component analysis

The preprocessing is done in accordance with the connectome computation system (CCS) pipeline which begins with leaving first four volumes followed by slice timing correction, motion realignment and intensity normalization. Nuisance variable regression is carried out after basic preprocessing to clean confounding variation due to physiological processes (heart beat and respiration), head motion, and low-frequency scanner. The global mean signal was included with nuisance variable.

Further to decompose the preprocessed fMRI data, SICA was accomplished, using the Group ICA fMRI Toolbox [126]. In group ICA method, images from all the subjects should be concatenated prior to ICA. To reduce the computational burden the concatenated data were first reduced to 75 components, and then further reduced to 50 components. The trimmed dataset was decomposed using the COMBI algorithm. Finally, the components were back reconstructed using the group ICA tool. Spatial maps were claimed as RSN on the basis of the values of dynamic range and the ratio of power at low frequency to higher frequency [127, 161]. Components were visually inspected and networks underlying the default mode network, lateralized fronto-parietal networks, BGN, and SN were interpreted on the basis of their spatial scope.

4.2.3 Functional network connectivity

The FNC analysis was executed, employing the FNC Toolbox (version 2.2), an add-on to the GIFT software. The FNC toolbox was earlier utilized by Jafri et al. [131] to examine FNC in schizophrenia. The toolbox computes a constrained maximal lag correlation between each pair of networks of interest by calculating Pearsons correlation and constraining the lag between the time courses. With six networks of interest, the number of possible pair-wise combinations to examine between-network

connectivity is 15. Subject specific timecourses were detrended and despiked, then filtered using a fifth-order Butterworth low-pass filter with a high-frequency cutoff of 0.15 Hz.

4.3 Static Connectivity Results

Each fMRI dataset was decomposed into 50 independent components, of which around 20 components were identified as resting state networks. Functional Network connectivity analysis was carried out among six cognitive RSNs i.e. DMN I, DMN II, LFPN, FPN, SN, and BGN. These networks are gathered in Fig.4.1, where orthogonal views of each of them are depicted for voxels with peak values. Default mode networks and the rest task positive networks are connected functionally. The FNC analysis was done for all the three groups of both cohorts separately. These correlation maps are depicted in Fig. 4.2, where the maps in the left are for the typically developing population and maps for the autistic patients are arranged to the right.

Cumulative observations are as follows 1) DMN I maintain negative correlations with anterior salience, basal ganglia and left executive control networks. 2) Connectivity between basal ganglia and the two executive control networks swings between the positive and negative correlation throughout the development trajectory. This swinging nature can be observed between BGN and DMN II and also between anterior salience and right frontparietal network. 3) Positive correlations have been found among the rest pairs of networks in all the three stages.

Exploring the differences in the connectivity of cognitive networks of the two cohorts at each developmental stage can shed light on the atypical functional integration of the networks that lead to the functional deficiency of autistic population. Theses sFNC differences are depicted as a connectogram for the three groups in Fig 4.3 Autistic children had FNC differences with the group of typically developing children viz., anterior salience has higher connectivity with the rest cognitive networks except with DMN II, FNC of DMN II with the rest of the networks are indifferent to the two groups. The connectivity among the two default networks and between BGN and LFPN is weaker, the two fronto-parietal networks had no connectivity while DMN I share a stronger functional connection with BGN.

For adolescence, the second neurodevelopment stage considered here, FNC differences were also found. At this stage, functional connectivity between nine pairs of networks of the autistic population was different than the other group. The two fronto-parietal networks of autistic adolescents were also functionally disconnected.

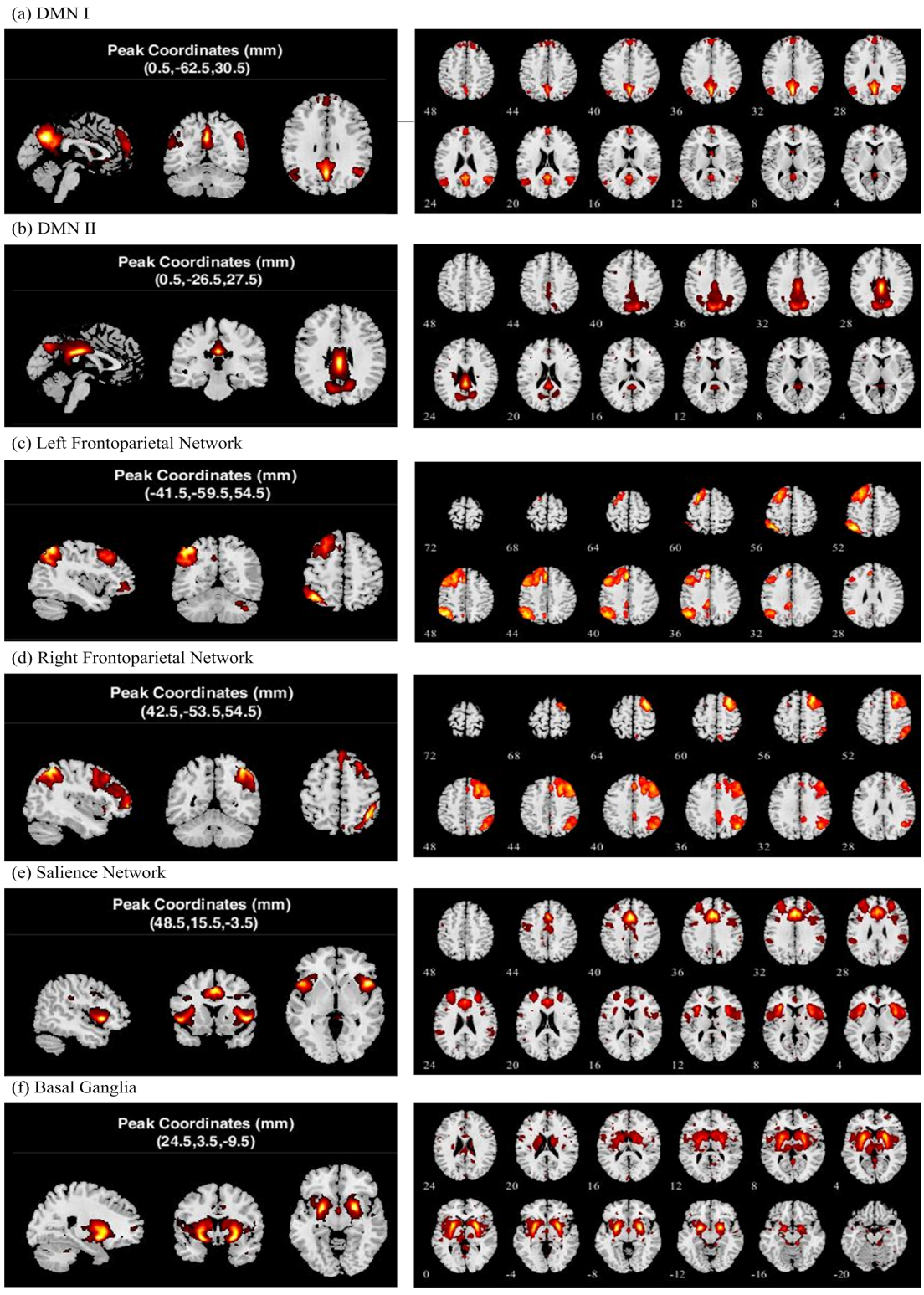

Fig. 4.1: Cognitive RSNs (a) DMN I, (b) DMN II, (c) LFPN (d) RFPN, (e) SN, and (f) BGN. The three orthogonal views, viz. saggital, coronal and axial of each network alongwith the peak MNI coordinates are depicted. Multiple axial slices of each network are kept for better visualization.

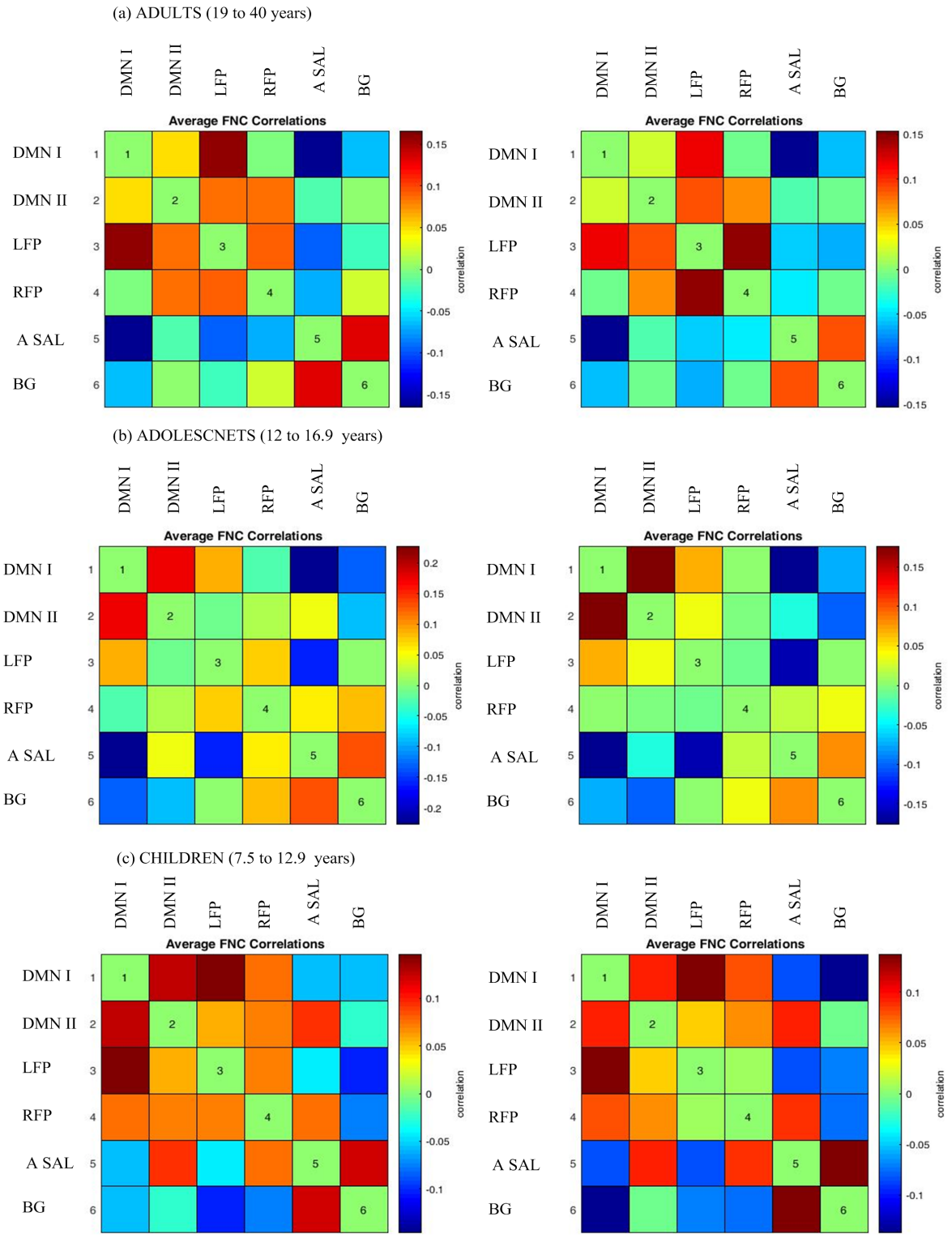

Fig. 4.2: Mean correlations (Fisher's Z scores) among six networks for neurotypicals and atypicals of three age groups. For each group correlation map in the left is for typically developing individuals and the map in right is for individuals with ASD. The vertical bar shows the correlation values.

The strength of four pairs of RSNs of atypically developing group was reversed from the previous stage and they are a) anterior salience and BGN, b) anterior salience and RFPN, c) DMN I and DMN II and d) DMN I and BGN. The DMN II shares stronger FC with BGN and LFPN while BGN and RFPN shares weaker bonding. Correlation between DMN II and salience network has positive value for typically developing adolescents but negative value for the autistic group.

The groups of neurotypical and atypical adults also have FNC differences . The LFPN and RFPN networks of the adult autistic brain have stronger connectivity while for the two earlier stages they had no connectivity. The FNC between the two default networks of the autistic brain was found weaker in adulthood too. The SN has weaker connectivity with LFPN, RFPN and BGN although for the group of autistic children it shares stronger functional bonding with them. The FNC of BGN and LFPN, which was indifferent compared to adolescents group of neurotypical and was weaker than typically developing cohorts for the group of children, is stronger for the adult autistic cohort. At this stage, BGN and RFPN have no connectivity in the atypical group.

4.4 Discussion

In order to investigate the underlying atypical functional integration among the cognitive RSNs which may lead to the behavioral manifestations of an autistic individual, a age-stratified study of between network connectivity was executed in this chapter. With six resting state networks of interest, 15 pair-wise combinations were possible to examine FNC. Mostly the connectivity of SN and BGN with each other and with other cognitive RSNs differ for the two cohorts for all developmental stages considered here. Hyperconnectivity of SN is found for autistic children and it matches with the previous findings of Uddin et. al. [78], even they have proposed this distinguishable feature to use as a biomarker to identify children suffering from ASD. Further, in advanced stages, SN shows hypoconnectivity with other networks.

One of the earliest manifestations of autism is enlarged head circumference. Infants and toddlers with ASD show signs of early brain overgrowth. Although the relationship between neuron density and brain size is fuzzy, post-mortem studies of children with ASD indicate that they have excess numbers of neurons in the prefrontal cortex. Some of these differences vanish with development, such that autistic and typically developing individuals are indifferent on measures of brain size. An overabundance of neurons in the prefrontal cortex which is a part of salience network may be responsible for the hyperconnectivity of SN while hypoconnectivity of it during the advanced stages may be the result of vanishing of differences mentioned above.

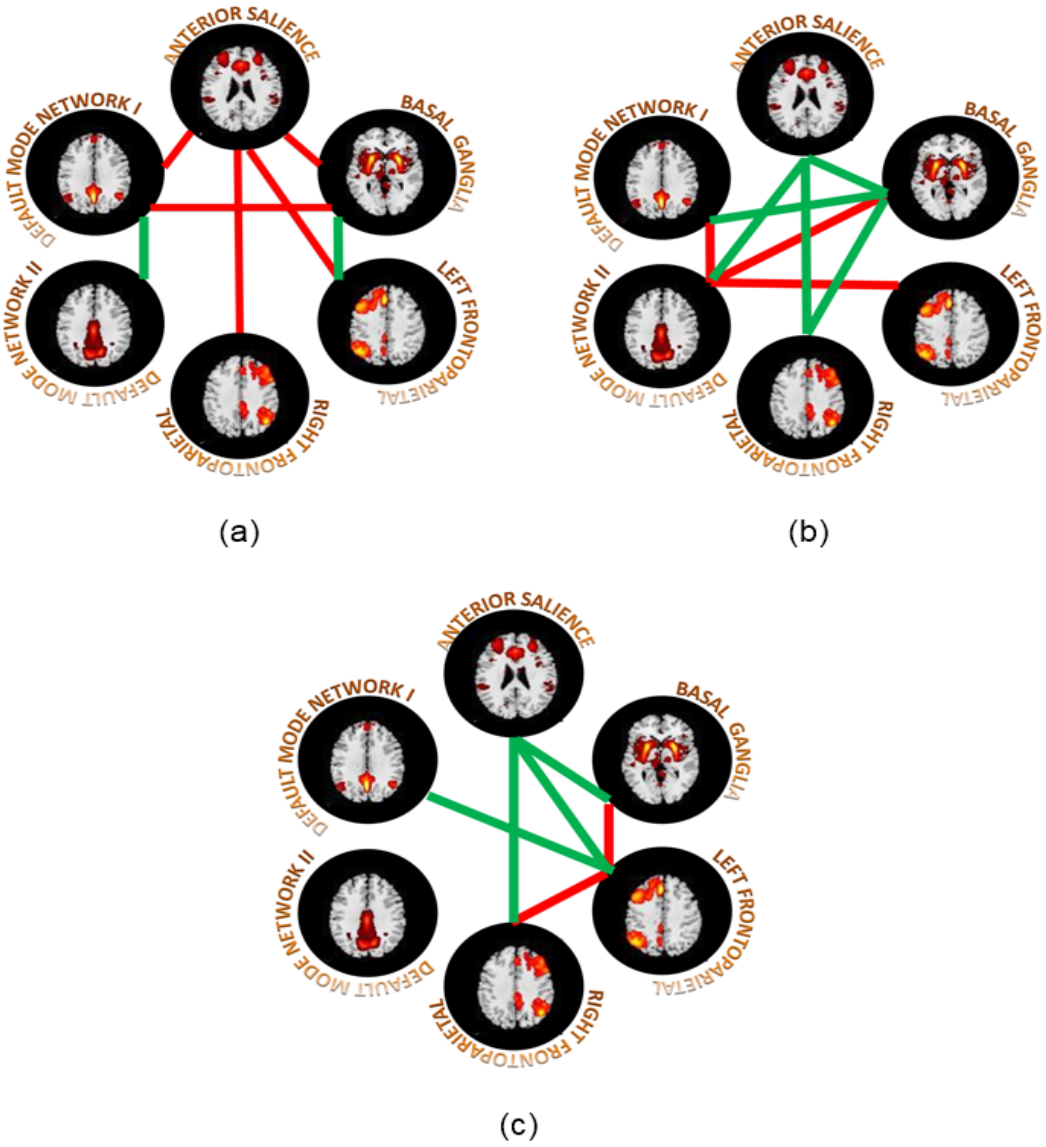

Fig. 4.3: The difference of functional network connectivity between the healthy cohorts and folks suffering from ASD at three developmental stages (a) childhood, (b) teenage, and (c) adulthood. The red lines represent stronger functional connectivity (FC) the green lines represent weaker FC. Anterior salience network in children with ASD have strong FC with basal ganglia and the two frontoparietal networks , while these functional connection gets weaker for the next two developmental stages in patients. The two default mode networks of ASD cohorts has weaker FC in first stage, stronger FC in intermediate stage and no FC difference in the last stage. The FC between salience network and basal ganglia in ASD cohorts is stronger in childhood, weaker in teenage and they have no FC difference between the two adult groups.

Lateralized fronto-parietal components have been associated with different functions, i.e., memory, language, attention and visual processes [150]. The absence of functional connectivity between these two networks may be responsible for deficiency in one or more functionality of autistic children and adolescents.

4.5 Summary

The SN manifest aberrant patterns of brain connectivity in the various stages of developmental trajectory. Attention allocation to stimuli that is salient to the individual is the conventional responsibility of the SN and atypical development of the salience network may lessen interest in social interaction, a signature characteristic of ASD. No connectivity between LFPN and RFPN during childhood and adolescence of atypical population may be one of the reasons behind their hallmark behavioral characteristics.

CHAPTER 5

AGE STRATIFIED FUNCTIONAL NETWORK BASED DYNAMIC FUNCTIONAL NETWORK CONNECTIVITY ANALYSIS IN AUTISM

Biomarkers have been investigated for the entire gamut of autism. Past work seeking for connectivity biomarkers responsible for signature manifestations of ASD had analyzed either toddlers, or mixed groups of youngsters and teenagers, or aged folks in autonomous investigations. Diverging from most examinations, authors explored entire functional organization and present the first age-stratified functional network-based dynamic connectivity analysis in autism. Findings of this work are dissimilar to the speculations that hyper-connectivity of brain networks are prevalent in young children with ASD, while hypo-connectivity are more common in young people and adults with the disorder when compared to typically developing cohorts. The statistically significant functional network connectivity differences (fdr<= 0.05) are sparse in the group of children and adults and even the significant intra-connectivity differences do not influence over the interconnectivity differences in the children's group of ASD.

5.1 Background and Motivation

Autism spectrum disorders (ASD) are symbolized by noteworthy social, pragmatics, and behavioral disabilities. The expression "spectrum disorders" alludes to the way that in spite of the fact that individuals with ASD share some basic symptoms, ASD influence distinctive individuals in various courses, with some encountering exceptionally gentle indications and others encountering extreme manifestations. ASD incorporate autistic disorder and the by and large less serious structures, Asperger's syndrome and pervasive developmental disorder-not otherwise specified (PDD-NOS). Youngsters with ASD may need enthusiasm for other individuals, experience difficulty appearing or discussing sentiments, and maintain a strategic distance from or oppose physical contact. A scope of communication issues are found in youngsters with ASD: some talk exceptionally well, while numerous kids with an ASD don't talk by any means. Another trademark norm for ASDs is the exhibit of prohibitive or fixated interests, for example, arranging toys, fluttering hands, shaking his or her body, or turning in circles. ASD is hereditary to a great extent [162, 163] and exceptionally pervasive [164] neurodevelopmental disorder.

The exact idea of the neuropathology in ASD is not completely caught on. Anatomical examinations and autopsy have recognized cellular and volumetric abnormalities of various brain areas [165–167]. Functional neuroimaging examinations have been correspondingly conflicting, with reports of atypical brain reaction in an assortment of regions. In any case, confirmation of aberrant localization, intensity, and inconstancy of neural action in ASD proposes extensively disorganized functional brain configuration [168, 169]. Conflicting reports of territorial brain atypicality from the norm are not especially astonishing given the formative idea of ASD. It is a firmly hereditary disorder set apart by early brain overgrowth [169, 170], irregular examples of white tissue advancement [170], and disability in various psychological spaces by age three. Such early aggravations without a doubt change formative directions for harrowed people in different and complex ways, and would subsequently not be anticipated to have surrounded neural impacts. Or maybe, impacts would be across the board, mirroring the continuous interaction of pathology, ordinary maturational procedures, and experience.

There is expanding conceptualization of conduct and discernment as being rising properties of brain networks. According to this archetype, a network comprises of numerous areas or hubs (that might be spatially inaccessible from each other) showing steady, systemized pattern of reproducible co-initiation when brain work is measured. This patterned co-actuation between hubs inside a network has been named Functional Connectivity (FC), and various methods might be utilized to look for and characterize networks, including blind source separation (e.g., ICA), seed-based, graph and clustering strategies. The impression is building of being many, stable networks in the human brain exist crosswise over people that have been related with particular behavioral or intellectual capacities, for example, vision [171]. Networks are robust to conditions, and many have been recognized amid assignment execution that relate to those found in the wakeful resting state [172], anesthesia and rest [173], proposing resting state neurocognitive formats as a good alternative of task based studies [174]. These observations cumulatively propose these large scale networks might be hereditary in human brain working, offering ascend to the moniker 'Intrinsic connectivity networks' (ICNs) [175]. Coactivations between ICNs is termed as Functional Network Connectivity (FNC). The FNC is derived between all the possible combinations of N networks, or [(NxN)- N]/2.

However these methodologies have utilized measures of brain connectivity averaged over several minutes subsequently blurring dynamics of brain action. Dynamics are conceivably much more conspicuous amid resting-state [45], amid which mental action is unconstrained, than in task based studies. By not catching the basic changes in dynamics essential contrasts are clouded and our capac-

ity to identify the practical brain changes that portray complex neuronal disorders is obscured. There is late enthusiasm for this point as a few new examinations have concentrated on powerful FNC changes. Concentrates in both animals and people showed that the unconstrained blood oxygen level dependent (BOLD) signals measured amid rest display inborn spatiotemporal dynamic association [176–179] This resting state fMRI (RsfMRI) investigation attempt to compare dynamics of whole-brain functional network connectivity in ASD and typically developing (TD) individuals utilizing an entirely information-driven approach. Authors investigated the characteristics and degree of functional contrasts both inside and between-networks when looking at ASD and TD people crosswise over three age gatherings $\rightarrow$ kids (under 11), teenagers (11 $\rightarrow$ 18), and adults (more than 18).

5.1.1 Sliding-Window dFNC

To comprehend the sliding window correlation it's numerical representation is simplified here. Sliding-window covariance for two time-series p and q with sampling period TR is defined as follows at scan k.

$$\begin{aligned} C_{pq}[k] &= cov(p[k-\triangle, k+\triangle], q[k-\triangle, k+\triangle]) \\ &= \frac{TR}{w} \sum_{j=k-\triangle}^{k+\triangle} (p_j - \bar{p_k})(q_j - \bar{q_k}) \end{aligned}$$

where

$$\begin{aligned} w &= (2\triangle + 1)TR \\ \bar{p_n} &= \frac{TR}{w} \sum_{j=k-\triangle}^{k+\triangle} p_j \end{aligned}$$

After some elementary manipulations

$$\begin{aligned} C_{pq}[k] &= \frac{TR}{w} \sum_{j=k-\triangle}^{k+\triangle} p_j(q_j - \bar{q_k}) - TR\frac{\bar{x}}{w} \sum_{j=k-\triangle}^{k+\triangle} (q_j - \bar{q_k}) \\ &= \frac{TR}{w} \sum_{j=k-\triangle}^{k+\triangle} p_j(q_j - \bar{q_k}) \\ &= \frac{TR}{w} \sum_{j=k-\triangle}^{k+\triangle} p_j q_j - \bar{q_k}\frac{TR}{w} \sum_{j=k-\triangle}^{k+\triangle} p_j \\ &= \frac{TR}{w} \sum_{j=k-\triangle}^{k+\triangle} p_j q_j - \bar{p_k}\bar{q_k} \end{aligned}$$

The sliding window correlation:

$$Corr_{pq}[k] = \frac{C_{pq}[k]}{\sqrt{C_{pp}[k]C_{qq}[k]}}$$

5.2 Methodology for Dynamic Functional Network Connectivity Analysis

5.2.1 Resting-state fMRI Images

The RsfMRI images in search for the functional connectivity based biomarker of ASD are gathered from the autism brain imaging data exchange (ABIDE I) website [84] along with the entire make up details and scanning details. ABIDEI is a subset of International Neuroimaging Information Sharing Initiative (INDI) and 1000 Functional Connectomes Project [180]. The RsfMRI data present in this repository are collected from around 16 different laboratories and the volunteers participated were from different age groups. Authors utilized the images shared by Stanford University, Leuven University, and Carnegie Mellon University and the participants got scanned at those venues belongs to different age groups, children, teenager, and adults respectively. Participants demographics are summarized in table5.1

5.2.2 Image Processing and Independent Component Analysis

The pre-processing is done as per the connectome computation system (CCS) protocol which starts with skipping initial four volumes followed by slice timing correction, motion realignment and intensity normalization. Confounding variables brought in either by scanner, head motion, breathing or pulsation are regressed out after primary processing of images. The global mean signal is incorporated with disturbance variable. The processed images are decomposed by spatial ICA (SICA), using the Group ICA for fMRI Toolbox [152]. A higher order model i.e. 100 is selected for SICA. The COMBI algorithm is utilized to break down the datasets [122]. At last, the parts are back reconstucted utilizing the group ICA tool. Spatial maps are guaranteed as ICN on the premise of the estimations of dynamic range and the proportion of power at low frequency to higher frequency. The MNI coordinates of the group maxima are changed to the Talairach stereotactic space. The brain areas are marked by the Talairach daemon tuned to an inquiry scope of 2mm. Components were visually inspected and RSNs are labelled on the basis of their spatial scope.

Table 5.1: Participants demographics

	ASD	**TD**
Children		
Mean age	9.96	9.95
Age range	7.5 —12.9	7.5 —12.9
Gender	16M/4F	16M/4F
FSIQ	78 —148	79 —136
Teenager		
Mean age	14.34	13.92
Age range	12.1 —16.8	12.1 —16.9
Gender	12M/3F	17M/3F
FSIQ	not available	not available
adults		
Mean age	26.35	26.84
Age range	19 —39	20 —40
Gender	11M/3F	10M/3F
FSIQ	95 —134	101 —129

5.2.3 Dynamic Functional Network Connectivity

The dynamic FNC are evaluated utilizing a sliding window approach instantiated in the dFNC toolbox in GIFT. First, the time-courses were detrended and despiked using 3D despike in the AFNI software then filtered using a fifth-order Butterworth low-pass filter with a high frequency cutoff of 0.15 Hz. Then, FNC covariance matrices were calculated between all pairwise ICN for each subject using the correlations derived from our ICA analysis by moving a Gaussian window in 1 TR increments across the subject TCs. Successive FNC matrices for each window were then concatenated to form a [33 x 33 x (number of window units)] array representing a state transition vector, or how the FNC state changed through time for each subject. Subsequently, a clustering analysis is done to examine the structure and frequency of FNC patterns that recurred in the state transition vectors. The k-means clustering algorithm was applied to the individual arrays of FNC covariance matrices using the City method and the algorithm iterated a maximum of 200 times before convergence.

5.3 The dFNC Results

The COMBI with a high order model was successfully used to decompose the fMRI images of typically developing (TD) subjects and patients with ASD. Spatial maps identified as ICN were bunched based on their neurocognitive function, and some exemplars of each group is displayed in Fig 5.1. These groups are cognitive control networks (CCN), default mode networks (DMN), auditory (AUD), visual (VIS), basal ganglia (BG), sensorimotor (SM), and fronto-parietal networks (FP). In this developmental study three groups of both the cohorts are made i.e. children, teenagers, and adults. Unlike conventional FNC analysis that averages the connectivity across the RsfMRI time courses, the dynamic approach can separate significant differences in patterns of abnormal connectivity and locate these in individual states, providing a more granular picture of the structure of functional connectivity in ASD. Here, the 6 state, 30 TR size window solution is displayed in Fig 5.25.35.4

Further the mean is computed for each cluster state of both the groups and they are displayed in the Fig 5.55.65.7. Number of subjects with finite correlations are shown in these figures as well as the pairs of resting state networks who qualify the two-sample t test are circled. The overall dFNC differences can be divided into within network connectivity differences and between network connectivity differences. Significant differences are sparse for the groups of children and adults. The VIS and AUD networks have no significant within network connectivity differences in all the five states of the children's group, though they have in the other two groups. Within network connectivity differences exist for SM, and BG networks but only in any single state.

The FP network is such an ICN who does not possess any statistically significant intra-connectivity differences for even a single state for all the three developmental stages under consideration. All ICN except FP have many between network connectivity differences for all the three groups. The pairs of ICN those having significant differences may have positive correlation, negative correlation, or opposite correlation for both the populations and it is summarized with bar graphs in Fig 5.8.

For all the states except state 2 of the two groups of children, opposite functional connections (OFC) are higher. For these combinations of ICN in state 4 and 6 ASD subjects have a higher number of positive functional connections (PFC), in state 2 HC have a higher number of PFC and in the rest two states both the groups have nearly equal PFC. For the unanimous functional connections (UFC) when both the populations show either positive correlation or negative correlations there are differences between the strength of the functional connections. Except in state 2, ASD subjects show stronger correlations and except in state 4 and state 5, they are strongly anti-correlated.

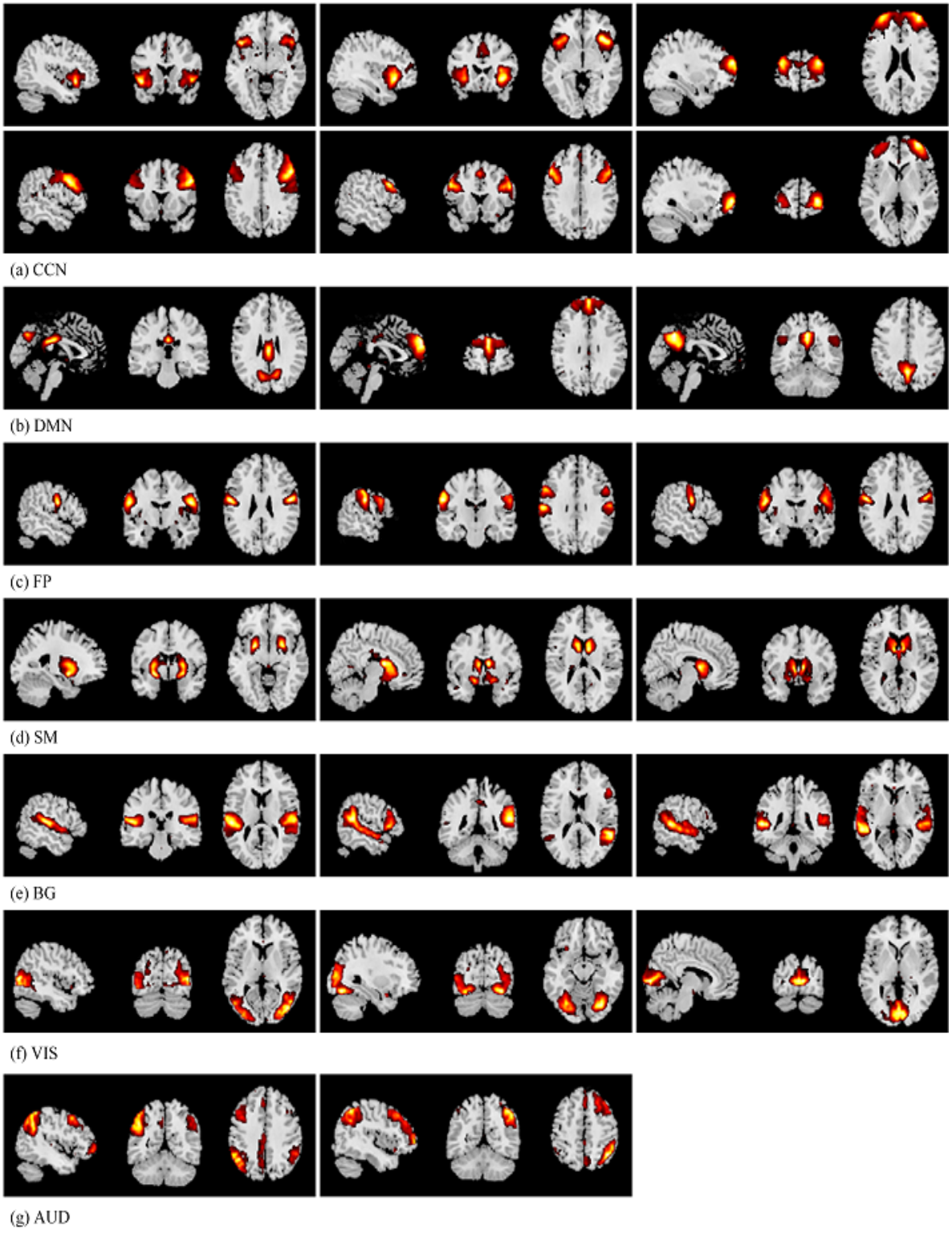

Fig. 5.1: Sagittal, coronal and axial alices of the exemplars of the seven ICNs viz., (a) CCN, (b) DMN, (c) FP, (d) SM, (e) BG, (f) VIS, and (g) AUD for peak intensity activation.

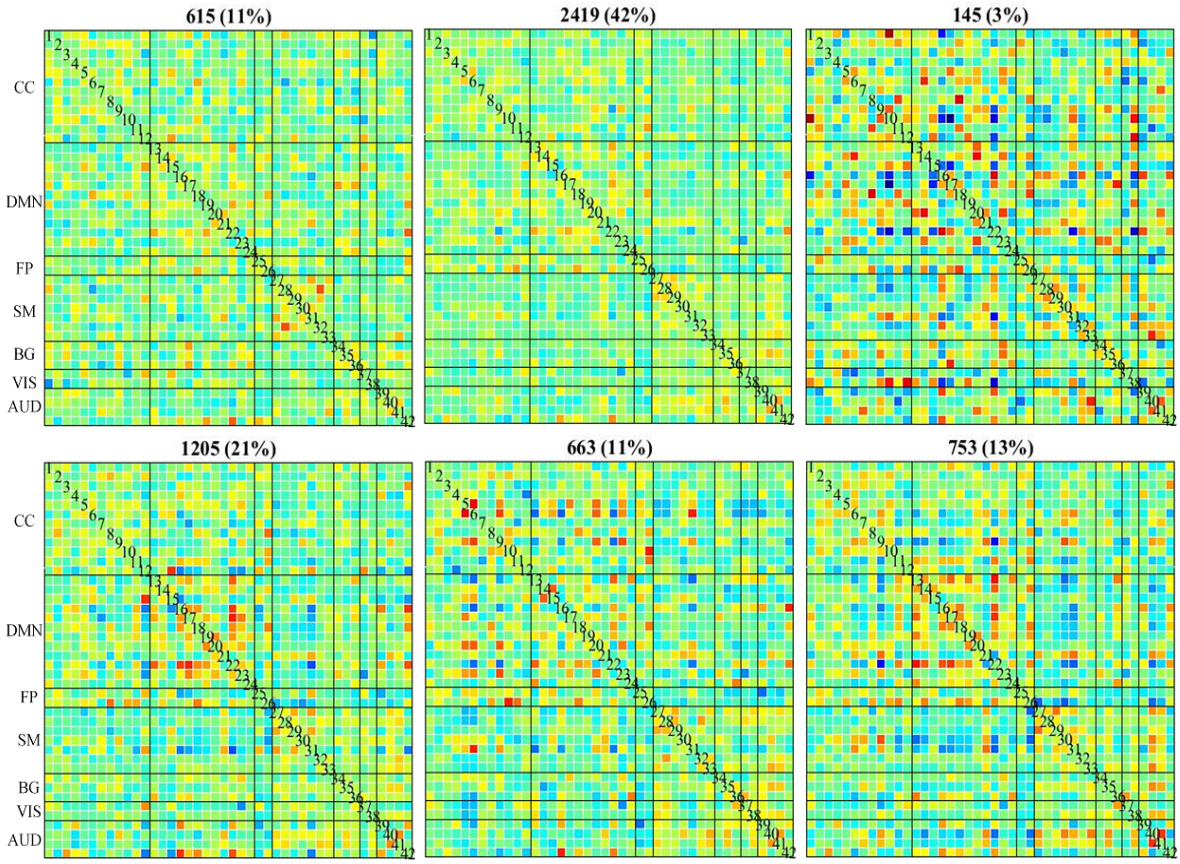

Fig. 5.2: Dynamic functional network connectivity states for the age group under 11. These states show FNC among six ICNs viz., CCN, DMN, FP, SM, BG, VIS, and AUD. The percentage of occurrence of states 1-6 are 11, 42, 3, 21, 11 and 13 respectively.

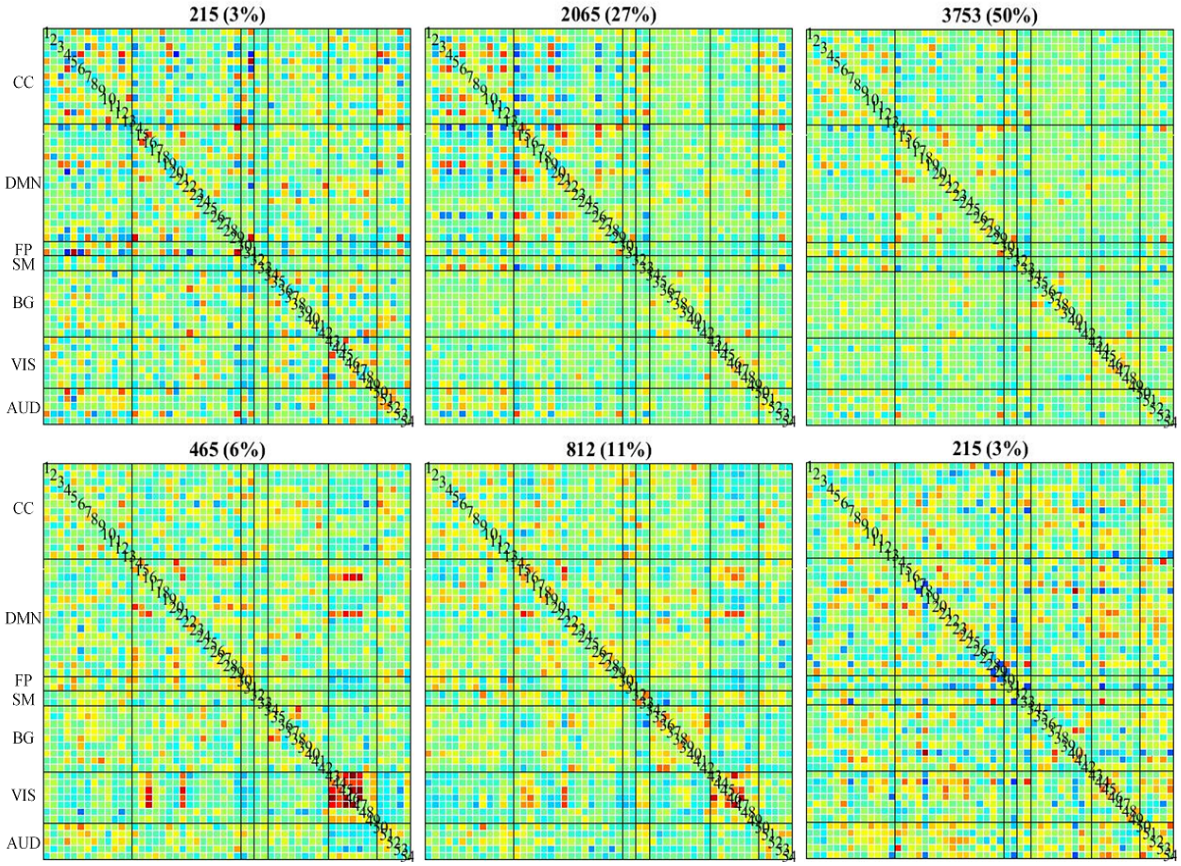

Fig. 5.3: Dynamic functional network connectivity states for age group (11-18). These states shows FNC among six ICNs viz., CCN, DMN, FP, SM, BG, VIS, and AUD. The percentage of occurrence of states 1-6 are 3, 27, 50, 6, 11, and 3 respectively.

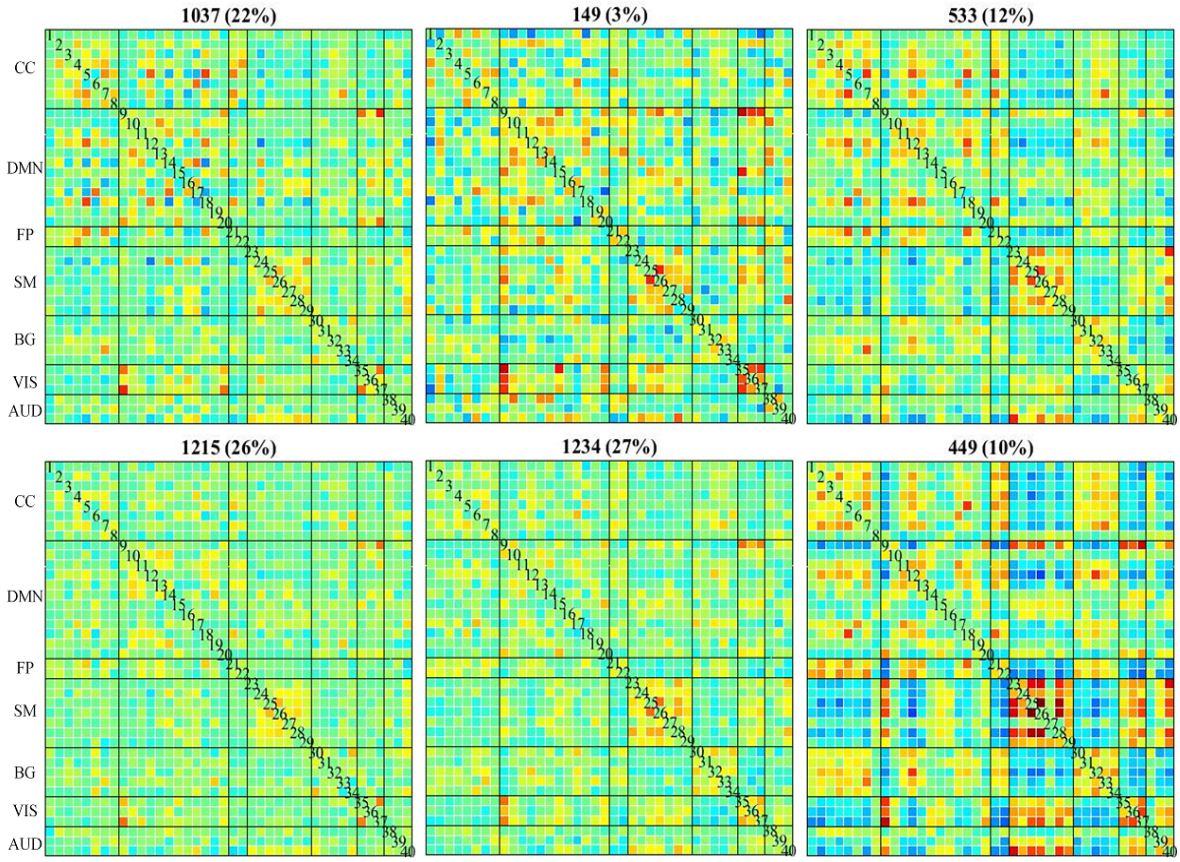

Fig. 5.4: Dynamic functional network connectivity states for age group above 18. These states shows FNC among six ICNs viz., CCN, DMN, FP, SM, BG, VIS, and AUD. The percentage of occurrence of states 1-6 for TD are 22, 3, 12, 26, 27 and 10 respectively.

The teenager's groups of the two cohorts have nearly equal OFC and UFC. In state 3 ASD folks have stronger anticorrelations. For the adult's groups also, only state 4 has a higher number of OFC and only in state 4 adult ASD folks has higher PFC. When the adult's group of the two cohorts are compared on the basis of UFC, only in the state 2 ASD folks have a higher number of strongly correlated or anticorrelated connections. Two sample t-test of mean dwell time (MDT), number of states, change between states, state span, and total distance between groups, HC and ASD, is also performed and it is arranged in table 5.2.

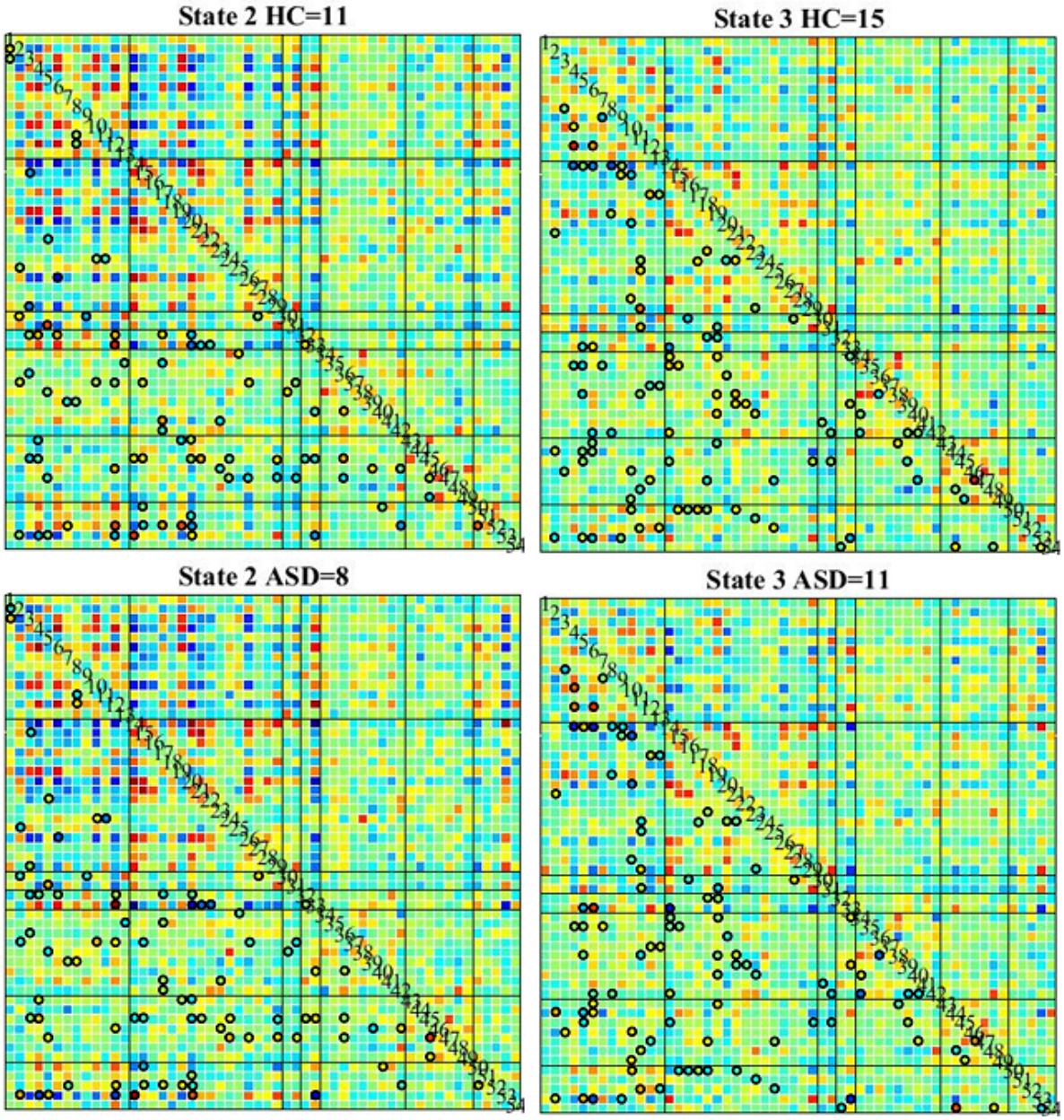

Fig. 5.5: Dynamic functional network connectivity states for ASD and TD cohorts for adolescents group. These states shows FNC among six ICNs viz., CCN, DMN, FP, SM, BG, VIS, and AUD. The pairs of ICN having statistically significant differences between the two group are circled.

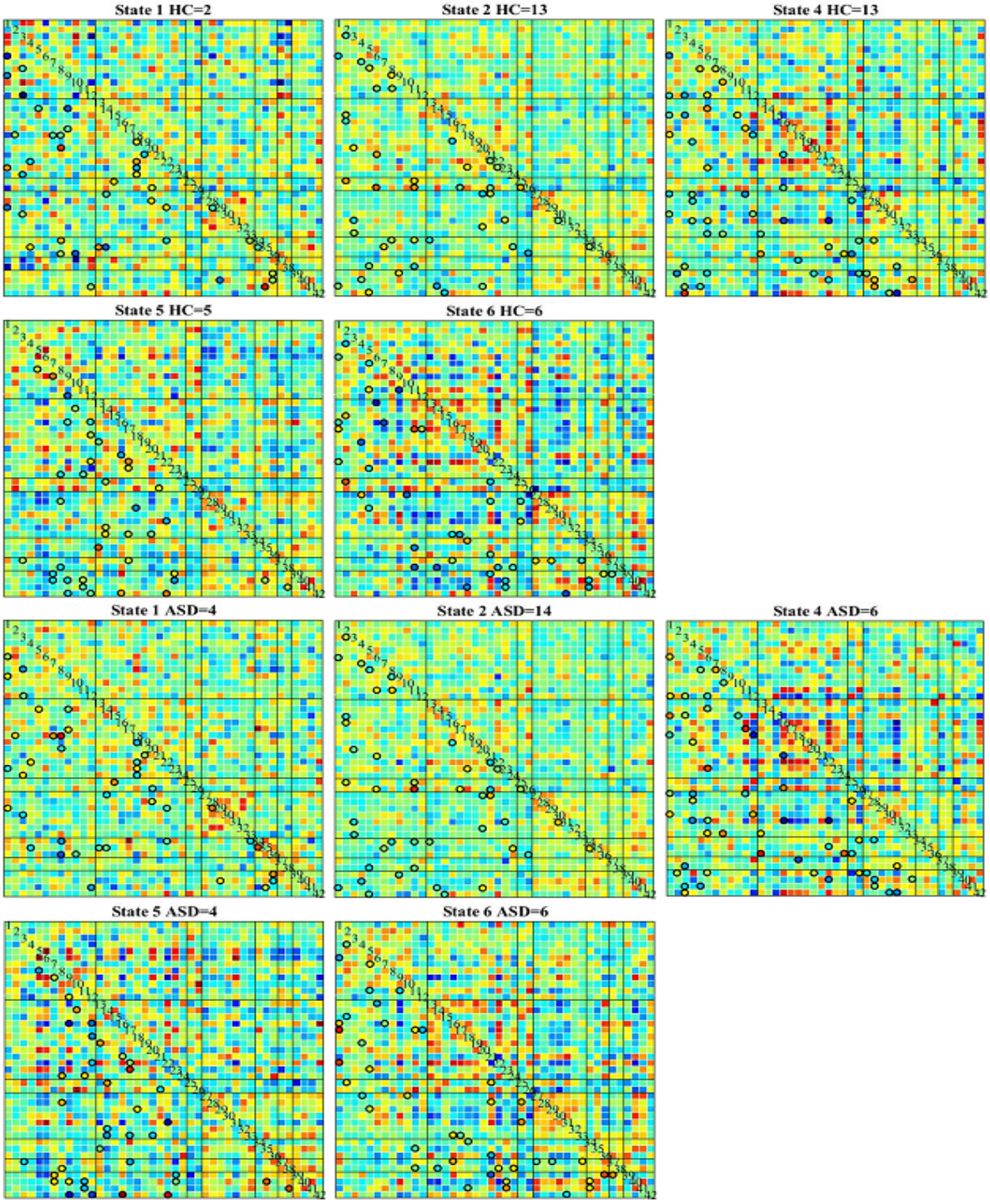

Fig. 5.6: Dynamic functional network connectivity states for ASD and TD cohorts for toddlers to school going children group. These states shows FNC among six ICNs viz., CCN, DMN, FP, SM, BG, VIS, and AUD. The pairs of ICN having statistically significant differences between the two group are circled.

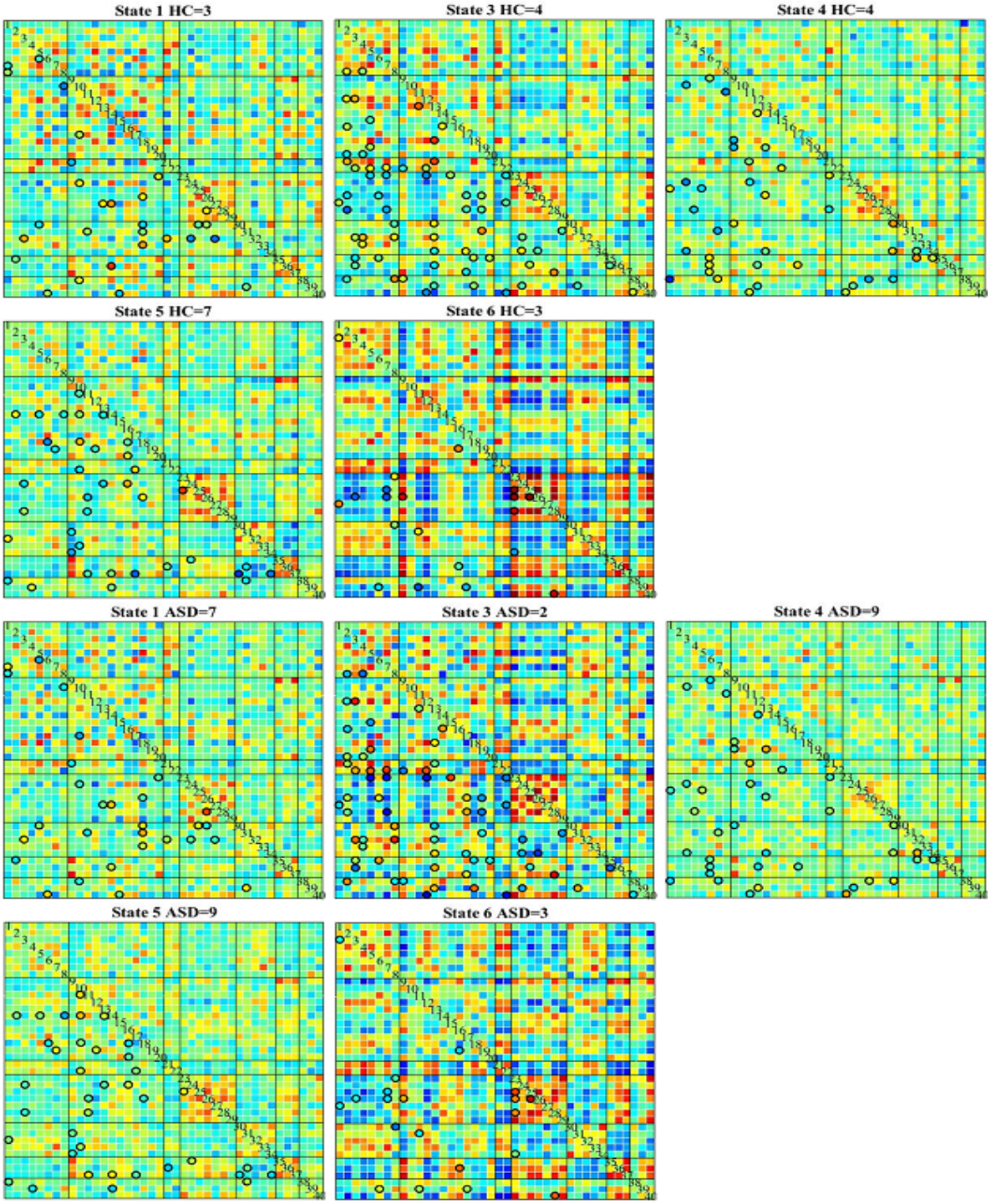

Fig. 5.7: Dynamic functional network connectivity states for ASD and TD cohorts for adult's group. These states shows FNC among six ICNs viz., CCN, DMN, FP, SM, BG, VIS, and AUD. The pairs of ICN having statistically significant differences between the two group are circled.

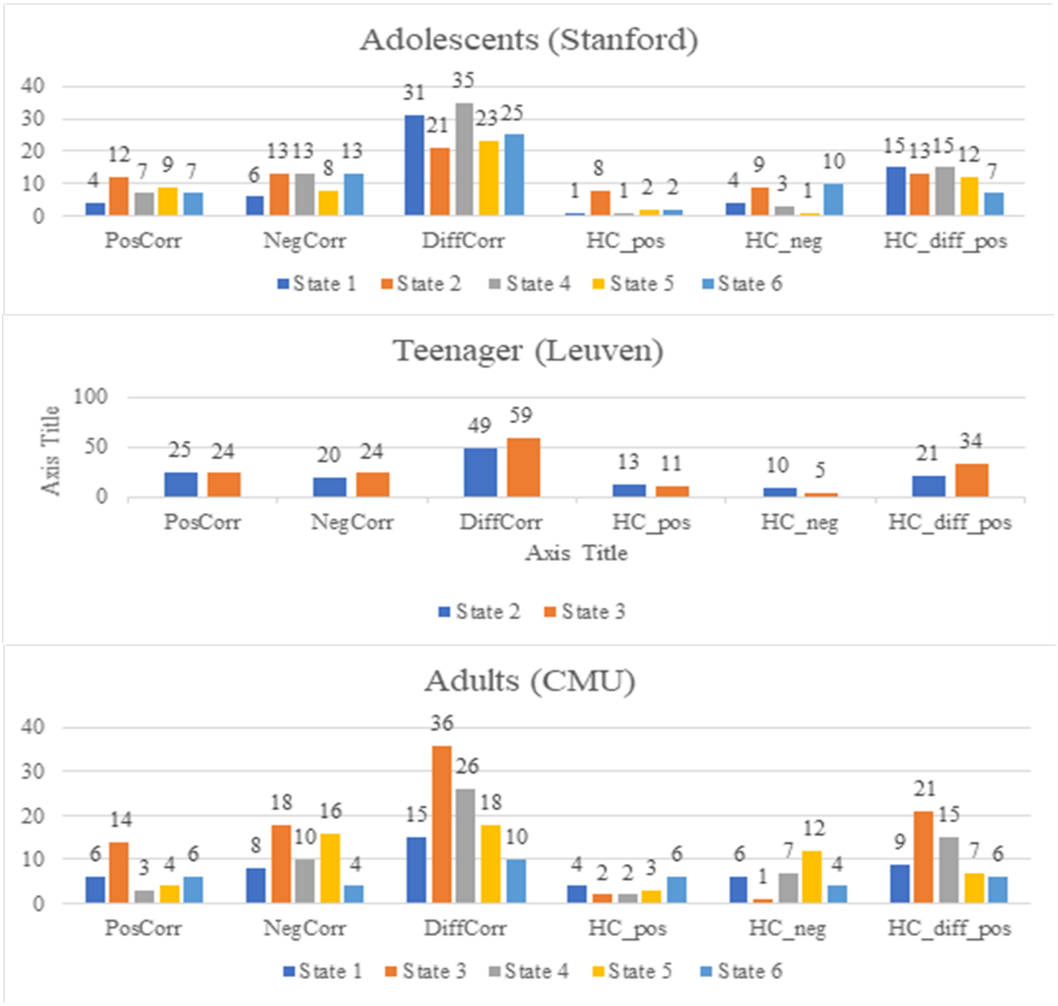

Fig. 5.8: Bar graph representation of the statistically significant dFNC differences between the three groups of ASD and HC cohorts in terms of direction and strength. The bar chart at the top is for the adolescent's group and in the middle, is for teenager's group and the bottom is for adult's group. The PosCorr, NegCorr, HC_pos, and HC_neg are the variables for unanimous functional connection (UFC) whereas DiffCorr and HC_diff_pos are for opposite functional connections (OFC). In the presence of UFC, the PosCorr and NegCorr represent the total number of RSN combinations those shows correlations and anticorrelations respectively. The HC_pos and HC_negative show the number of stronger correlation and stronger anticorrelation respectively manifested by HC folks. In the presence of different functional connections (DFC), DiffCorr represents the number of RSN combinations those are correlated for one group and anticorrelated for the other. The HC_diff_pos represents the number of RSN combinations who are positively correlated for HC folks.

Table 5.2: Two sample t-test of mean dwell time (MDT), number of states, change between states, state span, and total distance between groups, HC and ASD.

Children (MDT)			
State	p-value	T-value	
1	0.9141	0.1086	
2	0.1601	-1.4326	
3	0.3236	-1.0000	
4	0.0056	2.9396	
5	0.2836	-1.0876	
6	0.6468	-0.4618	
Method	Num States	Change Between States	State Span
K-means	Tval =0.3473, Pval =0.7303, Mean of Group1 =12.5000, Mean of Group2 =12.0500	Tval =0.1946, Pval =0.8468, Mean of Group1 =20.2000, Mean of Group2 =19.8500,	Tval =-1.2319, Pval =0.2256, Mean of Group1 =4.9000, Mean of Group2 =5.4000
Teenager (MDT)			
State	p-value	T-value	
1	0.2541	-1.1606	
2	0.1193	1.5991	
3	0.5512	0.6022	
4	0.0730	-1.8519	
5	0.0505	2.0299	
6	0.2541	-1.1606	
K-means	Tval =0.9310, Pval =0.3586, Mean of Group1 =16.7500,	Tval =0.4080, Pval =0.6859, Mean of Group1 =31.2000,	Tval =-1.9480, Pval =0.0600, Mean of Group1 =10.8500,

	Mean of Group2 =14.8667	Mean of Group2 =30.0667,	Mean of Group2 =13.0000
Adults (MDT)			
State	p-value	T-value	
1	0.7675	0.2989	
2	0.3086	1.0393	
3	0.1326	1.5547	
4	0.2900	-1.0811	
5	0.7780	0.2850	
6	0.4766	0.7226	
K-means	Tval =-0.3028, Pval =0.7645,	Tval =0.3910, Pval =0.6991,	Tval =-0.5400, Pval =0.5940,
	Mean of Group1 =22.6923,	Mean of Group1 =33.6923,	Mean of Group1 =9.3077,
	Mean of Group2 =23.5714	Mean of Group2 =32.4286,	Mean of Group2 =9.8571

The dynamic perspective of FNC results of this study completely reject the hypothesis that hyper-connectivity of brain networks is prevalent in young children with ASD, while hypo-connectivity are more common in young people and adults with the disorder when compared to typically developing cohorts. Few findings of this study are also not in accord to the previous results presented in the literature. Within network connectivity among the constituent ICNs of a modular organization is not unidirectional as expected, rather some are anticorrelated. The DMN is not strictly anticorrelated with task positive networks.

5.4 Discussion

Overall, the results demonstrate that children with ASD exhibit atypical within and between-network functional connectivity. Importantly, these results are completely not in accord with the developmental trajectory hypothesis proposed by [78] predicting hyper connectivity in young children with ASD and hypo-connectivity in adults with ASD. Additionally, the current results are in accord with previous ideas suggesting that increased within-network connectivity in children with ASD could be responsible for reduced between-network connectivity as tighter coupling within networks could

lead to reduced coupling between networks [78]. The justification for this hypothesis was based on previous research which have shown that ASD is characterized by increased head circumference in childhood [181] while in-vivo [182] and post-mortem studies [183] have shown increased neuronal growth in children with ASD from 2_5 years and 2_16 years respectively.

One previously proposed explanation for the findings of changing functional connectivity across development in ASD is that the pubertal period during adolescence is responsible for changes in underlying brain organization, and that pubertal hormones may differentially affect developmental trajectories in the disorder [184]. Hormonal changes during puberty have been linked with changes in both gray and white matter [185]. However, there have been no cross-sectional or longitudinal studies examining changes in functional connectivity that accompany the pubertal transition in humans, in either typical or atypical development. Unfortunately, a large amount of ASD research is conducted on adolescents and adults, probably due to the difficulty in acquiring artifact-free fMRI data from younger children, especially young children with psychiatric disorders such as ASD [186]. The previous study finding a lack of hypo-connectivity in adults [77] used only participants older than 18 years in a data-driven ICA analysis. However, two other studies using ICA with participants over 18 have found hypo-connectivity in ASD [86].

Although the ASD cohorts do possess statistically significant differences with TD patients in all the three developmental stages considered in this study, but it is the cumulative result of the time profiles of subnetworks of any ICN who establishes functional connections in various dynamic states. In such a scenario a RSN whose FNC is less dynamic should be considered for a reliable biomarker establishment. The biomarkers which contrast the FNC differences between the ASD and TD cohorts should be explored either in the children's group or in the adults group as the significant differences are sparse in these two stages. The FP network does not have any significant within network connectivity differences in all the three group. Besides this the significant interconnectivity differences of FP with other networks are in one or two states only.

5.5 Summary

The FNCs in ASD significantly fluctuated in literary works as a result of methodological and subject choice contrasts. Early examinations regularly centered around locale differences in activation during tasks, with more recent studies utilizing RsfMRI concentrated in seed based techniques and low-order ICA models. The current findings support adopting a developmental perspective to help reconcile the heterogeneous findings of functional hypo- and hyper-connectivity observed in the RsfMRI lit-

erature in ASD. The overall functional network connectivity differences between the two groups are determined in this work. A careful examination of these dFNC maps shows that few ICN deserves a separate exhaustive analysis of their time profile. By doing so concrete results can be drawn regarding the signature manifestation of ASD patients.

CHAPTER 6

CONCLUSION AND FUTURE SCOPE

6.1 Conclusion

The current work was done in order to explore the functional network connectivity aspect of understanding the etiology of ASD. The workflow begins with the decomposition of the preprocessed RsfMRI images into the autonomous components followed by the identification and labeling of ICN and at the last correlating the time profiles of the pairs of ICN. The CCS protocol of preprocessing was simply followed here to prepare the fMRI images for their use. These images were further decomposed by the ICA but instead of going with the most used algorithms (i.e. INFOMAX, FastICA) their suitability for fMRI images was compared with eight other ICA algorithms. The phantom as well as real fMRI images were used as the test images and the real images were based on both the task-based and resting state protocols. The COMBI algorithm was found superior or equivalent to the frequently used algorithms in terms of all the tests whether it was applied to decompose the real/synthetic fMRI images distinctively or the time consumption or the aggregate score of mutual information of all the combinations of autonomous components of the images. Further, throughout in this work, COMBI had been used to disintegrate the RsfMRI images into the dedicated individual components.

The very next step after the decomposition was to identify the components of interest and label them. For the purpose of their identification as an RSN, dynamic range and the ratio of low to high-frequency power can be used but the problem is with their optimum value which is not yet standardized and thus manual expertise is required for their recognition as the RSN/ICN. Some work on automatic labeling of ICN had already been done and it relies on the spatial correlation values between the 2D templates and the ICN. The component gets the name of the template with which it gets the highest score. The results of the above automatic labeling was found erroneous during the analysis in the present work and the alternative is suggested here. With the help of proposed 3D templates, an accurate programmed way can be built which relies on volumetric overlap matching rather than spot overlapping in two dimensions.

After proposing these two corrective measures in the baseline of FNC analysis, further static and dynamic FNC analysis were carried out longitudinally. The developmental changes in traditional static FNC analysis of the two population was explored here. The results of this sFNC are in accordance

with the hyper-hypo connectivity hypothesis of ASD cohorts. The SN and BGN of participants with ASD had the most FNC differences with typically developing cohorts. The SN had hyper-connectivity with the rest five networks for autistic children while hypoconnectivity were observed for adolescents and adults. The two lateralized frontoparietal networks had no connectivity for the two initial developmental stages however for adults with ASD they had stronger functional connectivity. The dFNC analysis was also performed here, but the results disagree with the hyper-hypo connectivity hypothesis. In this dynamic counterpart of FNC authors have found that the significant differences are rather sparse in the group of children and adults suffering from ASD. Instead of no connectivity differences between the adult's group of two groups, they do exist.

In nutshell, for determining the functional network connectivity-based biomarkers which can be thought of responsible for the peculiarities of the ASD population, the present work revolves around two hypotheses 1) The disrupted connectivity that postulates the deficiencies in the way the brain coordinates and synchronizes activity among different regions may account for the clinical symptoms of ASD. The most common version of this hypothesis proposes that individuals with ASD have weak connections between distant brain regions and increased connections within local regions and these abnormalities contribute to the social, cognitive, and behavioral phenotype. 2) Developmental changes in functional connectivity have received inadequate attention and the discrepancies between findings of autism-related hypo-connectivity and hyper-connectivity might be reconciled by taking developmental changes with varying age into account.

6.2 Future Scopes

During synthesizing the thesis author found few corrective measures which are described further as the possible avenues for future work.

6.2.1 Using A Larger Dataset

In the current work, 15-20 subjects are considered in each group of various developmental stages. The results should be verified with a larger number of subjects in each group and consequently, the statistical power will not be limited.

6.2.2 FNC Analysis With A Dataset Without Global Signal Regression

Effects of global regression of the signal on functional connectivity differences between typically developing and autistic population can be explored.

6.2.3 Other Pattern Recognition Algorithm

The K-means cannot converge even after the maximum preset iterations which are termed as the end criteria, most likely because of broad commotion in dFNC. In this manner, the subsequent connectivity states from K-means might be incorrect, which impacts the adequacy of the resulting biomarker.

6.2.4 Same dFNC States Among All The Developmental Stages

Any comparison is trustworthy when it is executed under the same circumstances and it was taken care of while doing the comparison of the functional connections of the diseased and healthy controls during individual developmental stages. Whenever it comes to the comparison of two or three developmental stages the differences were based on all the dynamic states i.e. they were not evaluated individual dynamic state-wise.

6.2.5 Fusion of EEG and fMRI

Electroencephalography (EEG) and functional magnetic resonance imaging (fMRI) are two frequently used noninvasive medical imaging techniques to probe the brain. Also, because of a remarkable level of complementarity between the two modalities, the blend of EEG and fMRI information has been effectively looked for over the most recent two decades. The fusion of these two extremities can definitely empower the brain explorers.

6.2.6 Comapring FNC patterns of Other Neurological Disorders Having Same Manifestations as ASD

Both the disorders are neurodevelopmental and their trademark manifestations are language and social deficiency. Genetic changes are not the prime patron of autism and schizophrenia development. Do they share the same FNC patterns is still an open question?

6.2.7 Time-Frequency Analysis

Utilizing a window of fixed length is the major disadvantage of sliding-window examination. A time-frequency analysis can dodge the need to choose a settled sliding-window estimate.

PUBLICATIONS FROM THE RESEARCH WORK

JOURNALS

1. **Sariya, Yogesh** and R. S. Anand, “Comparison of separation performance of independent component analysis algorithms for fMRI data," Journal of Integrative Neuroscience 16 (2017): 157-175. (**Science Citation Index Expanded**)

2. **Sariya, Yogesh** and R. S. Anand, “3D Templates for Resting State Networks Labeling," Network: Computation in Neural Systems, Taylor & Francis (Under review).

3. **Sariya, Yogesh** and R. S. Anand, “ICA based investigation of developmental changes of dynamic functional network connectivity in ASD," Cognitive Neurodynamics (Under review).

CONFERENCES

1. **Sariya, Yogesh** and R. S. Anand, “Assessment of social and cognitive dysfunction of autism spectrum disorder through functional network connectivity," in India Conference (INDICON), 2016 IEEE Annual, 2016, pp. 1-4.

Bibliography

[1] C. Rorden and H.-O. Karnath, "Using human brain lesions to infer function: a relic from a past era in the fMRI age?" *Nat Rev Neurosci*, vol. 5, no. 10, pp. 812–819, oct 2004. [Online]. Available: http://dx.doi.org/10.1038/nrn1521

[2] T. Gandhi, P. Swami, P. Sinha, and S. Anand, "Top down processing of faces in human brain: A behavioral study," 2009. [Online]. Available: https://www.scopus.com/inward/record.uri?eid=2-s2.0-77949586357&partnerID=40&md5=ee237e71e9053f125b4058bee6769b1d

[3] P. J. Phillips, R. Chellappa, and P. Sinha, "Face recognition by computers and humans," *Computer (IEEE Computer)*, 2009.

[4] M. Vissers, M. X Cohen, and H. Geurts, "Brain connectivity and high functioning autism: A promising path of research that needs refined models, methodological convergence, and stronger behavioral links," *Neuroscience and Biobehavioral Reviews*, vol. 36, no. 1, 2012.

[5] S. Shore and L. G. Rastelli, *Understanding autism for dummies*. John Wiley & Sons, 2011.

[6] P. Sinha, M. M. Kjelgaard, T. K. Gandhi, K. Tsourides, A. L. Cardinaux, D. Pantazis, S. P. Diamond, and R. M. Held, "Autism as a disorder of prediction," *Proceedings of the National Academy of Sciences*, vol. 111, no. 42, pp. 15 220–15 225, 2014.

[7] V. Menon and S. Crottaz-Herbette, *Combined EEG and fMRI Studies of Human Brain Function*, 2005, vol. 66.

[8] C. Mulert and L. Lemieux, *EEG-fMRI: physiological basis, technique, and applications*. Springer Science & Business Media, 2009.

[9] M. Ullsperger and S. Debener, *Simultaneous EEG and fMRI: recording, analysis, and application*. Oxford University Press, 2010.

[10] P. Jain and R. B. Pachori, "An iterative approach for decomposition of multi-component non-stationary signals based on eigenvalue decomposition of the Hankel matrix," *Journal of the Franklin Institute*, vol. 352, no. 10, pp. 4017–4044, oct 2015. [Online]. Available: http://www.sciencedirect.com/science/article/pii/S0016003215002288

[11] R. B. Pachori and V. Bajaj, "Analysis of normal and epileptic seizure EEG signals using empirical mode decomposition," *Computer Methods and Programs in Biomedicine*, vol. 104,

no. 3, pp. 373–381, dec 2011. [Online]. Available: http://www.sciencedirect.com/science/article/pii/S0169260711000745

[12] V. Bajaj and R. B. Pachori, "Automatic classification of sleep stages based on the time-frequency image of EEG signals," *Computer Methods and Programs in Biomedicine*, vol. 112, no. 3, pp. 320–328, dec 2013. [Online]. Available: http://www.sciencedirect.com/science/article/pii/S0169260713002265

[13] A. Deshmukh, V. Shivhare, R. Parihar, V. Gadre, D. Patkar, S. Shah, and S. Pungavkar, "Functional MRI activation signal detection using the periodicity transform," in *2004 International Conference on Signal Processing and Communications, SPCOM*, 2004.

[14] A. V. Deshmukh, V. Shivhare, R. S. Parihar, V. M. Gadre, D. P. Patkar, S. Shah, and S. Pungavkar, "Periodicity analysis of fmri data in the wavelet domain," in *Proceedings of the Eleventh National Conference on Communications: NCC-2005, 28-30 January, 2005*. Allied Publishers, 2005, p. 460.

[15] A. V. Deshmukh and V. M. Gadre, *Functional magnetic resonance imaging: novel transform methods*. Alpha Science International, Limited, 2008.

[16] P. Herscovitch, J. Markham, and M. Raichle, "Brain blood flow measured with intravenous H215O. I. Theory and error analysis," *Journal of Nuclear Medicine*, vol. 24, no. 9, 1983.

[17] G. Aguirre, E. Zarahn, and M. D'Esposito, "Empirical analyses of bold fmri statistics," *NeuroImage*, vol. 5, no. 3, pp. 199 – 212, 1997. [Online]. Available: http://www.sciencedirect.com/science/article/pii/S1053811997902640

[18] G. Aguirre and M. DŠEsposito, "Experimental design for brain fmri," *Functional MRI*, pp. 369–380, 1999.

[19] K. J. Friston, A. P. Holmes, K. J. Worsley, J.-P. Poline, C. D. Frith, and R. S. J. Frackowiak, "Statistical parametric maps in functional imaging: A general linear approach," *Human Brain Mapping*, vol. 2, no. 4, pp. 189–210, jan 1994. [Online]. Available: http://doi.wiley.com/10.1002/hbm.460020402

[20] K. J. Worsley, A. C. Evans, S. Marrett, and P. Neelin, "A three-dimensional statistical analysis for CBF activation studies in human brain," *Journal of Cerebral Blood Flow & Metabolism*, vol. 12, no. 6, pp. 900–918, 1992.

[21] R. J. Harris, *A primer of multivariate statistics*. Psychology Press, 2001.

[22] H. F. Kaiser, “The application of electronic computers to factor analysis,” *Educational and psychological measurement*, vol. 20, no. 1, pp. 141–151, 1960.

[23] K. J. Friston, C. D. Frith, P. F. Liddle, and R. S. J. Frackowiak, “Functional connectivity: the principal-component analysis of large (PET) data sets,” *Journal of Cerebral Blood Flow & Metabolism*, vol. 13, no. 1, pp. 5–14, 1993.

[24] C. Ecker, E. Reynaud, S. C. Williams, and M. J. Brammer, “Detecting functional nodes in largeâĂ?scale cortical networks with functional magnetic resonance imaging: A principal component analysis of the human visual system,” *Human brain mapping*, vol. 28, no. 9, pp. 817–834, 2007.

[25] C. Buchel and K. J. Friston, “Modulation of connectivity in visual pathways by attention: cortical interactions evaluated with structural equation modelling and fMRI.” *Cerebral Cortex*, vol. 7, no. 8, pp. 768–778, dec 1997. [Online]. Available: http://dx.doi.org/10.1093/cercor/7.8.768

[26] M. K. Bhuyan, D. A. Kumar, K. F. MacDorman, and Y. Iwahori, “A novel set of features for continuous hand gesture recognition,” *J. Multimodal User Interfaces*, vol. 8, no. 4, pp. 333–343, 2014. [Online]. Available: https://doi.org/10.1007/s12193-014-0165-0

[27] A. Choudhury, A. K. Talukdar, M. K. Bhuyan, and K. K. Sarma, “Movement epenthesis detection for continuous sign language recognition,” *J. Intelligent Systems*, vol. 26, no. 3, p. 471, 2017. [Online]. Available: https://doi.org/10.1515/jisys-2016-0009

[28] R. S. Richard A.Harshman, Christopher G.Thomas, “Noise Reduction in BOLD-Based fMRI Using Component Analysis,” *NeuroImage*, vol. 17, no. 3, pp. 1521–1537, nov 2002. [Online]. Available: http://www.sciencedirect.com/science/article/pii/S1053811902912000?via{%}3Dihub

[29] M. McKeown, S. Makeig, G. Brown, T.-P. Jung, S. Kindermann, A. Bell, and T. Sejnowski, “Analysis of fMRI data by blind separation into independent spatial components,” *Human Brain Mapping*, vol. 6, no. 3, 1998.

[30] V. Calhoun, T. Adali, G. Pearlson, and J. Pekar, “Spatial and temporal independent component analysis of functional MRI data containing a pair of task-related waveforms,” *Human Brain Mapping*, vol. 13, no. 1, pp. 43–53, may 2001. [Online]. Available: http://doi.wiley.com/10.1002/hbm.1024

[31] C. Beckmann, M. DeLuca, J. Devlin, and S. Smith, "Investigations into resting-state connectivity using independent component analysis," *Philosophical Transactions of the Royal Society B: Biological Sciences*, vol. 360, no. 1457, 2005.

[32] V. D. Calhoun, J. Liu, and T. Adali, "A review of group ICA for fMRI data and ICA for joint inference of imaging, genetic, and ERP data." *NeuroImage*, vol. 45, no. 1 Suppl, pp. 294–311, mar 2009. [Online]. Available: http://www.sciencedirect.com/science/article/pii/S1053811904006378?via{%}3Dihub

[33] V. Calhoun, T. Adali, N. Giuliani, J. Pekar, K. Kiehl, and G. Pearlson, "Method for multimodal analysis of independent source differences in schizophrenia: Combining gray matter structural and auditory oddball functional data," *Human Brain Mapping*, vol. 27, no. 1, pp. 47–62, jan 2006. [Online]. Available: http://doi.wiley.com/10.1002/hbm.20166

[34] V. Calhoun, T. Adali, G. Pearlson, and J. Pekar, "A method for making group inferences from functional MRI data using independent component analysis," *Human Brain Mapping*, vol. 14, no. 3, pp. 140–151, nov 2001. [Online]. Available: http://doi.wiley.com/10.1002/hbm.1048

[35] V. D. Calhoun, J. J. Pekar, V. B. McGinty, T. Adali, T. D. Watson, and G. D. Pearlson, "Different activation dynamics in multiple neural systems during simulated driving," *Human Brain Mapping*, vol. 16, no. 3, pp. 158–167, jul 2002. [Online]. Available: http://doi.wiley.com/10.1002/hbm.10032

[36] J. Liu, G. Pearlson, A. Windemuth, G. Ruano, N. I. Perrone-Bizzozero, and V. Calhoun, "Combining fMRI and SNP data to investigate connections between brain function and genetics using parallel ICA," *Human Brain Mapping*, vol. 30, no. 1, pp. 241–255, jan 2009. [Online]. Available: http://doi.wiley.com/10.1002/hbm.20508

[37] M. C. Stevens, P. Skudlarski, G. D. Pearlson, and V. D. Calhoun, "Age-related cognitive gains are mediated by the effects of white matter development on brain network integration," *NeuroImage*, vol. 48, no. 4, pp. 738–746, dec 2009. [Online]. Available: http://www.sciencedirect.com/science/article/pii/S105381190900706X?via{%}3Dihub

[38] S. Ogawa, T.-M. Lee, A. R. Kay, and D. W. Tank, "Brain magnetic resonance imaging with contrast dependent on blood oxygenation," *Proceedings of the National Academy of Sciences*, vol. 87, no. 24, pp. 9868–9872, 1990.

[39] J. R. Binder, "fMRI of Language Systems : Methods and Applications," *Functional MRI*, pp. 245–277, 2006.

[40] C. Giussani, F.-E. Roux, J. Ojemann, E. P. Sganzerla, D. Pirillo, and C. Papagno, "Is preoperative functional magnetic resonance imaging reliable for language areas mapping in brain tumor surgery? Review of language functional magnetic resonance imaging and direct cortical stimulation correlation studies," *Neurosurgery*, vol. 66, no. 1, pp. 113–120, 2010.

[41] J. S. Damoiseaux, S. A. R. B. Rombouts, F. Barkhof, P. Scheltens, C. J. Stam, S. M. Smith, and C. F. Beckmann, "Consistent resting-state networks across healthy subjects," *Proceedings of the National Academy of Sciences*, vol. 103, no. 37, pp. 13 848–13 853, 2006. [Online]. Available: http://www.pnas.org/cgi/doi/10.1073/pnas.0601417103

[42] M. D. Fox and M. E. Raichle, "Spontaneous fluctuations in brain activity observed with functional magnetic resonance imaging," *Nature reviews. Neuroscience*, vol. 8, no. 9, p. 700, 2007.

[43] M. Fox and M. Greicius, "Clinical applications of resting state functional connectivity," *Frontiers in Systems Neuroscience*, vol. 4, 2010.

[44] C. Beckmann and S. Smith, "Probabilistic Independent Component Analysis for Functional Magnetic Resonance Imaging," *IEEE Transactions on Medical Imaging*, vol. 23, no. 2, 2004.

[45] G. Deco, A. Ponce-Alvarez, D. Mantini, G. L. Romani, P. Hagmann, and M. Corbetta, "Resting-State Functional Connectivity Emerges from Structurally and Dynamically Shaped Slow Linear Fluctuations," *The Journal of Neuroscience*, vol. 33, no. 27, pp. 11 239 LP – 11 252, jul 2013. [Online]. Available: http://www.jneurosci.org/content/33/27/11239.abstract

[46] T. Mitchell, C. Hacker, J. Breshears, N. Szrama, M. Sharma, D. Bundy, M. Pahwa, M. Corbetta, A. Snyder, J. Shimony, and E. Leuthardt, "A novel data-driven approach to preoperative mapping of functional cortex using resting-state functional magnetic resonance imaging," *Neurosurgery*, vol. 73, no. 6, 2013.

[47] Y. Tie, L. Rigolo, I. Norton, R. Huang, W. Wu, D. Orringer, S. Mukundan, and A. Golby, "Defining language networks from resting-state fMRI for surgical planning- A feasibility study," *Human Brain Mapping*, vol. 35, no. 3, 2014.

[48] L. Zhu, Y. Fan, Q. Zou, J. Wang, J.-H. Gao, and Z. Niu, "Temporal reliability and lateralization of the resting-state language network," *PLoS ONE*, vol. 9, no. 1, 2014.

[49] C. C. Lee, H. A. Ward, F. W. Sharbrough, F. B. Meyer, W. R. Marsh, C. Raffel, E. L. So, G. D. Cascino, C. Shin, and Y. Xu, "Assessment of functional MR imaging in neurosurgical planning," *American journal of neuroradiology*, vol. 20, no. 8, pp. 1511–1519, 1999.

[50] C. Price, J. Crinion, and K. Friston, "Design and analysis of fMRI studies with neurologically impaired patients," *Journal of Magnetic Resonance Imaging*, vol. 23, no. 6, 2006.

[51] D. Hingwala, B. Thomas, A. Radhakrishnan, S. Nair N, and C. Kesavadas, "Correlation between anatomic landmarks and fMRI in detection of the sensorimotor cortex in patients with structural lesions," *Acta Radiologica*, vol. 55, no. 1, 2014.

[52] S. Lang, N. Duncan, and G. Northoff, "Resting-state functional magnetic resonance imaging: Review of neurosurgical applications," *Neurosurgery*, vol. 74, no. 5, 2014.

[53] O. Friman, J. Cedefamn, P. Lundberg, M. Borga, and H. Knutsson, "Detection of neural activity in functional MRI using canonical correlation analysis," *Magnetic Resonance in Medicine*, vol. 45, no. 2, 2001.

[54] C. Goutte, P. Toft, E. Rostrup, F. Å. Nielsen, and L. K. Hansen, "On clustering fMRI time series," *NeuroImage*, vol. 9, no. 3, pp. 298–310, 1999.

[55] P. Golland, Y. Golland, and R. Malach, "Detection of spatial activation patterns as unsupervised segmentation of fMRI data." *Medical image computing and computer-assisted intervention : MICCAI ... International Conference on Medical Image Computing and Computer-Assisted Intervention*, vol. 10, no. Pt 1, 2007.

[56] N. Ramnani, L. Lee, A. Mechelli, C. Phillips, A. Roebroeck, and E. Formisano, "Exploring brain connectivity: A new frontier in systems neuroscience," *Trends in Neurosciences*, vol. 25, no. 10, 2002.

[57] B. Horwitz, "The elusive concept of brain connectivity," *NeuroImage*, vol. 19, no. 2, 2003.

[58] L. Lee, L. Harrison, and A. Mechelli, "A report of the functional connectivity workshop, Dusseldorf 2002," *NeuroImage*, vol. 19, no. 2, 2003.

[59] W. Penny, K. Stephan, A. Mechelli, and K. Friston, "Modelling functional integration: A comparison of structural equation and dynamic causal models," *NeuroImage*, vol. 23, no. SUPPL. 1, 2004.

[60] V. Cherkassky, R. Kana, T. Keller, and M. Just, "Functional connectivity in a baseline resting-state network in autism," *NeuroReport*, vol. 17, no. 16, 2006.

[61] D. Kennedy and E. Courchesne, "The intrinsic functional organization of the brain is altered in autism," *NeuroImage*, vol. 39, no. 4, 2008.

[62] C. Monk, S. Peltier, J. Wiggins, S.-J. Weng, M. Carrasco, S. Risi, and C. Lord, "Abnormalities of intrinsic functional connectivity in autism spectrum disorders,," *NeuroImage*, vol. 47, no. 2, 2009.

[63] S.-J. Weng, J. Wiggins, S. Peltier, M. Carrasco, S. Risi, C. Lord, and C. Monk, "Alterations of resting state functional connectivity in the default network in adolescents with autism spectrum disorders," *Brain Research*, vol. 1313, 2010.

[64] G. Olivito, S. Clausi, F. Laghi, A. M. Tedesco, R. Baiocco, C. Mastropasqua, M. Molinari, M. Cercignani, M. Bozzali, and M. Leggio, "Resting-state functional connectivity changes between dentate nucleus and cortical social brain regions in autism spectrum disorders," *The Cerebellum*, vol. 16, no. 2, pp. 283–292, 2017.

[65] J.-J. Paakki, J. Rahko, X. Long, I. Moilanen, O. Tervonen, J. Nikkinen, T. Starck, J. Remes, T. Hurtig, H. Haapsamo, K. Jussila, S. Kuusikko-Gauffin, M.-L. Mattila, Y. Zang, and V. Kiviniemi, "Alterations in regional homogeneity of resting-state brain activity in autism spectrum disorders," *Brain Research*, vol. 1321, 2010.

[66] M. Assaf, K. Jagannathan, V. Calhoun, L. Miller, M. Stevens, R. Sahl, J. O'Boyle, R. Schultz, and G. Pearlson, "Abnormal functional connectivity of default mode sub-networks in autism spectrum disorder patients," *NeuroImage*, vol. 53, no. 1, 2010.

[67] I. Dinstein, K. Pierce, L. Eyler, S. Solso, R. Malach, M. Behrmann, and E. Courchesne, "Disrupted Neural Synchronization in Toddlers with Autism," *Neuron*, vol. 70, no. 6, 2011.

[68] A. Di Martino, C. Kelly, R. Grzadzinski, X.-N. Zuo, M. Mennes, M. Mairena, C. Lord, F. Castellanos, and M. Milham, "Aberrant striatal functional connectivity in children with autism," *Biological Psychiatry*, vol. 69, no. 9, 2011.

[69] J. Anderson, T. Druzgal, A. Froehlich, M. Dubray, N. Lange, A. Alexander, T. Abildskov, J. Nielsen, A. Cariello, J. Cooperrider, E. Bigler, and J. Lainhart, "Decreased interhemispheric functional connectivity in autism," *Cerebral Cortex*, vol. 21, no. 5, 2011.

[70] S. Ebisch, V. Gallese, R. Willems, D. Mantini, W. Groen, G. Romani, J. Buitelaar, and H. Bekkering, "Altered intrinsic functional connectivity of anterior and posterior insula regions in high-functioning participants with autism spectrum disorder," *Human Brain Mapping*, vol. 32, no. 7, 2011.

[71] J. Wiggins, S. Peltier, S. Ashinoff, S.-J. Weng, M. Carrasco, R. Welsh, C. Lord, and C. Monk, "Using a self-organizing map algorithm to detect age-related changes in functional connectivity during rest in autism spectrum disorders," *Brain Research*, vol. 1380, 2011.

[72] S. Gotts, W. Simmons, L. Milbury, G. Wallace, R. Cox, and A. Martin, "Fractionation of social brain circuits in autism spectrum disorders," *Brain*, vol. 135, no. 9, 2012.

[73] J. Rudie, L. Hernandez, J. Brown, D. Beck-Pancer, N. Colich, P. Gorrindo, P. Thompson, D. Geschwind, S. Bookheimer, P. Levitt, and M. Dapretto, "Autism-Associated Promoter Variant in MET Impacts Functional and Structural Brain Networks," *Neuron*, vol. 75, no. 5, 2012.

[74] E. von dem Hagen, R. Stoyanova, S. Baron-Cohen, and A. Calder, "Reduced functional connectivity within and between 'social' resting state networks in autism spectrum conditions," *Social Cognitive and Affective Neuroscience*, vol. 8, no. 6, 2013.

[75] C. Lynch, L. Uddin, K. Supekar, A. Khouzam, J. Phillips, and V. Menon, "Default mode network in childhood autism: Posteromedial cortex heterogeneity and relationship with social deficits," *Biological Psychiatry*, vol. 74, no. 3, 2013.

[76] S. Washington, E. Gordon, J. Brar, S. Warburton, A. Sawyer, A. Wolfe, E. Mease-Ference, L. Girton, A. Hailu, J. Mbwana, W. Gaillard, M. Kalbfleisch, and J. Vanmeter, "Dysmaturation of the default mode network in autism," *Human Brain Mapping*, vol. 35, no. 4, 2014.

[77] J. Tyszka, D. Kennedy, L. Paul, and R. Adolphs, "Largely typical patterns of resting-state functional connectivity in high-functioning adults with autism," *Cerebral Cortex*, vol. 24, no. 7, 2014.

[78] L. Uddin, K. Supekar, C. Lynch, A. Khouzam, J. Phillips, C. Feinstein, S. Ryali, and V. Menon, "Salience network-based classification and prediction of symptom severity in children with autism," *JAMA Psychiatry*, vol. 70, no. 8, 2013.

[79] E. Redcay, J. Moran, P. Mavros, H. Tager-Flusberg, J. Gabrieli, and S. Whitfield-Gabrieli, "Intrinsic functional network organization in high-functioning adolescents with autism spectrum disorder," *Frontiers in Human Neuroscience*, no. SEP, 2013.

[80] J. Nielsen, B. Zielinski, P. Fletcher, A. Alexander, N. Lange, E. Bigler, J. Lainhart, and J. Anderson, "Multisite functional connectivity MRI classification of autism: ABIDE results," *Frontiers in Human Neuroscience*, no. SEP, 2013.

[81] J. Maximo, C. Keown, A. Nair, and R.-A. Müller, "Approaches to local connectivity in autism using resting state functional connectivity MRI," *Frontiers in Human Neuroscience*, no. OCT, 2013.

[82] T. Starck, J. Nikkinen, J. Rahko, J. Remes, T. Hurtig, H. Haapsamo, K. Jussila, S. Kuusikko-Gauffin, M.-L. Mattila, E. Jansson-Verkasalo, D. Pauls, H. Ebeling, I. Moilanen, O. Tervonen, and V. Kiviniemi, "Resting state fMRI reveals a default mode dissociation between retrosplenial and medial prefrontal subnetworks in ASD despite motion scrubbing," *Frontiers in Human Neuroscience*, no. NOV, 2013.

[83] A. Di Martino, X.-N. Zuo, C. Kelly, R. Grzadzinski, M. Mennes, A. Schvarcz, J. Rodman, C. Lord, F. Castellanos, and M. Milham, "Shared and distinct intrinsic functional network centrality in autism and attention-deficit/hyperactivity disorder," *Biological Psychiatry*, vol. 74, no. 8, 2013.

[84] A. Di Martino, C.-G. Yan, Q. Li, E. Denio, F. Castellanos, K. Alaerts, J. Anderson, M. Assaf, S. Bookheimer, M. Dapretto, B. Deen, S. Delmonte, I. Dinstein, B. Ertl-Wagner, D. Fair, L. Gallagher, D. Kennedy, C. Keown, C. Keysers, J. Lainhart, C. Lord, B. Luna, V. Menon, N. Minshew, C. Monk, S. Mueller, R.-A. Müller, M. Nebel, J. Nigg, K. O'Hearn, K. Pelphrey, S. Peltier, J. Rudie, S. Sunaert, M. Thioux, J. Tyszka, L. Uddin, J. Verhoeven, N. Wenderoth, J. Wiggins, S. Mostofsky, and M. Milham, "The autism brain imaging data exchange: Towards a large-scale evaluation of the intrinsic brain architecture in autism," *Molecular Psychiatry*, vol. 19, no. 6, 2014.

[85] D. Abrams, C. Lynch, K. Cheng, J. Phillips, K. Supekar, S. Ryali, L. Uddin, and V. Menon, "Underconnectivity between voice-selective cortex and reward circuitry in children with autism," *Proceedings of the National Academy of Sciences of the United States of America*, vol. 110, no. 29, 2013.

[86] S. Mueller, D. Keeser, A. Samson, V. Kirsch, J. Blautzik, M. Grothe, O. Erat, M. Hegenloh, U. Coates, M. Reiser, K. Hennig-Fast, and T. Meindl, "Convergent Findings of Altered Functional and Structural Brain Connectivity in Individuals with High Functioning Autism: A Multimodal MRI Study," *PLoS ONE*, vol. 8, no. 6, 2013.

[87] R. Cardinale, P. Shih, I. Fishman, L. Ford, and R.-A. Müller, "Pervasive rightward asymmetry shifts of functional networks in autism spectrum disorder," *JAMA Psychiatry*, vol. 70, no. 9, 2013.

[88] X. You, M. Norr, E. Murphy, E. Kuschner, E. Bal, W. Gaillard, L. Kenworthy, and C. Vaidya, "Atypical modulation of distant functional connectivity by cognitive state in children with Autism Spectrum Disorders," *Frontiers in Human Neuroscience*, no. AUG, 2013.

[89] K. Alaerts, D. Woolley, J. Steyaert, A. Di Martino, S. Swinnen, and N. Wenderoth, "Underconnectivity of the superior temporal sulcus predicts emotion recognition deficits in autism," *Social Cognitive and Affective Neuroscience*, vol. 9, no. 10, 2013.

[90] M. Verly, J. Verhoeven, I. Zink, D. Mantini, L. Oudenhove, L. Lagae, S. Sunaert, and N. Rommel, "Structural and functional underconnectivity as a negative predictor for language in autism," *Human Brain Mapping*, vol. 35, no. 8, 2014.

[91] A. Nair, J. Treiber, D. Shukla, P. Shih, and R.-A. Müller, "Impaired thalamocortical connectivity in autism spectrum disorder: A study of functional and anatomical connectivity," *Brain*, vol. 136, no. 6, 2013.

[92] C. Keown, P. Shih, A. Nair, N. Peterson, M. Mulvey, and R.-A. Müller, "Local functional overconnectivity in posterior brain regions is associated with symptom severity in autism spectrum disorders," *Cell Reports*, vol. 5, no. 3, 2013.

[93] K. Alaerts, K. Nayar, C. Kelly, J. Raithel, M. P. Milham, and A. Di Martino, "Age-related changes in intrinsic function of the superior temporal sulcus in autism spectrum disorders," *Social cognitive and affective neuroscience*, vol. 10, no. 10, pp. 1413–1423, 2015.

[94] K. A. Doyle-Thomas, W. Lee, N. E. Foster, A. Tryfon, T. Ouimet, K. L. Hyde, A. C. Evans, J. Lewis, L. Zwaigenbaum, E. Anagnostou *et al.*, "Atypical functional brain connectivity during rest in autism spectrum disorders," *Annals of neurology*, vol. 77, no. 5, pp. 866–876, 2015.

[95] S. Robinson and V. Schopf, "ICA of fMRI studies: New approaches and cutting edge applications," *Frontiers in Human Neuroscience*, no. OCT, 2013.

[96] I. Daubechies, E. Roussos, S. Takerkart, M. Benharrosh, C. Golden, K. D'Ardenne, W. Richter, J. Cohen, and J. Haxby, "Independent component analysis for brain fMRI does not select for independence," *Proceedings of the National Academy of Sciences of the United States of America*, vol. 106, no. 26, 2009.

[97] W. Du, S. Ma, G.-S. Fu, V. Calhoun, and T. Adali, "A novel approach for assessing reliability of ICA for FMRI analysis," in *ICASSP, IEEE International Conference on Acoustics, Speech and Signal Processing - Proceedings*, 2014.

[98] N. Correa, Adali, O. Li, Y, and V. D. Calhoun, "Performance of blind source separation algorithms for fMRI analysis using a group ICA method," *Magnetic Resonance Imaging*, vol. 25, no. 5, pp. 684–694, Jun. 2007. [Online]. Available: http://www.sciencedirect.com/science/article/pii/S0730725X06003080

[99] N. Correa, T. Adali, Y.-O. Li, and V. Calhoun, "Comparison of blind source separation algorithms for FMRI using a new matlab toolbox: Gift," in *ICASSP, IEEE International Conference on Acoustics, Speech and Signal Processing - Proceedings*, vol. V, 2005.

[100] C. Pernet, J. Andersson, E. Paulesu, and J. Demonet, "When all hypotheses are right: A multifocal account of dyslexia," *Human Brain Mapping*, vol. 30, no. 7, 2009.

[101] B. Biswal, F. Zerrin Yetkin, V. M. Haughton, and J. S. Hyde, "Functional connectivity in the motor cortex of resting human brain using echo-planar mri," *Magnetic Resonance*

in Medicine, vol. 34, no. 4, pp. 537–541, Oct. 1995. [Online]. Available: http://doi.wiley.com/10.1002/mrm.1910340409

[102] B. B. Biswal, "Resting state fMRI: A personal history," *NeuroImage*, vol. 62, no. 2, pp. 938–944, 2012. [Online]. Available: http://www.sciencedirect.com/science/article/pii/S1053811912001073

[103] M. Greicius, K. Supekar, V. Menon, and R. Dougherty, "Resting-state functional connectivity reflects structural connectivity in the default mode network," *Cerebral Cortex*, vol. 19, no. 1, 2009.

[104] C. Honey, O. Sporns, L. Cammoun, X. Gigandet, J. Thiran, R. Meuli, and P. Hagmann, "Predicting human resting-state functional connectivity from structural connectivity," *Proceedings of the National Academy of Sciences of the United States of America*, vol. 106, no. 6, 2009.

[105] M. Moussa, M. Steen, P. Laurienti, and S. Hayasaka, "Consistency of Network Modules in Resting-State fMRI Connectome Data," *PLoS ONE*, vol. 7, no. 8, 2012.

[106] M. van den Heuvel and H. Hulshoff Pol, "Exploring the brain network: A review on resting-state fMRI functional connectivity," *European Neuropsychopharmacology*, vol. 20, no. 8, 2010.

[107] K. Pierce, "Early functional brain development in autism and the promise of sleep fMRI," *Brain Research*, vol. 1380, 2011.

[108] E. Redcay, D. Kennedy, and E. Courchesne, "fMRI during natural sleep as a method to study brain function during early childhood," *NeuroImage*, vol. 38, no. 4, 2007.

[109] M. Raichle and A. Snyder, "A default mode of brain function: A brief history of an evolving idea," *NeuroImage*, vol. 37, no. 4, 2007.

[110] M. Sabri, C. Humphries, M. Verber, E. Liebenthal, J. Binder, J. Mangalathu, and A. Desai, "Neural effects of cognitive control load on auditory selective attention," *Neuropsychologia*, vol. 61, no. 1, 2014.

[111] E. Erhardt, E. Allen, Y. Wei, T. Eichele, and V. Calhoun, "SimTB, a simulation toolbox for fMRI data under a model of spatiotemporal separability," *NeuroImage*, vol. 59, no. 4, 2012.

[112] V. D. Calhoun, T. Adali, L. K. Hansen, J. Larsen, and J. J. Pekar, "Ica of functional mri data: an overview," 2003.

[113] M. McKeown, L. Hansen, and T. Sejnowsk, "Independent component analysis of functional MRI: What is signal and what is noise?" *Current Opinion in Neurobiology*, vol. 13, no. 5, 2003.

[114] H. Gudbjartsson and S. Patz, "The rician distribution of noisy mri data," *Magnetic Resonance in Medicine*, vol. 34, no. 6, 1995.

[115] S. Rachakonda, E. Egolf, N. Correa, and V. Calhoun, "Group ica of fmri toolbox (gift) manual," *Dostupné z http://www. nitrc. org/docman/view. php/55/295/v1. 3d_ GIFTManual pdf [cit. 2011-11-5]*, 2007.

[116] A. J. Bell and T. J. Sejnowski, "An Information-Maximization Approach to Blind Separation and Blind Deconvolution," *Neural Computation*, vol. 7, no. 6, pp. 1129–1159, Nov. 1995. [Online]. Available: http://dx.doi.org/10.1162/neco.1995.7.6.1129

[117] A. Hyvarinen and E. Oja, "A Fast Fixed-Point Algorithm for Independent Component Analysis," *Neural Computation*, vol. 9, no. 7, 1997.

[118] J.-F. Cardoso and A. Souloumiac, "Blind beamforming for non-gaussian signals," in *IEE proceedings F (radar and signal processing)*, vol. 140, no. 6. IET, 1993, pp. 362–370.

[119] S. Cruces-Alvarez, A. Cichocki, and S.-I. Amari, "From blind signal extraction to blind instantaneous signal separation: Criteria, algorithms, and stability," *IEEE Transactions on Neural Networks*, vol. 15, no. 4, 2004.

[120] S. Cruces, L. Castedo, and A. Cichocki, "Robust blind source separation algorithms using cumulants," *Neurocomputing*, vol. 49, 2002.

[121] P. Georgiev and A. Cichocki, "Blind source separation via symmetric eigenvalue decomposition," in *6th International Symposium on Signal Processing and Its Applications, ISSPA 2001 - Proceedings; 6 Tutorials in Communications, Image Processing and Signal Analysis*, vol. 1, 2001.

[122] P. Tichavsky, Z. Koldovsky, E. Down, A. Yeredor, and G. Gomez-Herrero, "Blind signal separation by combining two ICA algorithms: HOS-based EFICA and time structure-based WASOBI," in *European Signal Processing Conference*, 2006.

[123] E. G. Miller and J. W. Fisher III, "Independent components analysis by direct entropy minimization," CALIFORNIA UNIV BERKELEY DEPT OF ELECTRICAL ENGINEERING AND COMPUTER SCIENCES, Tech. Rep., 2003.

[124] X. L. Li and T. Adali, "Independent component analysis by entropy bound minimization," *IEEE Transactions on Signal Processing*, vol. 58, no. 10, 2010.

[125] X. L. Li and T. Adali, "Blind spatiotemporal separation of second and/or higher-order correlated sources by entropy rate minimization," in *2010 IEEE International Conference on Acoustics, Speech and Signal Processing*, 2010, pp. 1934–1937.

[126] V. Calhoun, "Group ICA of fMRI toolbox (GIFT)," *Online at http://icatb. sourceforge. net*, 2004.

[127] E. Allen, E. Erhardt, E. Damaraju, W. Gruner, J. Segall, R. Silva, M. Havlicek, S. Rachakonda, J. Fries, R. Kalyanam, A. Michael, A. Caprihan, J. Turner, T. Eichele, S. Adelsheim, A. Bryan, J. Bustillo, V. Clark, S. Feldstein Ewing, F. Filbey, C. Ford, K. Hutchison, R. Jung, K. Kiehl, P. Kodituwakku, Y. Komesu, A. Mayer, G. Pearlson, J. Phillips, J. Sadek, M. Stevens, U. Teuscher, R. Thoma, and V. Calhoun, "A Baseline for the Multivariate Comparison of Resting-State Networks," *Frontiers in Systems Neuroscience*, vol. 5, pp. 2–2, 2011. [Online]. Available: http://journal.frontiersin.org/article/10.3389/fnsys.2011.00002

[128] S. Robinson, G. Basso, N. Soldati, U. Sailer, J. Jovicich, L. Bruzzone, I. Kryspin-Exner, H. Bauer, and E. Moser, "A resting state network in the motor control circuit of the basal ganglia," *BMC Neuroscience*, vol. 10, 2009.

[129] S. Ogawa, D. W. Tank, R. Menon, J. M. Ellermann, S. G. Kim, H. Merkle, and K. Ugurbil, "Intrinsic signal changes accompanying sensory stimulation: Functional brain mapping with magnetic resonance imaging," *Proceedings of the National Academy of Sciences of the United States of America*, vol. 89, no. 13, pp. 5951–5955, 1992.

[130] M. D. Greicius, G. Srivastava, A. L. Reiss, and V. Menon, "Default-mode network activity distinguishes Alzheimer's disease from healthy aging: evidence from functional MRI." *Proceedings of the National Academy of Sciences of the United States of America*, vol. 101, no. 13, pp. 4637–42, 2004. [Online]. Available: http://www.pubmedcentral.nih.gov/articlerender.fcgi?artid=384799{&}tool=pmcentrez{&}rendertype=abstract

[131] M. J. Jafri, G. D. Pearlson, M. Stevens, and V. D. Calhoun, "A method for functional network connectivity among spatially independent resting-state components in schizophrenia," *NeuroImage*, vol. 39, no. 4, pp. 1666–1681, 2008.

[132] C. Kesavadas, B. Thomas, S. Sujesh, R. Ashalata, M. Abraham, A. K. Gupta, and K. Radhakrishnan, "Real-time functional mr imaging (fmri) for presurgical evaluation of paediatric epilepsy," *Pediatric radiology*, vol. 37, no. 10, pp. 964–974, 2007.

[133] C. Kesavadas and B. Thomas, "Clinical applications of functional MRI in epilepsy," *Indian Journal of Radiology and Imaging*, vol. 18, no. 3, 2008.

[134] B. Thomas, W. Logan, E. Donner, and M. Shroff, "Assessment of cerebrovascular reactivity using real-time BOLD fMRI in children with moyamoya disease: A pilot study," *Child's Nervous System*, vol. 29, no. 3, 2013.

[135] P. Mandal, J. Joshi, and S. Saharan, "Visuospatial perception: An emerging biomarker for Alzheimer's disease," *Journal of Alzheimer's Disease*, vol. 31, no. SUPPL. 3, 2012.

[136] M. D. Greicius, K. Supekar, V. Menon, and R. F. Dougherty, "Resting-state functional connectivity reflects structural connectivity in the default mode network," *Cerebral cortex*, vol. 19, no. 1, pp. 72–78, 2009.

[137] P. Branco, D. Seixas, S. Deprez, S. Kovacs, R. Peeters, S. L. Castro, and S. Sunaert, "Resting-State Functional Magnetic Resonance Imaging for Language Preoperative Planning," *Frontiers in Human Neuroscience*, vol. 10, p. 11, feb 2016. [Online]. Available: http://www.ncbi.nlm.nih.gov/pmc/articles/PMC4740781/

[138] A. Meyer-Baese, A. Wismueller, and O. Lange, "Comparison of two exploratory data analysis methods for fMRI: Unsupervised clustering versus independent component analysis," *IEEE Transactions on Information Technology in Biomedicine*, vol. 8, no. 3, 2004.

[139] P. K. Mandal, D. Schifilliti, F. Mafrica, and V. Fodale, "Inhaled anesthesia and cognitive performance," *Drugs of Today*, vol. 45, no. 1, p. 47, 2009.

[140] K. Arfanakis, D. Cordes, V. Haughton, C. Moritz, M. Quigley, and M. Meyerand, "Combining independent component analysis and correlation analysis to probe interregional connectivity in fMRI task activation datasets," *Magnetic Resonance Imaging*, vol. 18, no. 8, 2000.

[141] F. Esposito, E. Formisano, E. Seifritz, R. Goebel, R. Morrone, G. Tedeschi, and F. Di Salle, "Spatial independent component analysis of functional MRI time-series: To what extent do results depend on the algorithm used?" *Human Brain Mapping*, vol. 16, no. 3, 2002.

[142] J. Damoiseaux, C. Beckmann, E. S. Arigita, F. Barkhof, P. Scheltens, C. Stam, S. Smith, and S. Rombouts, "Reduced resting-state brain activity in the âĂIJdefault networkâĂ? in normal aging," *Cerebral cortex*, vol. 18, no. 8, pp. 1856–1864, 2008.

[143] A. Demertzi, F. GÃşmez, J. S. Crone, A. Vanhaudenhuyse, L. Tshibanda, Q. Noirhomme, M. Thonnard, V. Charland-Verville, M. Kirsch, S. Laureys, and A. Soddu, "Multiple fmri system-level baseline connectivity is disrupted in patients with consciousness alterations," *Cortex*, vol. 52, pp. 35 – 46, 2014. [Online]. Available: http://www.sciencedirect.com/science/article/pii/S0010945213002803

[144] S. Vergun, W. Gaggl, V. A. Nair, J. I. Suhonen, R. M. Birn, A. S. Ahmed, M. E. Meyerand, J. Reuss, E. A. DeYoe, and V. Prabhakaran, "Classification and Extraction of Resting State Networks Using Healthy and Epilepsy fMRI Data ," p. 440, 2016. [Online]. Available: https://www.frontiersin.org/article/10.3389/fnins.2016.00440

[145] M. Chamberland, M. Bernier, D. Fortin, K. Whittingstall, and M. Descoteaux, "3D interactive tractography-informed resting-state fMRI connectivity ," p. 275, 2015. [Online]. Available: https://www.frontiersin.org/article/10.3389/fnins.2015.00275

[146] D. Tomasi and N. D. Volkow, "Association between functional connectivity hubs and brain networks," *Cerebral Cortex*, vol. 21, no. 9, pp. 2003–2013, 2011.

[147] N. Tzourio-Mazoyer, B. Landeau, D. Papathanassiou, F. Crivello, O. Etard, N. Delcroix, B. Mazoyer, and M. Joliot, "Automated Anatomical Labeling of Activations in SPM Using a Macroscopic Anatomical Parcellation of the MNI MRI Single-Subject Brain," *NeuroImage*, vol. 15, no. 1, pp. 273–289, 2002. [Online]. Available: http://linkinghub.elsevier.com/retrieve/pii/S1053811901909784

[148] W. R. Shirer, S. Ryali, E. Rykhlevskaia, V. Menon, and M. D. Greicius, "Decoding subject-driven cognitive states with whole-brain connectivity patterns," *Cerebral Cortex*, vol. 22, no. 1, pp. 158–165, 2012.

[149] S. Mesmoudi, V. Perlbarg, D. Rudrauf, A. Messe, B. Pinsard, D. Hasboun, C. Cioli, G. Marrelec, R. Toro, H. Benali, and Y. Burnod, "Resting State Networks' Corticotopy: The Dual Intertwined Rings Architecture," *PLoS ONE*, vol. 8, no. 7, 2013.

[150] C. Rosazza and L. Minati, "Resting-state brain networks: Literature review and clinical applications," *Neurological Sciences*, vol. 32, no. 5, pp. 773–785, 2011.

[151] P. Tewarie, M. M. Schoonheim, C. J. Stam, M. L. van der Meer, B. W. van Dijk, F. Barkhof, C. H. Polman, and A. Hillebrand, "Cognitive and Clinical Dysfunction, Altered MEG Resting-State Networks and Thalamic Atrophy in Multiple Sclerosis," *PLoS ONE*, vol. 8, no. 7, 2013.

[152] E. Egolf, K. A. Kiehl, and V. D. Calhoun, "Group ICA of fMRI toolbox (GIFT)," *Proc. HBM Budapest, Hungary*, 2004.

[153] G. H. Glover, "Overview of functional magnetic resonance imaging," *Neurosurgery Clinics of North America*, vol. 22, no. 2, pp. 133–139, 2011.

[154] M. R. Arbabshirani and V. D. Calhoun, "Functional network connectivity during rest and task: comparison of healthy controls and schizophrenic patients," in *Annual International Confer-*

ence of the IEEE Engineering in Medicine and Biology Society. IEEE, 2011, Conference Proceedings, pp. 4418–4421.

[155] P. K. Mandal, "Magnetic Resonance Spectroscopy (MRS) and its application in Alzheimer's disease," *Concepts in Magnetic Resonance Part A: Bridging Education and Research*, vol. 30, no. 1, pp. 40–64, jan 2007. [Online]. Available: http://doi.wiley.com/10.1002/cmr.a.20072

[156] T. K. Gandhi, P. Sinha, and S. Anand, "Impairment in sensory reactivity of children with autism spectrum disorder," in *PSYCHOPHYSIOLOGY*, vol. 47, 2010, pp. S23–S23.

[157] J. S. Nomi and L. Q. Uddin, "Developmental changes in large-scale network connectivity in autism," *NeuroImage: Clinical*, vol. 7, pp. 732–741, 2015.

[158] "ABIDEI," *Online at http://fcon1000.projects.nitrc.org/indi/abide/*.

[159] "fcon," *Online at FCP: http://fcon 1000.projects.nitrc.org/fcpClassic/FcpTable.html*.

[160] C. Lord, M. Rutter, and A. Le Couteur, "Autism diagnostic interview-revised: a revised version of a diagnostic interview for caregivers of individuals with possible pervasive developmental disorders," *Journal of autism and developmental disorders*, vol. 24, no. 5, pp. 659–685, 1994.

[161] S. Robinson, G. Basso, N. Soldati, U. Sailer, J. Jovicich, L. Bruzzone, I. Kryspin-Exner, H. Bauer, and E. Moser, "A resting state network in the motor control circuit of the basal ganglia," *BMC neuroscience*, vol. 10, no. 1, p. 1, 2009.

[162] S. Folstein and M. Rutter, "INFANTILE AUTISM: A GENETIC STUDY OF 21 TWIN PAIRS," *Journal of Child Psychology and Psychiatry*, vol. 18, no. 4, pp. 297–321, sep 1977. [Online]. Available: http://doi.wiley.com/10.1111/j.1469-7610.1977.tb00443.x

[163] J. Hallmayer, S. Cleveland, A. Torres, and et Al, "Genetic heritability and shared environmental factors among twin pairs with autism," *Archives of General Psychiatry*, vol. 68, no. 11, pp. 1095–1102, nov 2011. [Online]. Available: http://dx.doi.org/10.1001/archgenpsychiatry.2011.76

[164] E. Fonbonne, "Epidemiology of autistic disorder and other pervasive developmental disorders," *Journal of Clinical Psychiatry*, vol. 66, no. 10, pp. 3–8, 2005.

[165] I. Rapin and R. Katzman, "Neurobiology of Autism," *Annals of Neurology*, vol. 43, no. 1, pp. 7–14, jan 1998. [Online]. Available: http://doi.wiley.com/10.1002/ana.410430106

[166] G. Trottier, L. Srivastava, and C. D. Walker, "Etiology of infantile autism: a review of recent advances in genetic and neurobiological research." *Journal of Psychiatry*

and Neuroscience, vol. 24, no. 2, pp. 103–115, mar 1999. [Online]. Available: http://www.ncbi.nlm.nih.gov/pmc/articles/PMC1188990/

[167] D. K. Sokol and M. Edwards-Brown, "Neuroimaging in Autistic Spectrum Disorder (ASD)," *Journal of Neuroimaging*, vol. 14, no. 1, pp. 8–15, jan 2004. [Online]. Available: http://doi.wiley.com/10.1111/j.1552-6569.2004.tb00210.x

[168] H. Cody, K. Pelphrey, and J. Piven, "Structural and functional magnetic resonance imaging of autism," *International Journal of Developmental Neuroscience*, vol. 20, no. 3-5, pp. 421–438, jun 2002. [Online]. Available: http://linkinghub.elsevier.com/retrieve/pii/S0736574802000539

[169] E. Courchesne, E. Redcay, and D. P. Kennedy, "The autistic brain: birth through adulthood," *Current Opinion in Neurology*, vol. 17, no. 4, 2004. [Online]. Available: http://journals.lww.com/co-neurology/Fulltext/2004/08000/The{_}autistic{_}brain{_}{_}birth{_}through{_}adulthood.16.aspx

[170] E. Courchesne, C. M. Karns, H. R. Davis, R. Ziccardi, R. A. Carper, Z. D. Tigue, H. J. Chisum, P. Moses, K. Pierce, C. Lord, A. J. Lincoln, S. Pizzo, L. Schreibman, R. H. Haas, N. A. Akshoomoff, and R. Y. Courchesne, "Unusual brain growth patterns in early life in patients with autistic disorder: An MRI study ," *Neurology*, vol. 57, no. 2, pp. 245–254, jul 2001. [Online]. Available: http://www.neurology.org/content/57/2/245.abstract

[171] A. R. Laird, P. M. Fox, S. B. Eickhoff, J. A. Turner, K. L. Ray, D. R. McKay, D. C. Glahn, C. F. Beckmann, S. M. Smith, and P. T. Fox, "Behavioral Interpretations of Intrinsic Connectivity Networks," *Journal of Cognitive Neuroscience*, vol. 23, no. 12, pp. 4022–4037, jun 2011. [Online]. Available: http://dx.doi.org/10.1162/jocn{_}a{_}00077

[172] S. M. Smith, P. T. Fox, K. L. Miller, D. C. Glahn, P. M. Fox, C. E. Mackay, N. Filippini, K. E. Watkins, R. Toro, A. R. Laird, and C. F. Beckmann, "Correspondence of the brain's functional architecture during activation and rest," *Proceedings of the National Academy of Sciences*, vol. 106, no. 31, pp. 13 040–13 045, aug 2009. [Online]. Available: http://www.pnas.org/content/106/31/13040.abstract

[173] D. Zhang and M. E. Raichle, "Disease and the brain's dark energy," *Nat Rev Neurol*, vol. 6, no. 1, pp. 15–28, jan 2010. [Online]. Available: http://dx.doi.org/10.1038/nrneurol.2009.198http://www.nature.com/nrneurol/journal/v6/n1/suppinfo/nrneurol.2009.198{_}S1.html

[174] R. N. Spreng, J. Sepulcre, G. R. Turner, W. D. Stevens, and D. L. Schacter, "Intrinsic Architecture Underlying the Relations among the Default, Dorsal Attention, and Frontoparietal

Control Networks of the Human Brain," *Journal of Cognitive Neuroscience*, vol. 25, no. 1, pp. 74–86, aug 2012. [Online]. Available: http://dx.doi.org/10.1162/jocn{_}a{_}00281

[175] W. W. Seeley, V. Menon, A. F. Schatzberg, J. Keller, G. H. Glover, H. Kenna, A. L. Reiss, and M. D. Greicius, "Dissociable Intrinsic Connectivity Networks for Salience Processing and Executive Control," *The Journal of Neuroscience*, vol. 27, no. 9, pp. 2349 LP – 2356, feb 2007. [Online]. Available: http://www.jneurosci.org/content/27/9/2349.abstract

[176] Ü. Sakoglu, G. D. Pearlson, K. A. Kiehl, Y. M. Wang, A. M. Michael, and V. D. Calhoun, "A method for evaluating dynamic functional network connectivity and task-modulation: application to schizophrenia," *Magnetic Resonance Materials in Physics, Biology and Medicine*, vol. 23, no. 5, pp. 351–366, 2010. [Online]. Available: https://doi.org/10.1007/s10334-010-0197-8

[177] C. Chang and G. H. Glover, "TimeâĂŞfrequency dynamics of resting-state brain connectivity measured with fMRI," *NeuroImage*, vol. 50, no. 1, pp. 81–98, mar 2010. [Online]. Available: http://linkinghub.elsevier.com/retrieve/pii/S1053811909012981

[178] X. Liu and J. H. Duyn, "Time-varying functional network information extracted from brief instances of spontaneous brain activity," *Proceedings of the National Academy of Sciences*, vol. 110, no. 11, pp. 4392–4397, mar 2013. [Online]. Available: http://www.pnas.org/content/110/11/4392.abstract

[179] R. M. Hutchison, T. Womelsdorf, J. S. Gati, S. Everling, and R. S. Menon, "Resting-state networks show dynamic functional connectivity in awake humans and anesthetized macaques," *Human Brain Mapping*, vol. 34, no. 9, pp. 2154–2177, sep 2013. [Online]. Available: http://doi.wiley.com/10.1002/hbm.22058

[180] M. Mennes, B. B. Biswal, F. X. Castellanos, and M. P. Milham, "Making data sharing work: The FCP/INDI experience," *NeuroImage*, vol. 82, pp. 683–691, nov 2013. [Online]. Available: http://linkinghub.elsevier.com/retrieve/pii/S1053811912010671

[181] J. E. Lainhart, J. Piven, M. Wzorek, R. Landa, S. L. Santangelo, H. Coon, and S. E. Folstein, "Macrocephaly in children and adults with autism," *Journal of the American Academy of Child and Adolescent Psychiatry*, vol. 36, no. 2, pp. 282–290, feb 1997. [Online]. Available: http://www.sciencedirect.com/science/article/pii/S0890856709628094?via{%}3Dihubhttp://www.ncbi.nlm.nih.gov/entrez/query.fcgi?cmd=Retrieve{&}db=PubMed{&}dopt=Citation{&}list{_}uids=9031582{%}5Cnhttp://ac.els-cdn.com/S0890856709628094/1-s2.0-S0890856709628094-main.pdf

[182] G. Allen and E. Courchesne, "Differential Effects of Developmental Cerebellar Abnormality on Cognitive and Motor Functions in the Cerebellum: An fMRI Study of Autism," *American Journal of Psychiatry*, vol. 160, no. 2, pp. 262–273, feb 2003. [Online]. Available: https://doi.org/10.1176/appi.ajp.160.2.262

[183] E. Courchesne, M. PR, C. ME, and et Al, "Neuron number and size in prefrontal cortex of children with autism," *JAMA*, vol. 306, no. 18, pp. 2001–2010, nov 2011. [Online]. Available: http://dx.doi.org/10.1001/jama.2011.1638

[184] M. van den Heuvel, H. Hulshoff Pol, P. Tichavsky, P., and Z. Koldovsky, "Functional connectivity in the motor cortex of resting human brain using echo-planar mri," *Magnetic Resonance in Medicine*, vol. 34, no. 6, pp. 537–541, Oct. 1995. [Online]. Available: http://dx.doi.org/10.1162/neco.1995.7.6.1129

[185] M. M. Herting, E. C. Maxwell, C. Irvine, and B. J. Nagel, "The Impact of Sex, Puberty, and Hormones on White Matter Microstructure in Adolescents," *Cerebral Cortex*, vol. 22, no. 9, pp. 1979–1992, sep 2012. [Online]. Available: http://dx.doi.org/10.1093/cercor/bhr246

[186] B. E. Yerys, K. F. Jankowski, D. Shook, L. R. Rosenberger, K. A. Barnes, M. M. Berl, E. K. Ritzl, J. VanMeter, C. J. Vaidya, and W. D. Gaillard, "The fMRI success rate of children and adolescents: Typical development, epilepsy, attention deficit/hyperactivity disorder, and autism spectrum disorders," *Human Brain Mapping*, vol. 30, no. 10, pp. 3426–3435, oct 2009. [Online]. Available: http://doi.wiley.com/10.1002/hbm.20767